

**REGULATION AND ROLE OF MIRNA AND TARGET GENES
IN CELL CYCLE DURING OXIDATIVE STRESS-INDUCED
PREMATURE SENESCENCE IN MESENCHYMAL STEM CELL**

By

TAI LIHUI

A dissertation submitted to the Department of Pre-Clinical Science,
Faculty of Medicine and Health Sciences,
Universiti Tunku Abdul Rahman,
in partial fulfilment of the requirements for the degree of
Master of Medical Sciences

December 2016

ABSTRACT

REGULATION AND ROLE OF MIRNA AND TARGET GENES IN CELL CYCLE DURING OXIDATIVE STRESS-INDUCED PREMATURE SENESCENCE IN MESENCHYMAL STEM CELL

Tai Lihui

Multipotent mesenchymal stem cells (MSCs) exhibit self-renewal and multilineage differentiation capacity, thus possessing great potentials in regenerative medicine and therapeutic applications. However, on *in vitro* expansion, MSCs enter irreversible growth arrest and eventually senescence as a consequence of oxidative stress. microRNAs (miRNAs) are negative regulators of gene expression that mediate senescence pathways by targeting the cell cycle, but the mechanism is still unclear. This study aimed to develop an oxidative stress-induced premature senescence (OSIPS) model using Wharton's Jelly-derived mesenchymal stem cells (WJ-MSCs) to study the role of differentially expressed miRNAs associated with the G1/S-transition of the cell cycle during senescence. In Part (I), an OSIPS WJ-MSC model was established by treatment with 200 μ M hydrogen peroxide (H_2O_2). The senescence state in OSIPS WJ-MSCs was validated by morphological changes, senescence associated β -galactosidase assays and senescence biomarkers expression. Cell cycle analysis showed that in OSIPS WJ-MSCs, G1-phase cell population increased whilst S-phase population decreased. Evidences further demonstrated that OSIPS cells closely resembled replicative senescence in WJ-

MSCs. In Part (II), miRNA microarray analysis of OSIPS WJ-MSCs identified seven up-regulated and five down-regulated miRNAs that fulfilled the criteria of $\log_2(\text{fold change}) >1$ or <-1 and $p < 0.05$. The microarray data were confirmed by real-time RT-PCR. Focussing on the less studied miR-20b-5p and miR-106a-5p in the down-regulated group, time-course studies indicated rapid and irreversible down-regulation of the miRNAs in OSIPS WJ-MSCs. In Part (III), transient over-expression showed that miR-20b-5p and miR-106a-5p were interchangeable in promoting the growth of WJ-MSCs, with concurrent increases in DNA synthesis rate, suggesting a regulatory role for miR-20b-5p/miR-106a-5p in the cell cycle. Bioinformatics interrogation predicted that miR-20b-5p/miR-106a-5p targeted pro- and anti-proliferative genes of the G1/S-transition; such targeting was confirmed by luciferase assays. In OSIPS WJ-MSCs, down-regulated miR-20b-5p/miR-106a-5p expression was shown to be inversely correlated with increased mRNA and protein expression levels of CCND1, CDK6 and p21, but not E2F1. A model depicting the role of miR-17 miRNAs in regulating the G1/S-phase of the cell cycle in OSIPS MSCs was proposed. Taken together, the results demonstrated the participation of miR-20b-5p/miR-106a-5p in oxidative stress-induced senescence in MSCs by targeting the G1/S-phase factors of the cell cycle.

ACKNOWLEDGEMENTS

First and foremost, my sincere appreciation and gratefulness to my supervisor, Senior Professor Dr. Choo Kong Bung, for his continuous guidance, encouragement, patience and advice that have assisted me throughout the project. I would also like to thank my co-supervisor, Emeritus Professor Dr. Cheong Soon Keng, for his support and advice. My gratitude also goes to Professor Huang Chiu-Jung, Chinese Culture University, Taiwan, for her opinions and feedback throughout the work. I have learned and gained a lot of knowledge from all my teachers and have broadened my perspective in the field of stem cell research, and in Life.

I would like to thank Cryocord Sdn. Bhd. in providing the characterised Wharton's Jelly-derived mesenchymal stem cells, which was the cell lines used in this study, and also appreciation to Dr. Hans-Ingo Trompeter, University Düsseldorf, Germany, for his generous gift of the luciferase plasmids used in this work. This work was supported by HIR-MoE Grant (UM.C/625/1/HIR/MOHE/CHAN/03). My sincere thanks to the Faculty of Medicine and Health Sciences, UTAR, for provided me the opportunity to conduct this project with sufficient lab instruments and under good circumstances.

Not to forget my fellow lab-mates in the FMHS Postgraduate Lab, especially Nguyen Phan Nguyen Nhi, Michele Hiew Sook Yui, Chai Kit Man, Vimalan Rengganatan and Dr. Lim Kian Lam. I truly appreciate their sharing,

encouragements and supports throughout the project. Finally and yet importantly, I would like to express my thankfulness to my family for their emotional support and concern to have enabled me to carry out my research project smoothly.

APPROVAL SHEET

This dissertation entitled “**REGULATION AND ROLE OF MIRNA AND TARGET GENES IN CELL CYCLE DURING OXIDATIVE STRESS-INDUCED PREMATURE SENESENCE IN MESENCHYMAL STEM CELL**” was prepared by TAI LIHUI and submitted as partial fulfilment of the requirements for the degree of Master of Medical Sciences at Universiti Tunku Abdul Rahman.

Approved by:

(Senior Prof. Dr. Choo Kong Bung)
Senior Professor/Supervisor
Department of Pre-clinical Sciences
Faculty of Medicine and Health Sciences
Universiti Tunku Abdul Rahman

Date:

(Emeritus Prof. Dr. Cheong Soon Keng)
Senior Professor/Co-supervisor
Department of Medicine
Faculty of Medicine and Health Sciences
Universiti Tunku Abdul Rahman

Date:

FACULTY OF MEDICINE AND HEALTH SCIENCES
UNIVERSITY TUNKU ABDUL RAHMAN

Date: _____

SUBMISSION OF DISSERTATION

It is hereby certified that **Tai Lihui** (ID no: **14UMM05533**) has completed this final year project entitled “REGULATION AND ROLE OF MIRNA AND TARGET GENES IN CELL CYCLE DURING OXIDATIVE STRESS-INDUCED PREMATURE SENESCENCE IN MESENCHYMAL STEM CELL” under the supervision of Senior Prof. Dr. Choo Kong Bung (Supervisor) from the Department of Pre-clinical Sciences, Faculty of Medicine and Health Sciences, and Emeritus Prof. Dr. Cheong Soon Keng (Co-Supervisor) from the Department of Medicine, Faculty of Medicine and Health Sciences.

I understand that University will upload softcopy of my dissertation in pdf format into UTAR Institutional Repository, which may be made accessible to UTAR community and public.

Yours truly,

(Tai Lihui)

DECLARATION

I TAI LIHUI hereby declare that the dissertation is based on my original work except for quotations and citations which have been duly acknowledged. I also declare that it has not been previously or concurrently submitted for any other degree at UTAR or other institutions.

TAI LIHUI

Date: _____

TABLE OF CONTENTS

	PAGE
ABSTRACT	ii
ACKNOWLEDGEMENTS	iv
APPROVAL SHEET	vi
SUBMISSION SHEET	vii
DECLARATION	viii
LIST OF TABLES	xiv
LIST OF FIGURES	xv
LIST OF ABBREVIATIONS	xvii
CHAPTER	
1.0 INTRODUCTION	1
2.0 LITERATURE REVIEW	5
2.1 Mesenchymal Stem Cells (MSCs)	5
2.1.1 Self-renewal and Multilineage Differentiation Capacity of Mesenchymal Stem Cells (MSCs)	7
2.1.2 Mechanisms and Limitations of Mesenchymal Stem Cell-based Therapy	10
2.1.3 Wharton’s Jelly-derived Mesenchymal Stem Cells (WJ-MSCs) in Human Umbilical Cord (hUC)	14
2.2 Ageing	18
2.2.1 Cellular Replicative Senescence (RS) and Stress-induced Premature Senescence (SIPS)	20
2.2.2 Reactive Oxygen Species (ROS) and Free Radical Theory of Aging	21

2.2.3	Cellular Senescence and Cell Cycle Arrest	22
2.3	microRNAs (miRNAs)	26
2.3.1	microRNA Regulation of G1/S-phase of the Cell Cycle During Senescence	27
3.0	MATERIALS AND METHODS	29
3.1	Cell Lines	29
3.2	Cell Culture	29
3.2.1	Preparation of Cell Culture Media	30
3.2.2	Cell Revival from Liquid Nitrogen Frozen Stock	30
3.2.3	Cell Culture Maintenance and Sub-culturing	31
3.2.4	Cryopreservation of Cultured Cell	32
3.2.5	Hydrogen Peroxide (H ₂ O ₂) Treatment of WJ- MSCs	33
3.3	Senescence Associated β -galactosidase (SA- β -gal) Staining	34
3.4	Cell Cycle Analysis	34
3.5	RNA Preparation	35
3.5.1	RNA Isolation	35
3.5.2	RNA Quantification and Integrity Assessment	36
3.6	Determination of Messenger RNA (mRNA) Levels by qRT-PCR	37
3.6.1	Primers for mRNA qRT-PCR	37
3.6.2	cDNA Synthesis by Reverse Transcription	37
3.6.3	mRNA qRT-PCR	39
3.7	Global microRNA (miRNA) Expression Profiling Analysis	41
3.8	miRNA qRT-PCR	42
3.8.1	miRNA Primers for qRT-PCR	42
3.8.2	Polyadenylation and Reverse Transcription of miRNA	42
3.8.3	miRNA qRT-PCR	45

3.9	Transfection of Synthetic miRNA	45
3.10	Cell Proliferation Analysis	47
	3.10.1 Cell Growth Analysis	47
	3.10.2 <i>In vitro</i> Cell Viability Assay by MTT	48
	3.10.3 BrdU Cell Proliferation Assay	48
3.11	Validation of miRNA Targeted Transcripts by Luciferase Assays	49
	3.11.1 Transformation of Plasmid DNA	49
	3.11.2 Plasmid DNA Extraction	52
	3.11.3 Validation of Extraction Plasmid DNA	53
	3.11.4 Luciferase Reporter Assays	54
3.12	miRNA Target Prediction by Bioinformatics Analysis	55
3.13	Western Blot Analysis	56
	3.13.1 Buffers and Reagents Preparation	56
	3.13.2 Preparation of Cell Lysates and Quantification of Protein Lysates	58
	3.13.3 Protein Separation by SDS-polyacrylamide Gel Electrophoresis (SDS-PAGE)	59
	3.13.4 Semi-dry Transfer of Protein from Gel to Nitrocellulose Membrane	60
	3.13.5 Membrane Blocking	61
	3.13.6 Antibody Staining	62
	3.13.7 Chemiluminescence Detection	63
	3.13.8 Stripping and Reprobing	63
	3.13.9 Western Blot Densitometric Analysis	64
3.14	Statistical Analysis	64
4.0	RESULTS	65
4.1	Study Design	65
	<u>Part I: Establishment of Oxidative Stress-induced Premature Senescence (OSIPS) Model in Wharton’s Jelly-derived Mesenchymal Stem Cells (WJ-MSCs)</u>	

4.2	Optimisation of Hydrogen Peroxide (H ₂ O ₂) Concentration in Inducing Premature Senescence in WJ-MSCs	67
4.3	Validation of Senescence Characteristics in OSIPS WJ-MSCs	69
4.4	OSIPS WJ-MSCs Shared Similar Senescence Characteristics with Replicative Senescence (RS) WJ-MSCs	72
4.5	Cell Cycle Arrest in OSIPS WJ-MSCs	74

Part II: miRNA Profiling and Validation in Oxidative Stress-induced Premature Senescence in Wharton’s Jelly-derived Mesenchymal Stem Cells (OSIPS WJ-MSCs)

4.6	RNA Concentration and Integrity Test	76
4.7	Global miRNA Expression Profiling in OSIPS WJ-MSCs	79
4.8	miRNA Expression Profiling Analysis Revealed Differentially Expressed miRNAs in OSIPS WJ-MSCs	81
4.9	Experimental Validation of miRNA Expression in OSIPS and RS WJ-MSCs	87
4.10	Rapid and Irreversible Down-regulation of miR-20b-5p and miR-106a-5p in OSIPS WJ-MSCs	89

Part III: The Regulatory Role of miR-17 Family in the G1/S-phase of the Cell Cycle

4.11	miR-20b-5p and miR-106a-5p Promote Cell Proliferation in WJ-MSCs	92
4.12	miR-20b-5p and miR-106a-5p Target G1/S-phase Cell Cycle Genes	95
4.13	miR-20b-5p and miR-106a-5p Regulate G1/S-phase Cell Cycle Genes	100

5.0	DISCUSSION	105
5.1	Establishment of Premature Senescence in WJ-MSCs by Hydrogen Peroxide Treatment	105
5.2	Senescence-deregulated miRNAs are Frequently Associated with Cancer	107
5.3	miR-17 miRNAs are Important Regulators of G1/S-phase Transition of the Cell Cycle in OSIPS WJ-MSCs	111
5.4	A Proposed Model on the Role of miR-17 miRNAs in Oxidative-stress Senescence	112
6.0	CONCLUSIONS	116
6.1	Conclusions	116
6.2	Future Studies	117
	REFERENCES	119
	APPENDICES	131

LIST OF TABLES

Table		Page
3.1	Primers used in mRNA qRT-PCR	38
3.2	mRNA qRT-PCR reaction mixture	40
3.3	Primers used in miRNA qRT-PCR	43
3.4	miRNA qRT-PCR reaction mixture	46
3.5	Primers used in cloning of 3'-UTR into vector pmirGLO	50
3.6	Preparation of western blot buffers	56
4.1	Cell cycle analysis in H ₂ O ₂ -treated and untreated WJ- MSC lines	75
4.2	Purity and concentration of RNA samples isolated from untreated control and H ₂ O ₂ -treated WJ-MSCs for miRNA profiling analysis	77
4.3	Fifty top miRNAs up- or down-regulated in OSIPS WJ- MSCs	82
4.4	Differentially expressed miRNAs in OSIPS WJ-MSCs	86
5.1	Relative expression of miRNAs from the miR-17/92 and miR-106a/363 clusters in normal development, cancer, other diseases and age-related conditions	110

LIST OF FIGURES

Figure		Page
2.1	Sources and multipotent differentiation potentials of mesenchymal stem cells (MSCs)	6
2.2	Self-renewal mechanisms by stem cells, viz. obligatory asymmetric replication and stochastic differentiation model	8
2.3	Mesenchymal stem cell-based therapy in common immune and non-immune diseases	12
2.4	Cross-sectional diagram of human umbilical cord (hUC)	16
2.5	The hallmarks of ageing	19
2.6	Damaged cells enter cellular senescence via DDR, p16/pRb and p19/p53/p21 pathways, and eventually promote ageing	25
3.1	Workflow of miRNA qRT-PCR	44
4.1	Study design	66
4.2	Cell growth profile of H ₂ O ₂ -treated WJ-MSCs relative to the respective untreated control cells determined by cumulative population doubling level	68
4.3	Senescence characteristics of 200 µM H ₂ O ₂ -treated WJ-MSC lines	70
4.4	Expression of senescence biomarkers in H ₂ O ₂ -treated WJ-MSC lines WJ0619, WJ0706 and WJ2000 as determined by real-time PCR	71
4.5	Senescence characteristics in early passage (P) 7 and late passage 23, and H ₂ O ₂ -treated OSIPS WJ0706 cells	73
4.6	Integrity of RNA prepared from untreated control and OSIPS WJ-MSC lines WJ0619, WJ0706 and WJ2000	78
4.7	Differentially expressed miRNAs in H ₂ O ₂ -treated WJ-MSCs	80
4.8	Validation of differentially expressed miRNAs in H ₂ O ₂ -treated WJ-MSCs by real-time RT-PCR	88

4.9	Validation of differentially expressed miRNAs in H ₂ O ₂ -treated or late-passage WJ0706 cells by real-time RT-PCR	90
4.10	Down-regulated expression of miR-20b-5p and miR-106a-5p in H ₂ O ₂ -treated WJ-MSCs	91
4.11	miR-20b-5p and miR-106a-5p promote cell proliferation in MSCs	93
4.12	Predicted targets of the G1/S-phase cell cycle of the down-regulated miR-17 family miRNAs in OSIPS MSCs	96
4.13	G1/S-phase cell cycle targets of the miR-20b-5p and miR-106a-5p	98
4.14	Validation of targeting of miR-20b-5p (A) and miR-106a-5p (B) at the cell cycle transcripts in luciferase assays	99
4.15	Inhibition of the cell cycle genes by miR-20b-5p/miR-106a-5p	102
4.16	mRNA expression levels of the cell cycle target genes in H ₂ O ₂ -treated WJ-MSCs by real-time RT-PCR	103
4.17	Protein expression levels of p21, CDK6, CCND1 and E2F1 in OSIPS WJ-MSCs by western blot analysis	104
5.1	Schematic representation of the miR-17/92 and miR-106a/363 paralogs and their chromosomal location	109
5.2	A proposed model illustrating the role of miR-17 family miRNAs in oxidative stress-induced premature senescence	114

LIST OF ABBREVIATIONS

A ₂₆₀	Absorbance at 260nm wavelength
A ₂₈₀	Absorbance at 280nm wavelength
ALL	Acute lymphoblastic leukaemia
AML	Acute myeloid leukaemia
APS	Ammonium persulfate
ATM	Ataxia telangiectasia mutated
ATP	Adenosine triphosphate
ATR	Ataxia telangiectasia mutated -Rad3-related
B cells	Bone marrow-derived cells
BCL2	B-cell lymphoma 2
BLAST	Basic local alignment search tool
BM-MSC	Bone marrow-derived mesenchymal stem cell
BrdU	5-bromo-2'-deoxyuridine
BSA	Bovine serum albumin
CCND	D-type cyclin
CCNE	E-type cyclin
CD	Cluster of differentiation
cdc25A	Cell division cycle 25A
CDK	Cyclin dependent kinase
cDNA	Complementary deoxyribonucleic acid
CHK	Checkpoint kinase
CLL	Chronic lymphocytic leukaemia
CO ₂	Carbon dioxide

CPD	Cumulative population doubling
C _t	Cycle threshold
DDR	DNA damage response
DEPC	Diethylpyrocarbonate
DMEM	Dulbecco's Modified Eagle Medium
DNA	Deoxyribonucleic acid
dNTP	Deoxynucleoside triphosphate
E2F1	Elongation 2 promoter binding factor
EDTA	Ethylenediaminetetraacetic acid
ERBB2	Erb-B2 receptor tyrosine kinase 2
FBS	Foetal bovine serum
GAPDH	Glyceraldehyde 3-phosphate dehydrogenase
GLB1	Galactosidase beta 1
H2AX	Histone H2A histone-variant
H ₂ O ₂	Hydrogen peroxide
hAMSC	Human adipose tissue-derived mesenchymal stem cell
HCl	Hydrochloric acid
HCT-15	Human colorectal adenocarcinoma cell line
HEK293T	Human Embryonic Kidney 293 cell
HLA-DR	Human leukocyte antigen - antigen D related
HLA-G	Human leukocyte antigen G
hMESC	Human endometrium-derived mesenchymal stem cell
HRP	Horseradish peroxidase
hUC	Human umbilical cord
IgG	Immunoglobulin G

LB	Luria Bertani
LNA	Locked nucleic acid
MCL	Myeloid cell leukaemia
miR-	Mature form of the miRNA
miRNA	microRNA
MLL	Mixed lineage leukaemia
mRNA`	Messenger ribonucleic acid
MSCs	Mesenchymal stem cells
MTT	3-(4,5-dimethylthiazolyl-2)-2,5-diphenyltetrazolium bromide
NaCl	Sodium chloride
NCBI	National Center for Biotechnology Information
NF-κB	Nuclear factor-κB
NO`	Nitric oxide
O ₂	Superoxide anion
OH`	Hydrocyl radical
Opti-MEM	Reduced serum medium
OSIPS	Oxidative stress-induced premature senescence
P	Passage
p16	Cyclin-dependent kinase inhibitor 2A (CDKN2A)
p19	Cyclin-dependent kinase inhibitor 2D (CDKN2D)
p21	Cyclin-dependent kinase inhibitor 1A (CDKN1A)
p53	Tumor protein p53
PBS	Phosphate buffered saline
PD	Population doubling

pRb	Retinoblastoma protein
pre-miRNAss	Precursor microRNAs
pri-miRNA	Primary microRNAs
PTEN	Phosphatase and tensin homolog
qRT-PCR	Quantitative reverse transcription polymerase chain reaction
RBL1/p107	Retinoblastoma transcriptional corepressor like 1
RBL2/p130	Retinoblastoma transcriptional corepressor like 2
RIPA	Radioimmunoprecipitation assay
RNA	Ribonucleic acid
RNU6	Ribonucleic acid, U6 small nuclear 6
ROS	Reactive oxygen species
rRNA	Ribosomal ribonucleic acid
RS	Replicative senescence
RT	Reverse transcription
RT-PCR	Reverse transcription polymerase chain reaction
SA- β -gal	Senescence associated β -galactosidase
SD	Standard deviation
SDS	Sodium dodecyl sulphate
SDS-PAGE	Sodium dodecyl sulphate-polyacrylamide gel electrophoresis
SIPS	Stress-induced premature senescence
SIRT1	Sirtuin 1
SMAD	SMAD family member
T cells	Thymus cells

TBE	Tris /borate/ ethylenediaminetetraacetic acid (EDTA)
TBS	Tris-buffered saline
TBST	Tris-buffered saline with Tween-20
TEMED	Tetramethylethylenediamine
TGF β	Transforming growth factor beta
TopBP1	Topoisomerase (DNA) II binding protein 1
TP53INP1	Tumour protein p53 inducible nuclear protein 1
UDG	Uracil-DNA glycosylase
UTR	Untranslated region
UV	Ultraviolet
WJ	Wharton's Jelly
WJ-MSC	Wharton's Jelly-derived mesenchymal stem cell
WNT3A	Wnt family member 3A
$\Delta\Delta C_t$	Delta Delta C_t

CHAPTER 1

INTRODUCTION

Mesenchymal stem cells (MSCs) are multipotent adult stem cells that are able to self-renew and differentiate into cell types of mesodermal origin, including adipocyte, chondrocyte and osteocyte. Besides, MSCs are capable to home in on inflammation sites and exert immunomodulatory effects on immune cells to alleviate immune disorders (Ullah et al., 2015). MSCs exist in almost all adult tissues and can be isolated and expanded, thus possessing great therapeutic potentials in stem cell transplantation and regenerative cell therapy (Williams and Hare, 2011; Kim and Cho, 2013).

In recent years, stem cell therapy using adult MSCs has made important clinical advances. In autologous or allogenic stem cell transplantation, MSCs isolated from donors are expanded in culture to obtain adequate cell numbers for validation and therapeutic purposes (Power and Rasko, 2011; Kim and Cho, 2013). However, on extended *in vitro* culture, the proliferation rate of MSCs rapidly reduce and the MSCs eventually enter senescence, resulting in diminished self-renewal and differentiation potentials, and hampering clinical applications (Wagner et al., 2010; Gu et al., 2016).

Cellular or replicative senescence is a state of irreversible growth arrest in which the cells permanently lose their proliferation capability and stop

proliferation (Ohtani et al., 2009). In eukaryotic cells, the cell cycle comprises of two major stages, the interphase (G1, S and G2 phases) and the mitotic (M) phase, that duplicate the chromosomal DNA prior to the production of two daughter cells. Interphase cell cycle checkpoints play important roles in regulating cell division and maintaining genome stability. Defective or incomplete DNA replication is detected by the first checkpoint at the G1/S-transition, triggering cell cycle arrest and S-phase blockage for DNA repair purposes (Neganova and Lako, 2008; Bertoli et al., 2013). Once the damages are irreparable, the cells are permanently arrested at the G1/S-checkpoint, thus leading to irreversible cell cycle arrest and eventually senescence (Ohtani et al., 2009).

Senescence can also be triggered prematurely by multiple intrinsic factors such as mitogenic and oncogenic stimulation, DNA damage and exposure to high oxygen concentration. Onset of senescence induced by stresses is known as stress-induced premature senescence (SIPS). It has been reported that cells in replicative senescence and SIPS shared important features, including morphology, gene expression pattern, senescence-associated β -galactosidase activity, telomere shortening, reduced DNA repair capability and irreversible G1-phase cell cycle arrest (Sikora et al., 2011; Haines et al., 2013).

Oxidative stress is one of the factors that accelerate the onset of replicative senescence. Accumulation of reactive oxygen species (ROS) alters normal redox state of the cells and provokes oxidative stress. Endogenous- and

exogenous-induced oxidative stresses trigger DNA single- and double-stranded breaks, thus activating the DNA damage response (DDR). DDR in turn stimulates p53 and p21 cell cycle inhibitors, leading to cell cycle arrest, thereby accelerating the onset of replicative senescence (Haines et al., 2013; Jeong and Cho, 2015).

Interests on the regulatory role of microRNAs (miRNAs) on senescence have emerged with the discovery that miRNA lin-4 functions to regulate the lifespan in *Caenorhabditis elegans* (Boehm and Slack, 2005). miRNAs are small single-stranded endogenous non-coding RNAs that negatively regulate transcripts of target genes at the post-transcriptional level, primarily by recognizing the specific sites in the 3'-untranslated region (3'-UTR), resulting in translational repression or degradation of the targeted transcripts. Studies have been shown that miRNAs regulate a broad range of cellular functions, including cancer formation, stress response, cell proliferation, self-renewal and other physiological conditions (Chen et al., 2010; Bilslund et al., 2013; Guo et al., 2014). A number of miRNAs have previously been reported to be differentially expressed in senescence cells, however the miRNA-regulated targets and biological functions in senescence remain to be clearly elucidated (Li et al., 2009; Feliciano et al., 2011). It is essential to gain insight into the fundamental molecular mechanisms and possible interactions between miRNAs and target genes in relation with cell cycle that contribute to the onset of replicative and premature senescence.

In this study, it was hypothesised that oxidative stress caused premature senescence in MSCs and altered miRNA expression. The dysregulated miRNAs in oxidative stress-induced premature senescence MSCs were proposed to play important roles in cell cycle regulation during the senescence process. We anticipated microarray analysis to reveal a group of differentially expressed miRNAs in oxidative stress-induced senescence in MSCs, and that these miRNAs contribute to the senescence process by modulating G1/S-phase of the cell cycle.

The objectives for this study were:

- 1) To develop an oxidative stress-induced premature senescence (OSIPS) model of mesenchymal stem cells (MSCs)
- 2) To compare the miRNA expression profiles in young and OSIPS MSCs and to identify differentially expressed miRNAs in young MSCs relative to OSIPS MSCs by high-throughput miRNA microarray
- 3) To identify and validate putative targets of OSIPS-affected miRNAs in association to G1/S-transition of the cell cycle by bioinformatics approaches and miRNA transfection assays
- 4) To elucidate the functional role of OSIPS-affected miRNAs and targeted genes in regulating G1/S-phase of the cell cycle in senescence

CHAPTER 2

LITERATURE REVIEW

2.1 Mesenchymal Stem Cells (MSCs)

Interests in research in mesenchymal stem cells (MSCs) were first aroused in 1960s when a Soviet researcher, Alexander Friedenstein, discovered osteogenic potentials in a minor subpopulation of bone marrow cells. These osteogenic stem cells were described then as colony forming unit fibroblasts due to their ability to form single cell-derived colonies in an *ex vivo* assay (Friedenstein et al., 1966). The stromal cells were later named as “mesenchymal stem cell” by Caplan (1991), and the multilineage differentiation potentials were further characterised by Pittenger et al. (1999). Today, MSCs are known as multipotent stromal cells that are capable of self-renewal and differentiation into mature cells of endoderm, ectoderm and mesodermal origin. MSCs exist in almost all tissues and can be isolated from adult and embryonic tissues, including skeletal muscle, adipose tissue, bone marrow, peripheral blood, umbilical cord and many more (Figure 2.1) (Zuk et al., 2001; Cho et al., 2004; Kassis et al., 2006; Uccelli et al., 2008).

The Mesenchymal and Tissue Stem Cell Committee of the International Society for Cellular Therapy has defined the minimal criteria to verify human MSCs. First, MSCs display plastic adherence when cultured

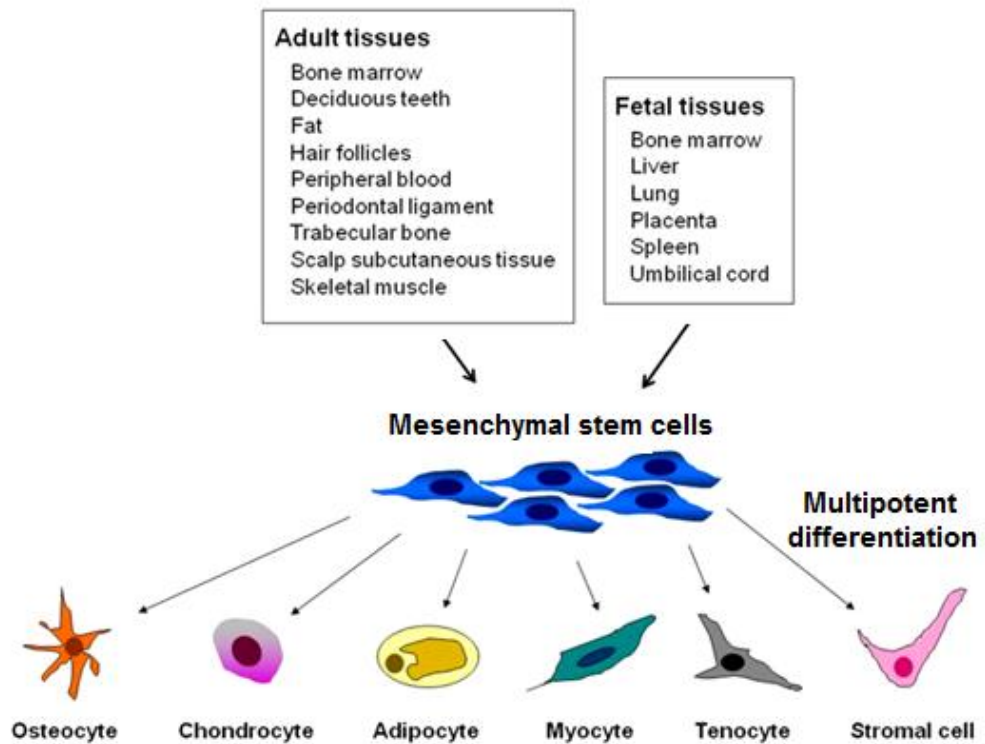


Figure 2.1 Sources and multipotent differentiation potentials of mesenchymal stem cells (MSCs). MSCs can be isolated from adult and foetal tissues and differentiate *in vitro* into mature cells of the same lineage. (Figure modified from Andrades et al., 2011)

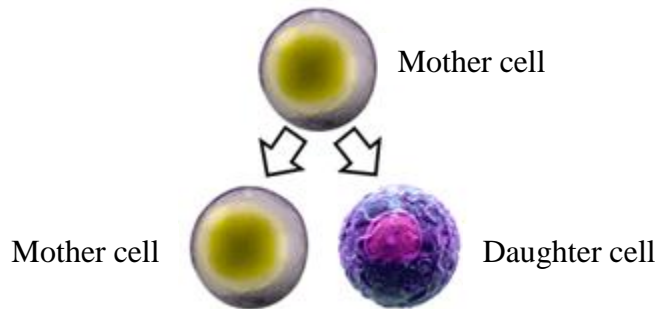
under standard culture condition; second, MSCs must stain positive for CD73, CD90 and CD105 surface markers, and negative for CD14, CD34, CD45 or CD79 α , CD11b or CD19 and HLA-DR hematopoietic markers; third, MSCs possess *in vitro* multi-lineage differentiation capability into osteoblasts, adipocytes and chondroblasts (Dominici et al., 2006).

2.1.1 Self-renewal and Multilineage Differentiation Capacity of Mesenchymal Stem Cells (MSCs)

Stem cells are defined by their self-renewal and multipotency potentials. MSCs are unspecialised stem cells with the capability to renew and retain the undifferentiated state while going through numerous cycles of cell divisions. During the division process, a MSC divides into a mother cell with stemness properties to maintain the stem cell pool (self-renewal), and a differentiated daughter cell to replace dead or damage tissues (proliferation) (Nombela-Arrieta et al., 2011). Although both the self-renewal and cell proliferation processes are dependent on cell division, the cell proliferation process involves division of various types of stem and progenitor cells while the self-renewal process is able to yield daughter cells with developmental potentials identical to the mother cell (Shenghui et al., 2009).

Generally, two self-renewal mechanisms are practiced by stem cells to maintain cellular homeostasis (Figure 2.2). In the obligatory asymmetric replication model in stem cell division, a mother cell identical to the original

Obligatory Asymmetric Replication



Stochastic Differentiation

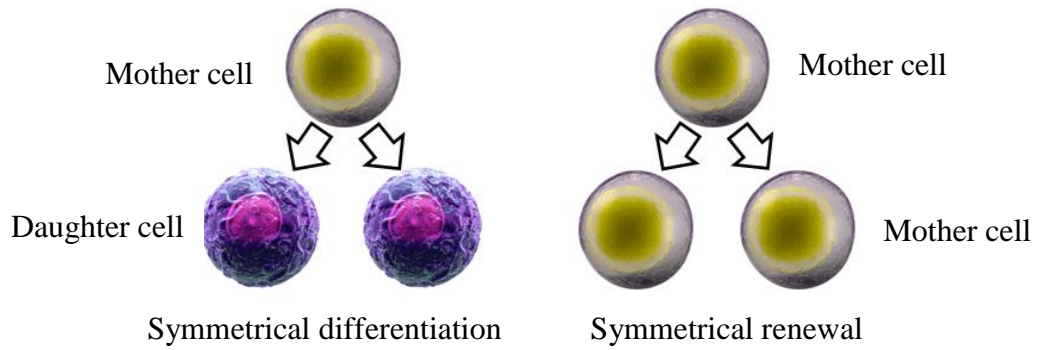


Figure 2.2 Self-renewal mechanisms by stem cells, viz. obligatory asymmetric replication and stochastic differentiation model. (Figure modified from Appelbaum et al., 2011)

one, and a specialised daughter cell are produced. In contrast, in the alternative stochastic differentiation model, two stem cells participated and formed either two identical mother cells through mitosis (symmetric renewal), or two differentiated daughter cells (symmetric differentiation) (Lander, 2009; Shenghui et al., 2009; Appelbaum et al., 2011).

Stem cell self-renewal is sustained by a balance between intrinsic actions of proto-oncogenes and tumour suppressors. Proto-oncogenes facilitate the self-renewal of stem cells whereas the gate-keeping tumour suppressors serve as a fail-safe programme to avoid uncontrolled proliferation and malignant transformation. Tumour suppressors, such as p53 and p16, which are also cell cycle-associated inhibitors, reduce stem cell regenerative capacity by delaying cell division or by inducing senescence upon activation by cellular stresses or DNA damages (Shenghui et al., 2009; Signer and Morrison, 2013). On the contrary, tumour suppressors when acting as a care-taker, function to maintain integrity of genome in stem cells through induction of DNA repair, detoxification of reactive oxygen species (ROS) and telomere maintenance (Kinzler and Vogelstein, 1997). Deprivation of care-taker tumour suppressors causes depletion in the stem cell pool and tissue regenerative capacity, triggering premature-ageing phenotypes. However, functional differences between the gate-keeping and care-taking roles of tumour suppressors are still unclear. As an example, the p53 tumour suppressor has both gate-keeping and care-taking functions (Lombard et al., 2005; Shenghui et al., 2009; Signer and Morrison, 2013). Disruption of the balance between activities of proto-

oncogenes, gate-keeping and care-taking tumour suppressors can induce ageing in stem cell or cancer.

During development and repair of injured tissues, multipotent MSCs are able to self-renew and differentiate into specialised mature cells, like osteocytes, chondrocytes, adipocytes, myocytes and tenocytes (Figure 2.1), depending on the extrinsic growth and differentiation stimuli received from the stem cell niche, which is a microenvironment comprises of stem cells, non-stem cells, extracellular matrix and molecular factors needed to maintain the potency of stem cells (Kassis et al., 2006; Uccelli et al., 2008). The niche cells provide MSCs with physical anchorage site and produce membrane-bound and -secreted factors that control stem cell cell cycle, survival and differentiation state, based on physiological demands (Morrison and Spradling, 2008; Zhang and Li, 2008; Andrades et al., 2011). In response to changing demands in development and ageing, embryonic, foetal, young and old adult MSCs have distinct self-renewal and multilineages differentiation potentials. However, the downstream mechanisms that regulate the cell cycle and developmental and differentiation potentials remain to be fully elucidated (Shenghui et al., 2009; Signer and Morrison, 2013).

2.1.2 Mechanisms and Limitations of Mesenchymal Stem Cell-based Therapy

The number of clinical trials on MSC-based cell therapy has been increasing since 2004. Today, multipotent MSCs, with no ethical and teratoma

formation issues, are emerging as therapeutic agents for treatment of both immune and non-immune diseases (Figure 2.3). In ischemic myocardial infarction, MSCs have been shown to reduce apoptosis and to differentiate into cardiac tissues to repair the damage (Jackson et al., 2001; Collins et al., 2007). Besides, *in vitro* ectodermal differentiation of MSCs into motor neurons and astrocytes, followed by cell engraftment to achieve cell replacement and neuroprotection was shown to increase the survival rate of neurons and delay the onset of amyotrophic lateral sclerosis (Lewis and Suzuki, 2014).

Apart from the multipotency property, MSCs are found to specifically migrate to inflammation sites of damaged tissues upon cell transplantation, in response to the inflammatory chemokines and cytokines (Honczarenko et al., 2006; Greco and Rameshwar, 2012). MSCs migration is dependent on the cell trafficking molecules, including chemokines, adhesion molecule and matrix metalloproteinases, which function to enhance MSCs *in vivo* engraftment efficacy, invasiveness and MSCs adherence to the damaged sites (Rüster et al., 2006; Son et al., 2006; Ding et al., 2009). At the injury sites, MSCs interact with the inflammation stimuli and secrete growth factors for tissue regeneration by mediating angiogenesis and preventing cell apoptosis (Caplan and Dennis, 2006; Crisostomo et al., 2008). Upon stimulation by inflammatory cytokines such as interferon- γ , interleukin-1 and tumour necrosis factor- α , MSCs subsequently exert immunomodulatory effects to decrease the chance of rejection following transplantation. MSCs suppress proliferation of B cells,

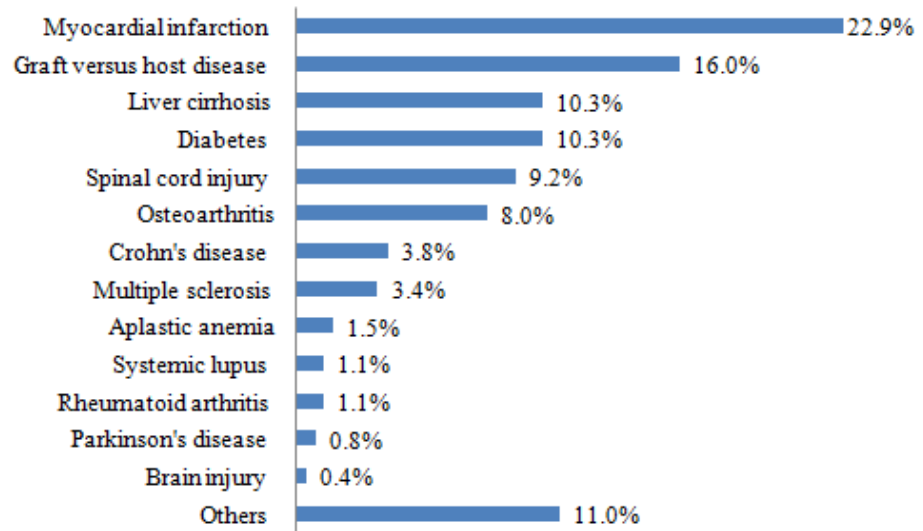


Figure 2.3 Mesenchymal stem cell-based therapy in common immune and non-immune diseases. (Figure modified from Wei et al., 2013)

T cells and natural killer cells, and inhibit the activation and maturation of dendritic cells. Moreover, MSCs interfere with different immune responses by direct cell-cell interactions and production of soluble factors to prevent the antigen presentation process, to reduce antibody production by B cells and secretion of cytokines by T cells and natural killer cells (De Miguel et al., 2012; Mundra et al., 2013; Kim and Cho, 2013). The therapeutic effects of MSCs are dependent on the nature and distinct microenvironment of different diseases (Kim and Cho, 2013). Further understanding on the underlying mechanisms of MSC homing effects, growth factor production and immune modulation is important to advance the application and efficacy of MSC-based cell therapy.

Although MSCs possess great therapeutic potentials in cell-based therapy, the difficulty in obtaining sufficient number of viable MSCs from the donor tissue has limited the application (Ullah et al., 2015). In order to yield adequate MSCs prior to transplantation, *in vitro* cell expansion is necessary. However, upon sub-culturing, MSCs lose their potency and display senescence phenotypes. It has been reported that during long-term *in vitro* culture, MSCs derived from adipose tissues or bone marrow demonstrated increased population doubling time, morphological changes and declined differentiation potentials and telomerase activities (Bonab et al., 2006; Alt et al., 2012). Another study demonstrated that during prolong *in vitro* culture, supplementation with essential serum and growth factors increased the probability of malignant transformation in MSCs (Røslund et al., 2009; Chen et al., 2014).

There are also growing evidences that age of the donors is associated with reduced efficiency of MSC-based cell therapy (Wei et al., 2013). During ageing, changes in systemic and local niches within tissues accumulate genetic and epigenetic damages that slowly impair MSCs functions (Duscher et al., 2014; Castorina et al., 2015). Previous studies have compared between human adipose tissue-derived MSCs (hAMSCs) from young and old donors. It was observed that hAMSCs from younger donors showed greater proliferation rate and higher growth factors production. On the other hand, hAMSCs from older donors displayed senescent features, as indicated by increased expression levels of p16, p21 and p53 senescence markers, senescence associated β -galactosidase staining and population doubling time, accompanied by granular, flatter and larger morphology (Stolzing et al., 2008; Khan et al., 2009; Alt et al., 2012). MSCs that are expanded *in vitro*, or isolated from elderly subjects, have shown reduction in stemness properties, which could affect the efficacy of regenerative MSC-based cell therapy. To date, studies on the MSCs self-renewal mechanisms and optimum *in vitro* culture microenvironment are actively being pursued with the goal of preserving the multipotency of MSCs (Ullah et al., 2015).

2.1.3 Wharton's Jelly-derived Mesenchymal Stem Cells (WJ-MSCs) in Human Umbilical Cord (hUC)

In recent years, researches have focused on utilising human umbilical cord (hUC) as the new source of MSCs in stem cell therapy. hUC is a tube-like elastic structure that connects the foetus to the mother's placenta during

prenatal development. MSCs are found in regions of the hUC, including the amniotic compartment (inner subamnion and outer amnion layer), the adventitia compartment of the walls of vessels, the perivascular compartment surrounding the vessels, the endothelial compartment, the umbilical cord blood and the Wharton's Jelly (WJ) compartment (Figure 2.4). hUC that is discarded after child birth is considered a biological waste, thus the collection and use of hUC do not have ethical issues as for embryonic stem cells (Can and Karahuseyinoglu, 2007; Jeschke et al., 2011).

As compared to other sources, high MSCs population is found in the WJ portion of an umbilical cord, which is the mucous proteoglycan-rich matrix that is embedded between the umbilical vessels and the amniotic epithelium. During pregnancy, WJ functions to prevent the compression, bending and torsion of the vessels, and provides bidirectional blood circulation between the foetus and the mother (Can and Karahuseyinoglu, 2007; Wang et al., 2016). MSCs isolated from WJ (WJ-MSCs) are maintained in an early embryological state, thus retaining primitive stemness properties and greater differentiation potentials than MSCs collected from the perivascular, subendothelial and umbilical cord lining compartments (Conconi et al., 2011).

WJ-MSCs are able to tolerate immune responses through the expression of placental HLA-G proteins that reduce cytolytic killing by cytotoxic T and natural killer cells, and enhance the production of

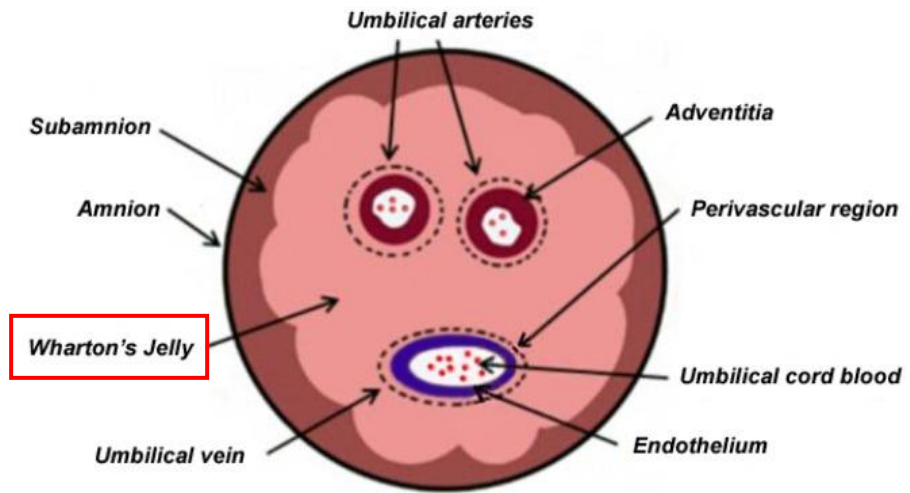


Figure 2.4 Cross-sectional diagram of human umbilical cord (hUC). The red box indicated the focus of this study. (Figure adapted from Kim et al., 2013)

immunosuppressive cytokines (Hunt et al., 2006; Batsali et al., 2013). Immuno co-stimulatory ligands, CD80 and CD86, that are essential to induce T cell activation and survival, are also absent in WJ-MSCs (Racz et al., 2014). The expression of placental HLA-G protein and the lack of co-stimulatory molecules reduce the immunogenicity of WJ-MSCs, making WJ-MSCs a prominent source for cell therapy, and possibly lower the chance of cellular rejection. WJ-MSCs hence also been shown to attenuate tumour growth *in vitro* and *in vivo* (Tamura et al., 2011). Although the mechanisms are not well understand, it was shown that WJ-MSCs reduced the tumour weight in human prostate and breast cancer cells by activating intrinsic apoptosis and inducing G2-phase arrest of the cell cycle (Ayuzawa et al., 2009; Han et al., 2014). WJ-MSCs also enhance the secretion of tumour suppressing proteins, thus improving the immune response against cancerous cells (Tamura et al., 2011; Watson et al., 2015).

Umbilical cord WJ has become the new MSC source in clinical applications, because WJ-MSCs can be harvested in abundance, show greater proliferation and differentiation capacity, low immunogenicity and tumour cells destruction potential. However, standard procedures for WJ-MSCs isolation is required to avoid MSCs heterogenicity and contamination (Jeschke et al., 2011).

2.2 Ageing

Ageing is a time-dependent life process in which organisms experience decline in cellular regeneration ability, imbalance in tissue homeostasis and compromised physiological functions. Stem cell ageing reduces the self-renewal, multipotency and regenerative capacities, leading to onset of age-associated diseases, and ultimately death. Nine cellular and molecular hallmarks that have been anticipated to contribute to ageing, are categorised into three groups, namely primary, antagonistic and integrative hallmarks of ageing (Figure 2.5) (López-otín et al., 2013; Yun, 2015).

The primary hallmarks are referred as the causes of damages which influence the cells negatively by inducing DNA damages and mutations, telomere shortening, epigenetic drift and proteostasis defects. In response to different intensities of the damages, antagonistic hallmarks provoke diverse effects, either beneficial or destructive to the cells. For instance, cellular senescence prevents tumorigenesis, but accumulation of senescent cells promotes ageing. Reactive oxygen species (ROS) is essential for cell signalling pathways, but high levels of ROS induce cellular damages. Likewise, excessive nutrient sensing and anabolism are pathological. Primary hallmarks accumulate with time and partly accelerates the onset of antagonistic, and finally integrative hallmarks, which deteriorate stem cells and intercellular communication and directly affect tissue homeostasis and functions (López-otín et al., 2013; Fukada et al., 2014). The three hallmarks are interconnected and can occur concurrently.

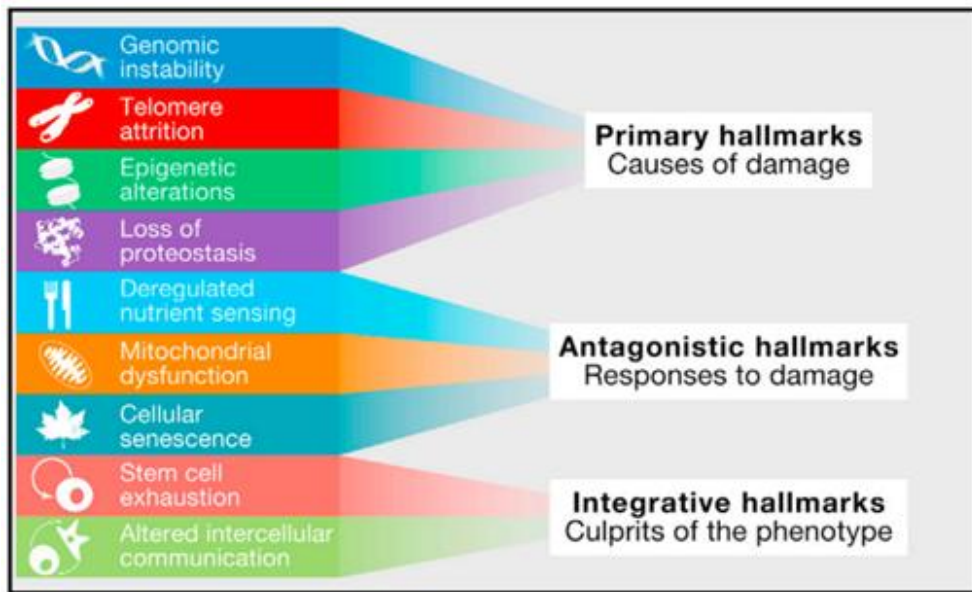


Figure 2.5 The hallmarks of ageing. The hallmarks are categorised into three groups: the primary, antagonistic and integrative hallmarks. (Figure adapted from López-otín et al., 2013)

2.2.1 Cellular Replicative Senescence (RS) and Stress-induced Premature Senescence (SIPS)

Cellular or replicative senescence (RS) was first described by Hayflick in human fibroblasts when the cells showed limited replicative lifespan in culture (Hayflick and Moorhead, 1961). Cellular senescence is an essential process whereby the cells enter a state of irreversible proliferation arrest, and no stimuli have been identified that can trigger RS cells to re-enter the cell cycle (Kuilman et al., 2010). Senescent cells are still metabolically active and experience phenotypic changes, including the activation of lysosomes and senescence associated β -galactosidase (SA- β -gal) activity (Dimri et al., 1995), up-regulation of senescence biomarkers such as p16, p21 and p53, nuclear and heterochromatin rearrangement, and increased production of secretory molecules like growth factors, proinflammatory cytokines and chemokines (Gu et al., 2016).

A major factor that contributes to the onset of replicative senescence both *in vitro* and *in vivo*, is the shortening of the telomere, a DNA protein structure with the repetitive non-coding DNA sequence TTAGGG that functions to protect the degradation of chromosome ends during DNA replication. Telomerase is an RNA-dependent DNA polymerase that inserts the telomeric DNA repeats to the telomeres. However, telomerase enzymes are only present in embryonic stem cells, some adult stem cells, cancer cells and a few somatic cells (Cong et al., 2002; Campisi, 2013). Thus, repeated cell division in somatic and stem cells with dysfunctional telomerase activity

results in the activation of p16/pRb and p53/p21 tumour suppressor pathways and eventually cell cycle arrest (see Section 2.2.3).

When cells are exposed to chronic stress or repeatedly sublethal intensity of stress, such as oxidative stress, UV light, oncogene activation and DNA damages, the onset of cellular senescence is accelerated. This type of senescence is known as stress-induced premature senescence (SIPS) (Toussaint et al., 2000). SIPS and RS cells share similar cellular and molecular senescence phenotypes, including flattened and enlarged morphology, irreversible growth arrest, increase SA- β -gal activity and activation of DNA damage checkpoint pathways. However, unlike RS, SIPS is independent of telomere shortening and function, but is a biological response against irreparable internal and external stresses. Hence, even cells with functional telomerase enzymes can undergo SIPS on exposure to stresses (Toussaint et al., 2000; Suzuki and Boothman, 2008; Raghuram and Mishra, 2014; Minieri et al., 2015).

2.2.2 Reactive Oxygen Species (ROS) and Free Radical Theory of Aging

There are multiple factors that can lead to cellular senescence and SIPS, but our focus here is the free radical theory of aging, which explains on the accumulation of reactive oxygen species (ROS) causes DNA damages and triggered senescence in stem cells (Harman, 2006). Unstable free radicals have unpaired electrons which include ROS that comprises of superoxide anion (O_2^-), nitric oxide (NO^-), hydroxyl radical (OH^-) and hydrogen peroxide

(H₂O₂). Under physiological conditions, low levels of ROS are produced by mitochondria as byproducts of metabolic processes, which can be removed by antioxidants such as glutathione peroxidase and catalase, or converted into toxic hydroxyl radicals (Pervaiz et al., 2009).

At low levels, ROS is an important cell signalling molecule in mediating proliferation and differentiation in MSCs (Kanda et al., 2011; Gauron et al., 2013). However, physiological ageing and exposure to external stresses such as chemicals, radiation and UV light lead to accumulation of ROS in stem cells, increasing the risk of oxidative damage. Oxidative stress occurs when there is an imbalance between ROS and the antioxidants levels, in which the antioxidants fail to remove the excessive ROS. Oxidative stress also causes damages to macromolecules, including lipid peroxidation, single- and double-strand DNA breaks, DNA adducts and crosslinks formation, and telomere shortening, which in turn induces cell cycle arrest, accompanied by morphological and functional changes (Hekimi et al., 2011; Chaudhari et al., 2014; Jeong and Cho, 2015). Prolonged exposure to ROS also correlated to cellular transformation of diseases, including diabetes, neurodegeneration and tumorigenesis (Pan et al., 2009).

2.2.3 Cellular Senescence and Cell Cycle Arrest

In response to oxidative stress and telomere shortening in stem cells, DNA damage response (DDR) is activated to initiate cell cycle arrest and to repair the DNA damages. When oxidative stress induces DNA single- and

double-strand breaks, DNA damage checkpoint protein kinases, ataxia telangiectasia mutated (ATM) and ATM-Rad3-related (ATR), are recruited and activated at the damage sites, followed by phosphorylation of the histone H2A histone-variant (H2AX). H2AX is important for further recruitment and activation of DNA-checkpoint proteins that control cell cycle progression and DNA repair. When the activities of ATM and ATR exceed the threshold, checkpoint kinase CHK2 and CHK1 are stimulated respectively, leading to phosphorylation of tumour suppressor protein p53. Activated p53 induces the expression of cyclin-dependent kinase (CDK) inhibitor p21, which in turn initiates cell cycle arrest at the G1-phase for DNA repair purpose (Insinga et al., 2014; Olivieri et al., 2015). If the DDR repair mechanisms fail to maintain the DNA integrity due to extensive damages, the cells are forced to enter permanent cell cycle arrest, and eventually cellular senescence (Zou, 2007). As dysfunctional telomeres are irreparable, particularly in somatic cells, persistent activation of the DDR pathway and the p53 protein enhances the onset of senescence (Lombard et al., 2005).

Senescence in stem cells can result in decrease proliferative and regenerative capacities, loss of stem cell pool, premature differentiation and tissue degeneration (Nelson et al., 2012; Acosta et al., 2013). Although detailed mechanisms that affect the stem cell functions are still unclear, it is known that the p16/pRb and p19/p53/p21 tumour suppressor pathways negatively regulate stem cells by initiating cell cycle arrest, apoptosis and senescence. Another CDK inhibitor, p16 has been shown to enhance ageing by reducing the regenerative capacity in liver, muscle and brain cells

(Krishnamurthy et al., 2006; Molofsky et al., 2006). p19 that regulates and stabilises p53 is still not well understood, but high levels of p53 was reported previously to enhance ageing and causes stem cell death (Dumble et al., 2007; Lee et al., 2010). Both p16/pRb and p19/p53/p21 pathways cross-regulate each other to regulate cellular senescence. As a downstream effector of p53, p21 hinders the activation of cyclin-CDK4/6 and CCNE-CDK2 complexes during onset of senescence. At the same time, p16 inhibits the CCND1-CDK4/6 complex and phosphorylation of pRb. Inactive pRb binds tightly to the elongation 2 promoter binding factor (E2F), thus inhibiting G1/S-phase progression (Insinga et al., 2014; Raghuram and Mishra, 2014). An overview on the activation of DDR, p16/pRb and p19/p53/p21 pathways by oxidative stress, leading to cell cycle arrest and senescence is illustrated in Figure 2.6.

Cellular senescence prevents uncontrolled proliferation of damaged cells by initiating cell cycle arrest, thus maintaining tissue homeostasis and avoids tumorigenesis. However, persistent and irreparable damages lead to accumulation of senescence cells, and cause stem cell dysfunctions, contributing to ageing (López-otín et al., 2013).

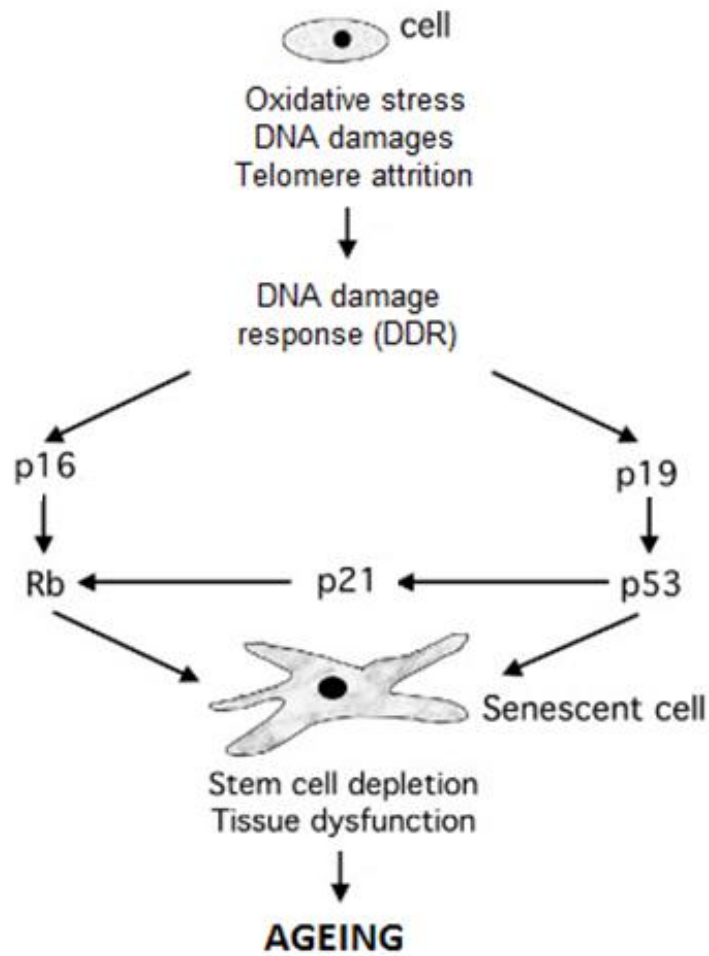


Figure 2.6 Damaged cells enter cellular senescence via DDR, p16/pRb and p19/p53/p21 pathways, and eventually promote ageing. When cells are exposed to oxidative stress, DNA damages and telomere attrition, DDR, p16/pRb and p19/p53/p21 mechanism are activated. Persistent activation of the mechanisms by unrepaired damages eventually causes cell cycle arrest and senescence. Progressive deterioration of tissue maintenance and stem cell pool eventually promote the ageing. (Figure modified from Lombard et al., 2005)

2.3 **microRNAs (miRNAs)**

microRNAs (miRNAs) are short endogenous non-coding RNAs that negatively regulate gene expression at the post-transcriptional level. miRNAs are encoded within the genome and are transcribed as long primary transcripts (pri-miRNAs) in the nucleus. Before being transported into the cytoplasm, the pri-miRNAs are processed into stem-loop precursor miRNAs (pre-miRNAs) by Drosha ribonuclease-III. Dicer ribonuclease-III then cleaves the pre-miRNAs to produce single-stranded mature miRNAs with approximately 18 to 24 nucleotides. The mature miRNA is incorporated into the RNA-induced silencing complex which in turn recognises the 3'-untranslated region (3'-UTR) of the target mRNAs through complementary base-pairing and results in mRNA degradation or translational repression (Kim, 2005).

The specificity of the miRNA targeting is dependent on the 6 to 11 nucleotides seed sequence at the miRNA 5'-end, enabling each miRNA to target hundreds of mRNAs, or a single mRNA may be targeted by different miRNAs (Bartel, 2009). Approximately 1,000 human miRNAs have been identified and predicted to regulate more than 50% of total cellular proteins in the gene regulatory network. However, the targets of most of the miRNAs are yet to be determined as experimental validation of miRNA-mRNA interactions is costly and time-consuming (Park and Kim, 2013). Although the biological roles of many miRNAs are still unknown, miRNAs are now believed to regulate diverse cellular functions, including cell proliferation (Lenkala et al., 2014), stem cell renewal and differentiation (Melton and

Blelloch, 2010), senescence (Faraonio et al., 2012), apoptosis and cancer (Lynam-Lennon et al., 2009).

2.3.1 microRNA Regulation of G1/S-phase of the Cell Cycle During Senescence

Several miRNAs have been shown to regulate the p53/p21 and pRb cell cycle pathways to induce onset of cellular senescence (Wagner et al., 2008; Lynam-Lennon et al., 2009). In response to stresses, the miR-15a/16-1 cluster, that comprises of mature miR-15a and miR-16 from the miR-15 family, triggers cell cycle arrest at the G1/S-transition by negatively regulating cell cycle factors such as CDK1,CDK2 and CDK6, CCND1/D3/E1 and E2F (Aqeilan et al., 2010; Ivey et al., 2010). Meantime, other miRNAs also mediate the expression of factors of the p53/p21 and pRb pathways. A positive feedback loop between miR-34a, sirtuin 1 (SIRT1) and p53 was observed, in which the activation of p53 enhanced the expression of miR-34a, and miR-34a in turn targeted and inhibited SIRT1, thus preventing SIRT1-mediated degradation of p53 activity (Yamakuchi and Lowenstein, 2009; Christoffersen et al., 2010). miR-34a also was shown to down-regulate the E2F transcription factor in human colon cancer cells, leading to cell proliferation suppression and senescence induction (Tazawa et al., 2007).

The E2F transcription factors are important regulators for cells progression into the S-phase of the cell cycle for DNA synthesis and mitosis purposes. Recent studies have discovered an auto-regulatory feedback loop

between miR-17-5p and miR-20a, both members of the miR-17/92 cluster, and E2F factors. It was observed that E2F factors bind directly to the miR-17/92 cluster, and concurrently the miRNA cluster can inhibit E2F expression to prevent irregular accumulation of the E2F factors. The miR-15a/16-1 and miR-17/92 miRNA clusters are not directly involved in the E2F-directed S-phase entry, but only inhibited expression of the cell cycle genes and the E2F targets, thus preventing replicative stress (O'Donnell et al., 2005; Sylvestre et al., 2007; Pickering et al., 2009). Interestingly, it was observed in proliferating cells that miR-369-3 and let-7 family members inhibited the translation process, but these miRNAs were shown to enhance translation in quiescent cells, suggesting that whether the miRNAs function to induce or repress translation is dependent on different stages in the cell cycle (Vasudevan et al., 2007). More supporting evidences are needed to further understand the interactions between miRNAs and cell cycle control in proliferation and cellular senescence via the p53/p21-pRb pathways.

CHAPTER 3

MATERIALS AND METHODS

3.1 Cell Lines

Wharton's Jelly derived-mesenchymal stem cell lines WJ0619, WJ0706 and WJ2000 at early passages were supplied by Cryocord Sdn. Bhd, Selangor, Malaysia (<http://www.cryocord.com.my>). All WJ-MSCs were isolated from foetal cord blood under informed consent and the MSCs phenotype was confirmed at Cryocord according to standard protocols (Leow et al., 2015). Human colorectal adenocarcinoma cell line HCT-15 was obtained from American Type Culture Collection (ATCC, Manassas, VA, USA).

3.2 Cell Culture

Cell culture was performed in an Airstream Class II Biological Safety Cabinet (ESCO, Singapore) under aseptic environment. All cells were maintained in a 37 °C cell culture incubator (ESCO) supplied with 5% CO₂. Disposable 6-cm and 10-cm cell culture dishes (BD Biosciences, New Jersey, USA), 6-well, 24-well and 96-well plates (SPL Life Sciences, Gyeonggi-do, South Korea), 5-mL and 10-mL serological pipettes (SPL Life Sciences) and 15-mL and 50-mL conical centrifuge tubes (BD Biosciences) were used for

cell culture work. Media bottles and pipette tips were sterilised at 121 °C for 15 min at the pressure of 975 kPa before use. An inverted phase contrast light microscope (Nikon, Tokyo, Japan) was used to examine the cultured cells and to capture cell images.

3.2.1 Preparation of Cell Culture Media

Dulbecco's Modified Eagle Medium (DMEM)/F12 and DMEM/high glucose (GIBCO, California, USA) were prepared according to the manufacturer's instruction. DMEM/F12 or DMEM/high glucose powder was dissolved with 1.2 g or 3.7 g sodium bicarbonate (Merck KGaA, Darmstadt, Germany), respectively, in 900 mL nuclease-free ddH₂O by constant stirring. The pH of the medium was then adjusted to pH 7.2 – pH 7.4 topped up with ddH₂O to one litre. The medium was filter sterilised with a 0.2-µm cellulose acetate membrane filter unit (Techno Plastic Product, Trasadingen, Switzerland) using a vacuum pump system (GAST, Michigan, USA). For preparation of the complete culture medium, 10% (v/v) foetal bovine serum (FBS, GIBCO) and 1% 100 units/mL penicillin (GIBCO) were added to the filter-sterilised medium. All media were kept at 4 °C for storage.

3.2.2 Cell Revival from Liquid Nitrogen Frozen Stock

A cryo-vial of frozen cells was retrieved from the liquid nitrogen tank and positioned in a 37 °C water bath until the cells thawed. The cell suspension was then transferred to a sterile 15-mL centrifuge tube, mixed with

9 ml pre-warmed complete culture medium, and centrifuged at 1,000 rpm for 3 min in a benchtop centrifuge machine (Allegra® X-15R, Beckman Coulter, California, USA). The supernatant was discarded and the pellet was re-suspended in 1 mL complete culture medium. The cell suspension was then transferred into a 10-cm culture dish and was maintained at 37 °C, 5% CO₂ in the cell culture incubator. The next day, the medium was replaced with fresh complete medium.

3.2.3 Cell Culture Maintenance and Sub-culturing

WJ-MSC cells were cultured in DMEM/F12 medium and HCT-15 cells were maintained in DMEM/high glucose medium in a 37 °C cell culture incubator with 5% CO₂. Culture medium was replaced every two to three days. Sub-culturing of cells was performed when the cells reached 80-90% confluency. Initial culture medium was removed and the cells were washed twice with 1X PBS, pH 7.4 (Amresco, Ohio, USA) to remove all trace of serum which inhibited trypsin activity. One mL 0.25% Trypsin-EDTA solution (GIBCO) was then added and the dish was incubated at 37 °C to disperse the cells. After five minutes of incubation, the cells were inspected under an inverted phase contrast microscope to ensure all cells were completely detached. Two mL serum-containing culture medium was added to inactivate trypsin activity. The cell suspension was gently transferred into a new sterile 15-mL centrifuge tube and centrifuged at 1,500 rpm for 5 min. Following centrifugation, the supernatant was discarded and the pellet was re-suspended in 1 mL culture medium. The cells were diluted with 0.4% (w/v)

trypan blue solution (MP Biomedicals, California, USA) and total cell number was determined using a hemocytometer (Hirschmann, Eberstadt, Germany). Cell concentration was determined by the formula:

$$\text{Cell number per mL} = (\text{the average counted cells}) \times (\text{dilution factor}) \\ \times (10^4)$$

The cell suspension was then diluted to a cell seeding ratio of 1:4 onto new flasks.

3.2.4 Cryopreservation of Cultured Cell

Cells at early passages were trypsinised following the protocols described in Section 3.2.3. The cells were pelleted by centrifugation at 1,500 rpm for 5 min. The supernatant was removed and the cells were re-suspended in a mixture containing 90% (v/v) FBS and 10% (v/v) dimethyl sulfoxide (Sigma-Aldrich, Missouri, USA). Aliquots of the cell suspension were transferred into sterile cryovials (Corning, New York, USA) and stored overnight at -80 °C. The next day, the cryovials were transferred into a liquid nitrogen container (Chart Industries, Ohio, USA) at approximately -180 °C for long-term storage.

3.2.5 Hydrogen Peroxide (H₂O₂) Treatment of WJ-MSCs

WJ-MSCs at early passages 6 - 10 were seeded at a cell density of 5,000 cells/cm² upon 70-80% confluency. Dose-response test was carried out in WJ0706 line with media containing different concentrations of hydrogen peroxide (H₂O₂) (Calbiochem, Merck Millipore, Massachusetts, USA) at 200 μM, 400 μM or 600 μM. After 2 h incubation, the treated cells were replaced with fresh complete cell culture medium for cell recovery. Cumulative Population Doubling (CPD) was calculated with the formula (Schellenberg et al., 2011):

$$PD_i = \log_2 (h_i / s_i)$$

$$CPD = \sum_{i=1}^n PD_i$$

n = total number of passages

s_i = number of cells seeded at passage *i*

h_i = number of cells harvested at passage *i*

For subsequent experiments, WJ-MSC lines were treated with 200 μM H₂O₂ in complete cell culture medium for 2 h. Upon reaching confluency, untreated control MSCs were re-plated at a density of 5,000 cells/cm² while H₂O₂-treated cells were split at 2,000 cells/cm². Cell count was done with a Neubauer counting chamber.

In the time-course experiments to assess the H₂O₂ repression of miRNA expression, WJ0706 line was treated with 200 μM H₂O₂ for different duration, followed by cell recovery for 24 h before RNA preparation. In the

miRNA stability test, the H₂O₂-treated cells were cultured in complete medium for different time points before being harvested for RNA preparation.

3.3 Senescence Associated β -galactosidase (SA- β -gal) Staining

The positive blue staining of senescence associated β -galactosidase (SA- β -gal) was used as a biomarker of cellular senescence. For assessment of SA- β -gal activity, the cells were washed with 1X PBS and stained with the Cellular Senescence Assay Kit (Cell Biolabs Inc., San Diego, USA) according to the manufacturer's protocols. Stained cells were incubated overnight at 37 °C and the expression of SA- β -gal activity in untreated controls and H₂O₂-treated WJ-MSC lines was examined under a phase contrast microscope (Nikon) on the following day. At the suboptimal pH 6.0, lysosomal SA- β -gal activities only increased in senescent cells and are not detected in pre-senescent or immortal cells. The assay was done in sub-confluent cultures displaying comparable cell density to avoid false-positive staining in serum starvation or confluence cell population rather than to proliferative senescence.

3.4 Cell Cycle Analysis

Untreated controls and H₂O₂-treated WJ-MSCs were harvested by trypsinisation, washed with 1X PBS and fixed overnight with 70% iced cold ethanol at -20 °C. After fixation, the cells were treated with 100 μ g/mL

RNase A (Thermo Fisher Scientific) and stained with 10 µg/mL propidium iodide (Nacalai tesque, Kyoto, Japan) in dark for 30 min at 37 °C, followed by analysis on a FACS Canto-II analyzer (BD Biosciences). A total of 100,000 events were recorded for each sample. DNA distribution in different phases of the cell cycle was analysed using the ModFit LT™ software (BD Biosciences).

3.5 RNA Preparation

3.5.1 RNA Isolation

Total RNA was isolated from cells using the TRIzol® reagent (Invitrogen, California, USA) according to manufacturer's guidelines. Cells were harvested by trypsinisation and pelleted by centrifugation at 1,500 rpm for 5 min. The cell pellets were homogenised in 500 µL TRIzol® reagent and the homogenate was stood for 10 min at room temperature. Chloroform (Amresco) (100 µL) was added to the homogenate and vortex vigorously for 15 s, followed by incubation for 15 min at room temperature. The homogenate was then separated into three phases by centrifugation at 12,000 xg for 15 min at 4 °C. The upper transparent phase containing RNA was transferred into a new microcentrifuge tube, mixed with 250 µL of isopropanol (Merck KGaA) and stood for 10 min at room temperature. The mixture was centrifuged at 12,000 xg for 15 min at 4 °C and the supernatant was discarded. Ethanol (Merck KGaA) (75%, 500 µL) was added and centrifuged at 12,000 xg for 5 min at 4 °C. The supernatant was discarded and the pellet was air-dried for

5 min before eluted with 30 μ L RNase-free water. All centrifuge steps were carried out in a Herarus Merck Millipore 21 refrigerated microcentrifuge (Thermo Scientific, Illinois, USA). RNA was quantified and kept at -80 °C for future use.

3.5.2 RNA Quantification and Integrity Assessment

The concentrations of isolated total RNAs were determined by NanoPhotometer (Implen, Munich, Germany). The ratio of the readings at 260 nm and 280 nm (A_{260}/A_{280}) provides an estimation of RNA purity. A_{260}/A_{280} ratios of isolated RNAs with values within 1.8 – 2.0 were used for downstream miRNA profiling analysis and subsequent quantitative real-time reverse transcription PCR (qRT-PCR) assays.

RNA integrity was examined by agarose gel electrophoresis. An aliquot of isolated RNAs (200 ng) was mixed with 2 μ L of 6X loading dye (Thermo Fisher Scientific) and topped up with distilled water to a final volume of 10 μ L. The RNA mixtures were subjected to 1% agarose gel electrophoresis at 90 V for 45 min using 1X TBE running buffer (Vivantis, California, USA). The gel was pre-stained with 3X GelRed nucleic acid stain (Biotium, California, USA) and visualised by exposure to 302 nm UV light under BioSpectrum Imaging System (Ultra-Violet Products Ltd, California, USA). RNA preparation displaying bands of 28S and 18S ribosomal RNA (rRNA) with a ratio of approximately 2:1 were considered intact. RNAs that lacked the sharp ribosomal bands were discarded.

3.6 Determination of Messenger RNA (mRNA) Levels by qRT-PCR

3.6.1 Primers for mRNA qRT-PCR

To avoid amplification of non-specific sequences, primer pairs for GAPDH (Zhang et al., 2011), CCND1, CDK6, E2F1, GLB1, p16, p21, and p53 genes were designed using National Center for Biotechnology Information (NCBI) Primer-BLAST (Ye et al., 2012). In the mRNA qRT-PCR, all gene primers were tested using Basic Local Alignment Search Tool (BLAST) and global alignment algorithm to ensure that the primer sequences were specific and did not non-specifically match with other gene sequence published in the NCBI database. All primers (Table 3.1) were custom synthesised by First BASE Oligos (Singapore).

3.6.2 cDNA Synthesis by Reverse Transcription

Total RNA was reversed transcribed to synthesise cDNA by using the Phusion RT-PCR kit (Thermo Fisher Scientific) according to manufacturer's protocols. One μg total RNA was pre-denatured in a mixture of 0.25 mM dNTP and 100 ng oligo(dT) primer at 65 °C for 5 min. Then, 1X RT buffer, RT enzyme mix and RNase-free water were added to the mixture at a final volume of 20 μL . The reaction tube was briefly spun down and incubated in a 96-well Thermal Cycler (Takara, Shiga, Japan) at 25 °C for 10 min for primer extension, 40 °C for 30 min for cDNA synthesis and 85 °C for 5 min for termination of reaction.

Table 3.1 Primers used in mRNA qRT-PCR

Gene	Accession ¹	Primer sequence (5' – 3')	Amplicon size (bp)
CCND1	NM_053056	F: ACAAACAGATCATCCGCAAACAC R: TGTTGGGGCTCCTCAGGTTC	144
CDK6	NM_001259	F: CGGAAAGCCCTCTTGAAGCAAAGA R: CGTGGGAAAGGAGCAAGAGCAT	105
E2F1	NM_005225	F: GCCGCCATCCAGGAAAAGGTGTG R: CGGCAGCCCAGTTCAGGTCG	138
GLB1	NM_004985	F: CCTACATCTGTGCAGAGTGG R: TTCATCTTGGGCAGAAGGAC	139
p16	NM_002439	F: GAAGGTCCCTCAGACATCCCC R: CCCTGTAGGACCTTCGGTGAC	94
p21	NM_005215	F: GCCTGGACTGTTTTCTCTCG R: ATTCAGCATTGTGGGAGGAG	134
p53	NM_000875	F: CCCAAGCAATGGATGATTTGA R: GGCATTCTGGGAGCTTCATCT	91
GAPDH	NM_001256799	F: GAAATCCCATCACCATCTTCCAGG R: GAGCCCCAGCCTTCTCCATG	120

¹NCBI was used in data derivation. F: forward primer; R: reverse primer

3.6.3 mRNA qRT-PCR

After the reverse transcription process, cDNA was subjected to qRT-PCR using SYBR® Select Master Mix (Thermo Fisher Scientific) containing a mixture of AmpliTaq® DNA Polymerase, SYBR® GreenER™ fluorescent dye, heat-labile uracil-DNA glycosylase (UDG), dNTPs with dUTP/dTTP blend, ROX passive reference dye and optimised buffer components (Table 3.2). The targeted mRNA sequence was amplified using gene-specific forward and reverse primers (Table 3.1). A negative control was included in each assay by substituting cDNA with DEPC-treated water to ensure no contamination in the PCR reaction. The mixtures were incubated in a Rotor Gene Q cycler (Qiagen, California, USA) for UDG activation at 50 °C for 2 min, UDG inactivation and hot-start DNA polymerase activation at 95 °C for 10 min, followed by 40 amplification cycles of denaturing step at 95 °C for 15 seconds and primer annealing and extension step at 60 °C for 1 min. Melt-curve analysis was performed to determine the specificity and quality of amplified products by heating the PCR products from 60 °C to 95 °. All experiments were carried out in triplicates and were normalised to the C_t value of the housekeeping gene, GAPDH. Relative mRNA expression levels were calculated using the comparative C_t ($\Delta\Delta C_t$) method.

Table 3.2: mRNA qRT-PCR reaction mixture

PCR components	Volume per reaction	Final concentration /amount
2X SYBR GreenER qPCR SuperMix	10 μ L	1X
Forward primer (10 μ M)	0.2 μ L	100 nM
Reverse primer (10 μ M)	0.2 μ L	100 nM
cDNA template (10 ng/ μ L)	1 μ L	10 ng
DEPC-treated water	8.6 μ L	-
Total volume	20 μ L	

3.7 Global microRNA (miRNA) Expression Profiling Analysis

For miRNA profiling analysis, the 7th Gen. version of miRCURY LNA™ microRNA Arrays (Exiqon, Vedbaek, Denmark), which contain validated and T_m -normalised LNA™-based capture probes, were used. The arrays included 1,896 of the 1,921 annotated human miRNAs in the miRBase 18.0, and 25 proprietary miRPlus™ human miRNAs that were not yet annotated in the miRBase. The microarray analysis experiments were conducted at Exiqon Services, Denmark. The quality of the total RNA was first verified by an Agilent 2100 Bioanalyzer profile. Total RNAs (450 ng) from both the experimental samples and the references were labelled with Hy3™ or Hy5™ fluorescent labels, respectively, using the miRCURY LNA™ microRNA Hi-Power Labeling Kit, Hy3™/Hy5™ (Exiqon) following established protocol of the manufacturer. The Hy3™-labelled experimental and a Hy5™-labelled reference RNA samples were mixed pair-wise and hybridised to the miRCURY LNA™ microRNA Arrays using a Tecan HS4800™ hybridisation station (Tecan, Grödig, Austria). After hybridisation, the microarray slides were scanned and stored in an ozone-free atmosphere to prevent bleaching of the fluorescent dyes. The array slides were scanned using the Agilent G2565BA Microarray Scanner System (Agilent Technologies Inc., CA, USA) and image analysis was carried out using the ImaGene® 9 miRCURY LNA™ microRNA Array Analysis Software (Exiqon). The quantified signals were background-corrected (Normexp with offset value 10) (Ritchie et al., 2007) and normalised using the global LOcally WEighted

Scatterplot Smoothing (Lowess) regression algorithm. The arrays were done in four replicate spots.

3.8 miRNA qRT-PCR

3.8.1 miRNA Primers for qRT-PCR

For miRNA qRT-PCR, mature sequences of selected miRNAs were obtained from miRBase ver. 21 (www.mirbase.org) and synthesised as specific forward primers; the Universal qPCR Primer (Invitrogen) was used as the reverse primer. All primers (Table 3.3) were synthesised by First BASE Oligos (Singapore).

3.8.2 Polyadenylation and Reverse Transcription of miRNA

Total RNA containing miRNAs were reverse transcribed to cDNA using NCode™ miRNA First-Strand cDNA Synthesis Kit (Invitrogen) according to manufacturer's instructions, as outlined in Figure 3.1. Briefly, 1 µg total RNA was subjected to polyadenylation in a 20 µL reaction volume containing polyA polymerase, 100 µM ATP and 2.5 mM MnCl₂ in 1X miRNA Reaction Buffer and incubated for 15 min at 37 °C in 96-well Thermal Cycler (Takara). First strand cDNA was immediately reverse transcribed using the polyA-tailed RNA preparation. PolyA-tailed RNA (4 µL) was mixed with the Universal RT Primer and Annealing Buffer and was first incubated at 65 °C

Table 3.3: Primers used in miRNA qRT-PCR

miRNA	Accession¹	Forward primer sequence (5' – 3')
miR-146a-5p	MI0000477	GCGTGAGAACTGAATTCCATGGGTT
miR-146b-5p	MI0003129	GCGCTGAGAACTGAATTCCATAGGCT
miR-17-5p	MI0000071	GCCAAAGTGCTTACAGTGCAGGTAG
miR-20a-5p	MI0000076	GCGCTAAAGTGCTTATAGTGCAGGTAG
miR-20b-5p	MI0001519	GCGTAAAGTGCTCATAGTGCAGGTAG
miR-106a-5p	MI0000113	GCGAAAAGTGCTTACAGTGCAGGTAG
RNU6	X07425	F: CTCGCTTCGGCAGCACA R: AACGCTTCACGAATTTGCGT

¹miRBase version 20 was used in data derivation. F: forward primer; R: reverse primer

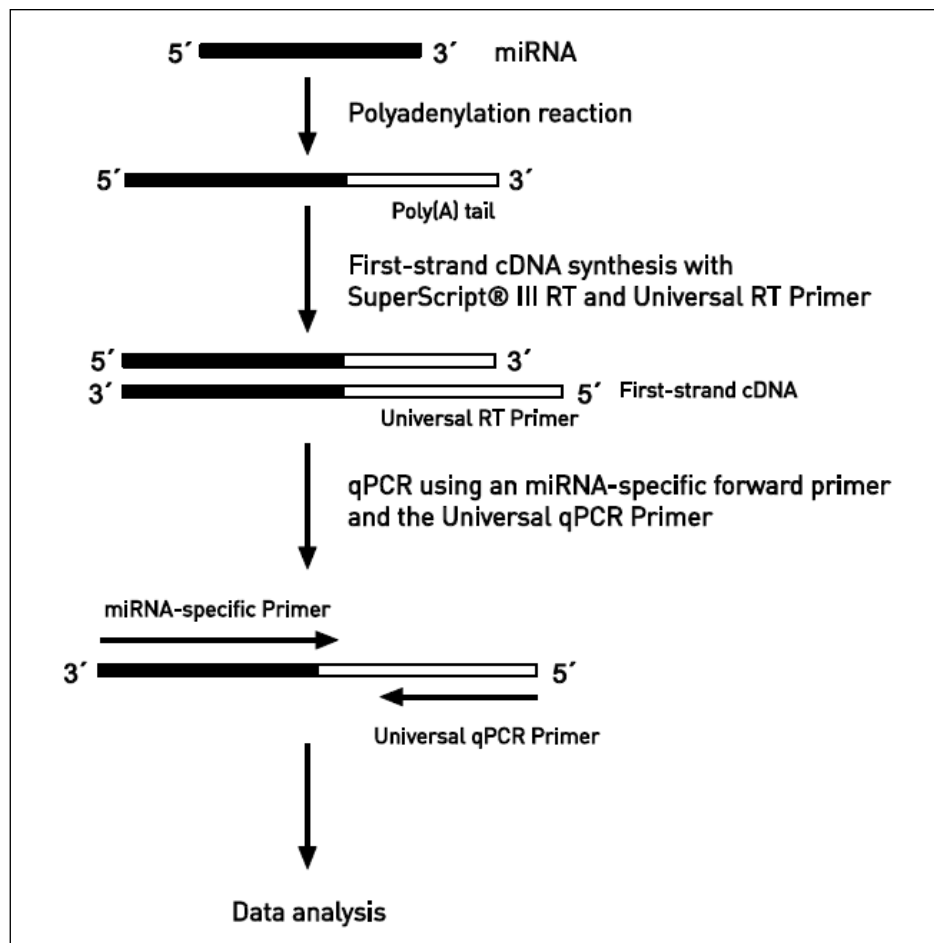


Figure 3.1: Workflow of miRNA qRT-PCR. (Invitrogen, USA)

for 5 min, followed by addition of 1X First-Strand Reaction Mix and SuperScript III Reverse Transcriptase/RNaseOUT Enzyme Mix to the mixture and incubation at 50 °C for 50 min, and 85 °C for 5 min in 96-well Thermal Cycler (Takara).

3.8.3 miRNA qRT-PCR

Synthesised cDNA was subjected to qRT-PCR using SYBR®_Select Master Mix (Thermo Fisher Scientific) in the presence of a specific forward primer designed (Table 3.3) and the Universal qPCR primer (Invitrogen) (Table 3.4). Negative controls were included in the assay by substituting cDNA with DEPC-treated water to ensure no contaminant was detected in the PCR reactions. The miRNA qRT-PCR conditions were as the mRNA qRT-PCR condition described in Section 3.6.3. All experiments were carried out in triplicates and were normalised to the data of the internal control, the small nuclear RNA U6. Relative miRNA expression levels were calculated using the comparative C_t ($\Delta\Delta C_t$) method.

3.9 Transfection of Synthetic miRNA

Early or late passage replicative senescence WJ0706 cells were seeded in a 6-well plate at a cell density of 7.5×10^4 per well. After 24 h, 25 nM or 50 nM of miRNA mimics or a validated nonspecific mimic negative control (Ambion, Thermo Fisher Scientific), respectively, was diluted in 100 μ L Opti-

Table 3.4: miRNA qRT-PCR reaction mixture

PCR components	Volume per reaction	Final concentration /amount
2X SYBR GreenER qPCR SuperMix	10 μ L	1X
Forward primer (10 μ M)	0.2 μ L	100 nM
Universal qPCR primer (10 μ M)	0.2 μ L	100 nM
cDNA template (10 ng/ μ L)	1 μ L	10 ng
DEPC-treated water	8.6 μ L	-
Total volume	20 μ L	

MEM medium (Gibco); 2.5 μ L Lipofectamine 2000 (Invitrogen) was also diluted in 100 μ L Opti-MEM medium (Gibco). Both diluted synthetic miRNAs and Lipofectamine 2000 were mixed and incubated for 15 min at room temperature. The synthetic miRNA-lipofectamine complex was then added to the cells and incubated in a 37 °C cell culture incubator for 24 h. At 24 h post-transfection, the medium was changed to fresh DMEM/F12 medium; 48 h post transfection, the cells were trypsinised for RNA preparation, cell cycle analysis and cell proliferation assays.

3.10 Cell Proliferation Analysis

3.10.1 Cell Growth Analysis

Early passage WJ0706 cells were transfected for 48 h as described in Section 3.9, followed by treatment with 200 μ M H₂O₂ for 2 h. Subsequently, the cells were cultured in fresh medium for 24 h to allow cell recovery. For late-passage (P23) replicative senescence WJ0706 cells, the cells were miRNA-transfected for 48 h. The H₂O₂-treated OSIPS and the replicative senescence WJ0706 cells were later reseeded at a density of 1×10^4 cells in a 12-well plate, followed by total cell count every second day using a hemocytometer (Hirschmann). The growth curve presented was from three independent experiments.

3.10.2 *In vitro* Cell Viability Assay by MTT

Effects of miRNA transfection on cell growth was determined by MTT [3-(4,5-dimethylthiazolyl-2)-2,5-diphenyltetrazolium bromide] assays (Sigma-Aldrich). After transfection with synthetic miRNAs (Section 3.9) for 48 h, cells were trypsinised and were seeded at a density of 1×10^4 cells in a 24-well plate in a final volume of 500 μ l/well. After 24 h incubation, 50 μ L 5 mg/mL MTT was added to each well and the plates were incubated for 2.5 h at 37 °C. Medium was subsequently replaced with 0.2 mL dimethyl sulfoxide (Sigma-Aldrich) per well followed by measurements in a Infinite M200 PRO Microplate Reader in triplicates (Tecan, Männedorf, Switzerland) at 570 nm. The MTT assays were performed in three independent biological experiments.

3.10.3 BrdU Cell Proliferation Assay

To determine DNA synthesis rates, 48 h post-miRNA transfection as stated in Section 3.9, cells were seeded at a density of 5×10^3 cells in a 96-well plate. 5-bromo-2'-deoxyuridine (BrdU) cell proliferation assay kit (Cell Signaling, Massachusetts, USA) was used to detect BrdU incorporation into newly synthesised DNA during cell proliferation. After 24 h, 1X BrdU solution was added to the medium and incubated at 37 °C for 2 h. Medium was then removed and 100 μ L fixing/denaturing solution was added and incubated at room temperature for 30 min. Antibody solution (100 μ L) was added and incubated for another hour. Washing step was carried out three times using 1X washing solution before incubation with 100 μ L of horseradish peroxidase

(HRP)-conjugated secondary antibody solution for 30 min. The treated cells were again washed with 1X washing solution before addition of 100 μ L tetramethylbenzidine substrate. After incubation for 30 min in the dark, 100 μ L STOP solution was added and the absorbance was measured at 450 nm in Infinite M200 PRO Microplate Reader (Tecan). All incubation steps were carried out at room temperature. The BrdU proliferation assay was performed in triplicates in three independent experiments.

3.11 Validation of miRNA Targeted Transcripts by Luciferase Assays

3.11.1 Transformation of Plasmid DNA

Recombinant plasmid constructs containing PCR products of full-length or segments of 3'-untranslated region (UTR) covering predicted miRNA binding sites of target genes were cloned into the dual luciferase (*Firefly/Renilla*) reporter vector pmirGLO using the restriction enzyme combination SacI/XbaI or Sall/XhoI (Table 3.5) (Trompeter et al., 2011). Transformation of plasmid DNA was carried out using One Shot® TOP10 Chemically Competent *E. coli* (Thermo Fisher Scientific). The competent cells were placed on ice for 10 to 15 min until the cells were completely thawed. Plasmid DNA (4 μ L) at approximately 50 ng was added directly to the cells and mixed by gentle stirring, immediately followed by incubation on ice for 30 min. The cells were heat shock for exactly 30 sec in a 42 °C water bath, and were immediately returned to ice for another 2 min. Room

Table 3.5 Primers used in cloning of 3'-UTR into vector pmirGLO

Gene (RE sites)	Accession¹	Primer sequence (5' – 3')	Amplicon size (bp)
RBL1 (<i>XhoI</i> , <i>SalI</i>)	NM_002895	F:GCATATCTCGAGTGTGTTCTTGTTCCTATGATAAAAGCACTTTC R:GCATATGTCGACTGATAATAGTTTACAAAAGAAGAAAGTGCCC	984
RBL2 (<i>SacI</i> , <i>XbaI</i>)	NM_005611	F:GCATATGAGCTCTGTGCAATGTCTGAGTGAACCTG R:GCATATTCTAGAACATTCCCAAAGGTGGCTATAGG	218
CCND1 (<i>SacI</i> , <i>XbaI</i>)	NM_053056	F:GCATATGAGCTCCCTGATAAAGCACAGCTGTAGTGG R:GCATATTCTAGACATGGATATTCCCAAACCATTCCATTAG	594
CCND2 (<i>SacI</i> , <i>XbaI</i>)	NM_001759	F:GCATATGAGCTCGGTGCTGATTGGCATGTCTGG R:GCATATTCTAGAGCTTCATTACCTGTCAATTACAATTGTGC	602
E2F1 (<i>SacI</i> , <i>XbaI</i>)	NM_005225	F:GCATATGAGCTCGTGAACATACACCTCTGTGTGTGC R:GCATATTCTAGAGACCTTTCTTCGAGTTATGAGGCTC	897

Table 3.5 continue

Gene (RE sites)	Accession ¹	Primer sequence (5' – 3')	Amplicon size (bp)
CDKN1A (<i>SacI</i> , <i>XbaI</i>)	NM_078467	F:GCATAT GAGCTC CTTTCTGGACTCAGACCTG R:GCATAT TCTAGACT CTACTGCCACCATCTTAAAATGTC	790

The primers were designed based on Trompeter et al., 2011. ¹NCBI was used in data derivation. In the primer sequences, nucleotide in bold indicate the sequences of the restriction enzymes. RE: restriction enzyme; F: forward primer; R: reverse primer

temperature recovery medium (250 μ L) was then added to the cells, and the mixture was incubated in a shaking incubator at 250 rpm for 1 h at 37 $^{\circ}$ C. After the incubation, 80 μ L transformed cells was plated on pre-warmed Luria Bertani (LB, Sigma-Aldrich) agar plate containing 100 μ g ampicillin (Amresco). The plates were incubated overnight at 37 $^{\circ}$ C for colony formation.

3.11.2 Plasmid DNA Extraction

Single-colonies of transformed cells were picked from the agar plate with a pipette tip and dropped in pre-warmed LB broth (Sigma-Aldrich) containing 100 μ g ampicillin (Amresco), and were incubated overnight at 37 $^{\circ}$ C with 250 rpm shaking. Plasmid DNA was purified using GeneJet Plasmid Miniprep Kit (Thermo Fisher Scientific). The bacterial culture was harvested by centrifugation at 8,000 rpm for 5 min in a Sorvall Legend centrifuge X1R machine (Thermo Fisher Scientific). The supernatant was removed and the pelleted bacterial cells were resuspended in 250 μ L resuspension solution until no cell clumps were observed. The cell suspension was transferred to a new microcentrifuge tube, added with 250 μ L lysis solution and immediately inverted four to six times until the solution became viscous and slightly clear. Next, 350 μ L neutralization solution was added to the bacterial lysate and mixed thoroughly until the lysate turned cloudy, followed by centrifugation at 12,000 rpm for 5 min in a Sigma 1-14 benchtop centrifuge machine (Sartorius Corporation, New York, USA). The supernatant was pipetted to a new GeneJET spin column and centrifuged at 12,000 rpm for 1 min. The flow-through was discarded and the column was returned to the

same collection tube. Washing step was carried out twice by adding 500 μ L wash solution to the spin column and centrifuged at 12,000 rpm for 60 sec. The flow-through was discarded and the column was centrifuged for additional 1 min to get rid of residual wash solution. The spin column was then placed on a new 1.5-mL microcentrifuge tube and 50 μ L elution buffer was added to the centre of the spin column membrane. The spin column was stood for 2 min at room temperature before centrifugation at 12,000 rpm for 60 sec to elute the plasmid DNA. The purified plasmid DNA was stored at -20 °C for future use.

3.11.3 Validation of Extracted Plasmid DNA

Purified plasmid DNA was subjected to restriction enzymes double digestion to confirm that the pmirGLO plasmid contained the full length or designated fragments of 3'-UTR of the target transcripts. Briefly, plasmid DNA at 250 ng was digested in a 0.2-mL microcentrifuge tube containing 0.5 μ L of each restriction enzyme (New England Biolabs, Massachusetts, USA), 1 μ L of 1X CutSmart buffer and topped up to a final volume of 10 μ L with DEPC-treated water (Table 3.5). The reaction mixture was mixed well and incubated in a 37 °C water bath for 2 h. Undigested pmirGLO plasmid was used as the control. Immediately after the digestion, the mixtures were subjected to 1% agarose gel electrophoresis at 90 V for 45 min using 1X TBE running buffer. The gel was pre-stained with 3X GelRed nucleic acid stain (Biotium) and visualised by exposure to 302 nm UV light under BioSpectrum Imaging System (Ultra-Violet Products Ltd).

3.11.4 Luciferase Reporter Assays

The Dual-Luciferase® Reporter Assay System (Promega, Wisconsin, USA) was used to identify the direct targeting of selected miRNAs. The colorectal cancer cell line HCT-15 was co-transfected in 24-well plates using 1 µL Lipofectamine 2000 (Invitrogen) with 200 ng empty pmirGLO or the pmirGLO/3'-UTR construct, and 10 µM miRNA mimic or a validated nonspecific negative control miRNA mimic (Ambion). Forty-eight hours post transfection, the medium was discarded and the cells were washed twice with 1X PBS before addition of 100 µL 1X Passive Lysis Buffer to the transfected cells and rocking at room temperature for 15 min. Cell lysate (20 µL) was then transferred to a 96-well plate predisposed with 100 µL Luciferase Assay Reagent II to measure the *Firefly* activity in a Infinite M200 PRO Microplate Reader (Tecan). After quantifying the *Firefly* luminescence, 100 µL Stop & Glo® Reagent was added simultaneously to the same well to initiate *Renilla* activity. The luciferase reporter assays were performed in two or more independent biological experiments each with transfection triplicates.

3.12 miRNA Target Prediction by Bioinformatics Analysis

Online web-based miRNA target prediction algorithms were used to identify miRNA putative targets and their biological functions in the regulatory network of transcription factor–miRNA–mRNA. The algorithms used included miRBase (www.mirbase.org), microT-CDs (<http://diana.imis.athena-innovation.gr>), TargetScan Release 6.2 (<http://www.targetscan.org/>), microRNA.org (www.microrna.org), miRTarBase (www.mirtarbase.mbc.nctu.edu.tw) and miRDB (www.mirdb.org).

3.13 Western Blot Analysis

3.13.1 Buffers and Reagents Preparation

Table 3.6 Preparation of western blot buffers

Buffer	Methods of preparation
10% (w/v) Sodium dodecyl sulphate (SDS) solution	A total of 10 g SDS (Omnipur, Merck KGaA) was dissolved in 90 mL distilled water. When dissolved, the volume was topped up to 100 mL with distilled water and stored at room temperature.
10% (w/v) Ammonium persulfate (APS)	A total of 0.1 g of APS (Merck KGaA) was dissolved in 1 mL distilled water. APS was prepared freshly as required.
1.5 M Tris, pH 8.8	A total of 18.15 g of Tris base (Norgen Biotek, Ontario, Canada) was dissolved in 60 mL distilled water and adjusted to pH 8.8 with 6 M HCl (Nacalai Tesque). The solution was topped up to 100 mL with distilled water and stored at 4 °C.
0.5 M Tris, pH 6.8	A total of 6 g of Tris base was dissolved in 60 mL of distilled water and adjusted to pH 6.8 with 6 M HCl. The solution was topped up to 100 mL with distilled water and stored at 4 °C.
SDS-PAGE running buffer (0.05 M Tris, 0.1% SDS, 0.384 M glycine)	A total of 12 g of Tris base, 57.6 g of Glycine (Merck KGaA) and 2 g of SDS were dissolved in 500 mL distilled water. The volume was made up to 2 L with distilled water and stored at room temperature.

Table 3.6 continue

Buffer	Methods of preparation
10X Tris-buffered saline (TBS) (1.5 M NaCl, 0.5 M Tris)	A total of 60.57 g of Tris base and 87.66 g of NaCl (Bio Basic Inc., Ontario, Canada) were dissolved in 500 mL distilled water. Then, it was adjusted to pH 7.5 with 6 M HCl. The volume was made up to 1 L with distilled water and stored at room temperature.
Washing buffer: 1X Tris-buffered saline with 0.05% Tween-20 (TBST)	To make 1X TBST, 100 mL of concentrated 10X TBS was diluted to 1X by adding 900 mL distilled water, and 500 µL Tween-20 (Omnipur, Merck KGaA) was added to the diluted TBS and mixed well.
Blocking buffer: washing buffer with 5% milk	A total of 2 g non-fat milk powder (Bio Basic Inc.) was dissolved in 40 mL of 1X TBST. It was prepared freshly as required.
1X Transfer buffer (25 mM Tris, 20% methanol, 192 mM glycine)	A total of 3.03 g of Tris base and 14.4 g of glycine were dissolved in 500 mL distilled water and the solution was then added with 200 mL of methanol (Merck KGaA, Germany). The volume was made up to 1 L with distilled water and stored at room temperature.
Mild stripping buffer	A total of 1.5 g of glycine, 0.1 g SDS and 1 mL Tween-20 were dissolved in 50 mL distilled water. The solution was adjusted to pH 2.2 with 6 M HCl. The volume was made up to 100 mL with distilled water and stored at room temperature.

3.13.2 Preparation of Cell Lysates and Quantification of Protein Lysates

Protein lysates were prepared from untreated and H₂O₂-treated cells by lysing the cells in RIPA Lysis Buffer (Nacalai Tesque) according to manufacturer's protocol. First, culture medium was removed from a 10-cm cell culture dish with 90% cell confluency (approximately 5 x 10⁶ cells) and the cells were washed twice with ice-cold 1X PBS. Then, 250 µL RIPA Lysis Buffer was added to the dish followed by scrapping of adherent cells with an ice-cold plastic cell scraper. The cell suspension was transferred to a pre-cold microcentrifuge tube and incubated on ice for 15 min, followed by centrifugation at 12,000 rpm for 15 min at 4 °C in a Herarus Fresco 21 refrigerated microcentrifuge (Thermo Scientific). The supernatant was collected into a new microcentrifuge tube and the cell pellet was discarded. All steps were performed on ice to prevent protein denaturation.

To standardise the protein amount loaded into the gel, protein quantification was performed using Quick Start Bradford Protein Assay (Bio-Rad, California, USA). A Protein Standard Curve was constructed based on serial dilution of concentrated bovine serum albumin (BSA), ranged from 125 to 2,000 µg/mL. Diluted protein standards (5 µL) and 5X diluted unknown samples were pipetted into a 96-wells microplate. Then, 250 µL 1X Dye Reagent (Bio-Rad) was added to each well, mixed and incubated in the dark for 15 min. The proteins in the microplate were then measured at absorbance of 595 nm in a Infinite M200 PRO Microplate Reader (Tecan). Every standard or sample was performed in triplicate. The concentration of the protein lysate

was calculated based on average absorbance reading of the protein lysates and the BSA protein standard curve.

3.13.3 Protein Separation by SDS-polyacrylamide Gel Electrophoresis (SDS-PAGE)

A Mini-PROTEAN Tetra Cell system (Bio-Rad) was used in SDS-polyacrylamide gel electrophoresis (SDS-PAGE). A short plate was placed on top of a spacer plate (1.0 mm thickness) and was secured on a casting stand to form a gel cassette assembly. A 10% resolving gel was prepared from 2.5 mL 1.5 M Tris (pH 8.8), 100 μ L 10% SDS, 3.3 mL 30% (w/v) Bis/Acrylamide (Bio-Rad) and 4.1 mL distilled water and mixed well. Tetramethylethylenediamine (TEMED, Calbiochem, Merck Millipore) (5 μ L) and 50 μ L 10% APS were added last to the resolving gel solution. All the components were mixed well and pipetted in between the glass plates assembled on the gel casting stand. The resolving gel was gently overlaid with 50 μ L isopropanol (Merck KGaA) to remove any bubble formation. After 45 min when the resolving gel was polymerised, isopropanol was rinsed off with distilled water and the residual was removed with Kimwipes tissue paper. A 5% stacking gel was prepared from 1 mL 0.5 M Tris (pH 6.8), 30 μ L 10% SDS, 0.67 mL 30% (w/v) Bis/Acrylamide and 1.9 mL distilled water and mixed well. A total of 3.3 μ L TEMED and 30 μ L 10% APS were added last to the stacking gel solution and mixed well. The stacking gel solution was then layered on the polymerised resolving gel. A 10-well 1.0 mm comb was inserted immediately into the stacking gel layer without forming air bubbles.

When the stacking gel polymerised, the gel cassette was clamped onto an electrode assembly and placed into the Mini-PROTEAN Tatra Tank. The comb was removed and the formed wells were rinsed with 1X running buffer. The electrode assembly was filled with SDS-PAGE running buffer until full, and the tank was filled to the indicated level. Then, four volumes of protein lysate at a final concentration of 50 µg was mixed with one volume of 5X Lane Marker Reducing Sample Buffer (Thermo Scientific), and the mixture was denatured at 95 °C for 10 min in a block heater (Stuart Scientific, Staffordshire, UK). Aliquots of denatured protein sample buffer mixture and 5 µL MagicMark™ XP Western Protein Standard (Thermo Fisher Scientific) were loaded into the wells accordingly. The electrophoresis was performed at a constant of 120 V for approximately 75 min.

3.13.4 Semi-dry Transfer of Protein from Gel to Nitrocellulose Membrane

While performing the gel electrophoresis, Hybond ECL nitrocellulose membrane (GE Healthcare, Little Chalfont, UK) and western blotting filter paper (Thermo Scientific) were cut to the dimension of the gel, approximately 10 cm x 6 cm. When the dye front was approaching the bottom of the resolving gel, the power was turned off and the electrophoresis apparatus was disassembled. The gel was removed gently from the gel cassette and the stacking gel layer was removed, leaving only the resolving gel with separated proteins. The resolving gel, together with the nitrocellulose membrane and two

pieces of blotting papers were soaked in 1X transfer buffer (Table 3.6) and equilibrated for 12 to 15 min.

The polyacrylamide gel was subjected to semi-dry electro-transfer by using Trans-Blot® SD Semi-Dry Electrophoretic Transfer Cell (Bio-Rad). A transfer sandwich was arranged accordingly. One piece of equilibrated blotting paper was placed on the bottom, followed by buffer-equilibrated nitrocellulose membrane, then the buffer-equilibrated polyacrylamide gel and finally another piece of blotting paper. The transfer sandwich was then placed on the anode of the semi-dry transfer cell. A centrifuge tube was used as a roller to exclude all trapped bubbles before the upper cathode was placed onto the stack. Separated protein samples on the gel were blotted to membrane with a constant voltage of 15 V for 15 min. The nitrocellulose membrane was removed from the sandwich and the gel orientation was marked on the membrane with pencil. The membrane was washed with distilled water for 5 min with gentle agitation on a gyratory rocker. The membrane was stained with RedAlert Stain (Novagen, Merck KGaA) to verify the transfer of proteins before western blot analysis. The RedAlert stain was removed by rocking the membrane in distilled water. The membrane was ready for blocking.

3.13.5 Membrane Blocking

The transferred nitrocellulose membrane was blocked with 5% milk to prevent non-specific binding of the antibodies onto the membrane. The membrane was incubated in 10 mL of blocking buffer (Table 3.6) for 1 h at

room temperature with gentle agitation on a gyratory rocker. The blocking solution was discarded and the membrane was washed with 10 mL washing buffer (Table 3.6) three times for 5 min with gentle agitation on a gyratory rocker, with fresh changes of washing buffer.

3.13.6 Antibody Staining

After the washing step, the membrane was probed with 5 mL primary rabbit antibodies against CDK6 (ab151247, Abcam, Cambridge, UK) diluted at 1:1,000 with washing buffer and incubated overnight at 4 °C with slight agitation. The membrane was washed with 10 mL washing buffer with agitation on a gyratory rocker and the step was repeated for two more times. The membrane was then incubated in 5 mL HRP-conjugated goat anti-rabbit IgG secondary antibody (ab97051, Abcam) diluted at 1:5,000 with washing buffer and incubated 1 h at room temperature with agitation. The membrane was again washed with 10 mL washing buffer with agitation and the step was repeated twice.

The expression levels of other proteins including E2F1 (ab94888, Abcam), CCND1 (ab137875, Abcam), p21 (#2947, Cell Signaling) and housekeeping gene GAPDH (#3683, Cell Signaling) were also detected. GAPDH protein was used as the loading control in the same SDS-PAGE gel to ensure even transfer to nitrocellulose membrane.

3.13.7 Chemiluminescence Detection

After the washing step, the excessive wash buffer was drained off from the washed blot. The membrane was placed on a sheet of transparent paper, with the protein side facing upward. Detection Solution 1 and 2, supplied in the Amersham Enhanced Chemiluminescent Western Blotting Detection Reagent (GE Healthcare), were mixed at a ratio of 1:1 and the mixture was added directly onto the membrane. Cumulative chemiluminescent signal emitted from the membrane after an exposure time of 15 min was captured by CCD camera of BioSpectrum Imaging System (Ultra-Violet Products Ltd). The image was saved for further analysis.

3.13.8 Stripping and Reprobing

After chemiluminescence detection, the primary and secondary antibodies on the membrane were removed for further use of the membrane. The developed membrane was rinsed with the wash buffer followed by incubation in 7 mL mild stripping buffer (Table 3.6) for 10 min at room temperature twice, with gentle agitation. The membrane was washed with 7 mL 1X PBS twice for 10 min, and with 7 mL washing buffer twice for 5 min. Subsequently, the stripped membrane was again blocked in the blocking buffer, followed by staining with primary and secondary antibodies and chemiluminescent signal detection as described in Section 3.13.5, Section 3.13.6 and Section 3.13.7.

3.13.9 Western Blot Densitometric Analysis

Band densitometric analysis was carried out using ImageJ 1.49v (National Institutes of Health, Maryland, USA) to measure intensity of the protein bands developed in the western blot membrane. The band intensity values obtained were first normalised to that of the loading control GAPDH. The protein levels were quantified in the three OSIPS WJ-MSC lines under study relative to the respective untreated control WJ-MSC lines.

3.14 Statistical Analysis

Statistical analysis was performed in Microsoft Excel 2010 using the statistical formula to obtain mean values, deviation and variance and to perform probability tests. Real-time RT-PCR results were reported as average of $\log(\text{fold change}) \pm \text{standard error}$. Data were analysed by Student's *t*-test (two-tailed distribution) by comparing the differences of miRNA or mRNA expression levels between the untreated control and the H₂O₂-treated WJ-MSC lines. Statistical significance was accepted at $p < 0.05$.

CHAPTER 4

RESULTS

The main objective of the study was to investigate the role of miRNAs and targeted transcripts in the regulation of G1/S-transition of the cell cycle in the oxidative stress-induced premature senescence (OSIPS) in mesenchymal stem cells (MSCs).

4.1 Study Design

The study design was divided into three main parts to achieve the objectives (Figure 4.1):

Part I : The development of OSIPS model of MSCs

Part II : miRNA profiling of OSIPS MSCs

Part III : Elucidation of functional role of OSIPS-affected miRNAs and targeted genes in association to the G1/S-phase of the cell cycle

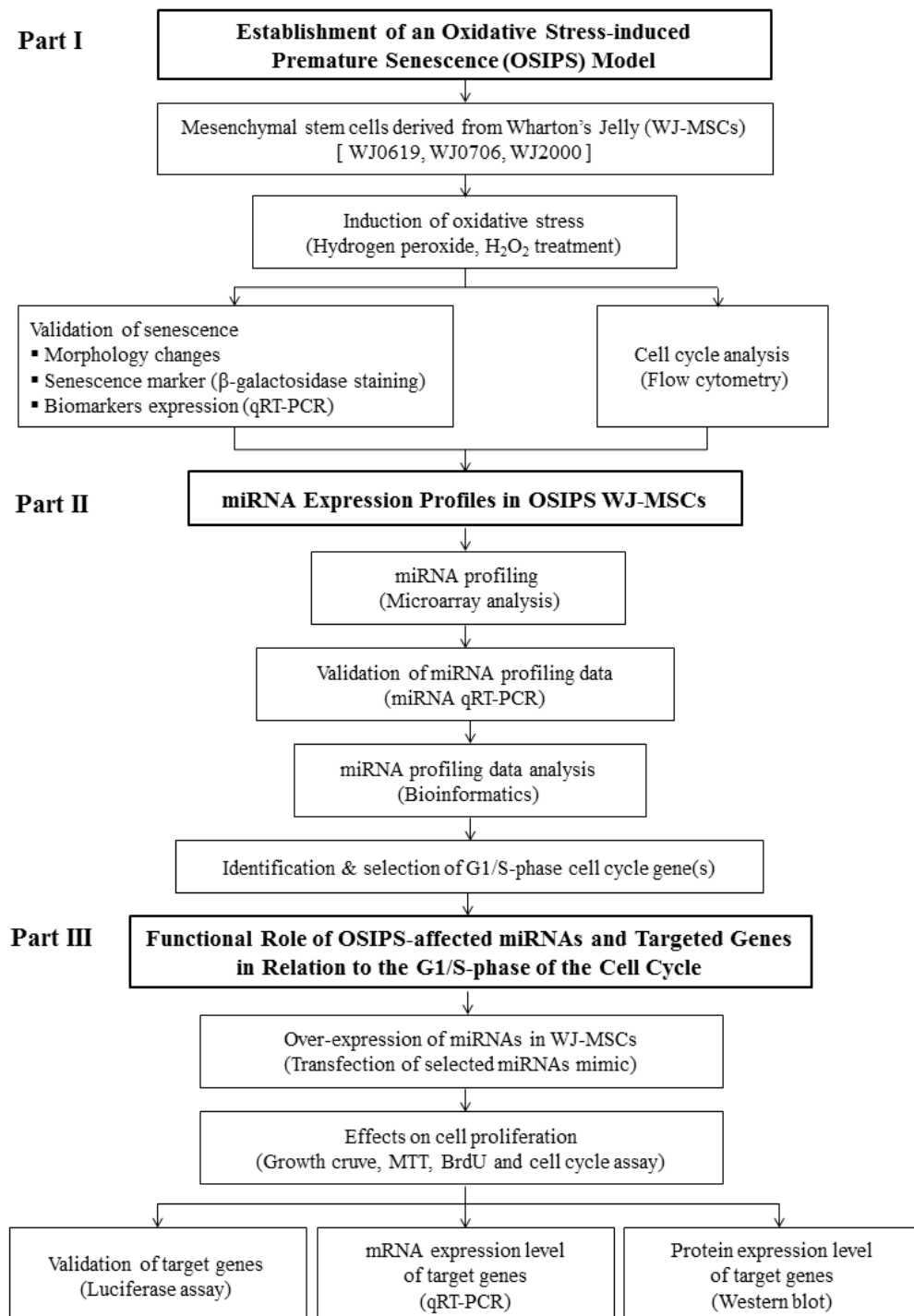


Figure 4.1 Study design. The study was divided into three main parts. The WJ-MSC lines used were stated in the square brackets; the assays carried out were described in round brackets.

Part I

Establishment of Oxidative Stress-induced Premature Senescence (OSIPS) Model in Wharton's Jelly-derived Mesenchymal Stem Cells (WJ-MSCs)

4.2 Optimisation of Hydrogen Peroxide (H₂O₂) Concentration in Inducing Premature Senescence in WJ-MSCs

Hydrogen Peroxide (H₂O₂) was used to induce premature senescence in Wharton's Jelly-derived mesenchymal stem cells (WJ-MSCs) at early passages 6 - 10. To determine the optimal concentration of H₂O₂ in inducing senescence, WJ-MSC line WJ0706 was cultured in a medium containing different concentrations of H₂O₂ as described in Section 3.2.5. Analysis on cumulative population doubling as an indicator of cell proliferation revealed that treatment of H₂O₂ at 200 µM retarded the growth of WJ0706 and the cells entered complete growth arrest (Figure 4.2A). In contrast, H₂O₂ treatment at higher concentrations of 400 µM or 600 µM caused immediate cell death on H₂O₂ treatment. The H₂O₂ concentration at 200 µM was reproducibly applied to four different independent WJ-MSC lines WJ0706, WJ0003, WJ2433 and WJ2000 to obtain similar growth profile when all the H₂O₂-treated WJ-MSC lines entered growth arrest (Figure 4.2B). H₂O₂ concentration at 200 µM was optimal to induce premature senescence in WJ-MSCs and was used in subsequent experiments.

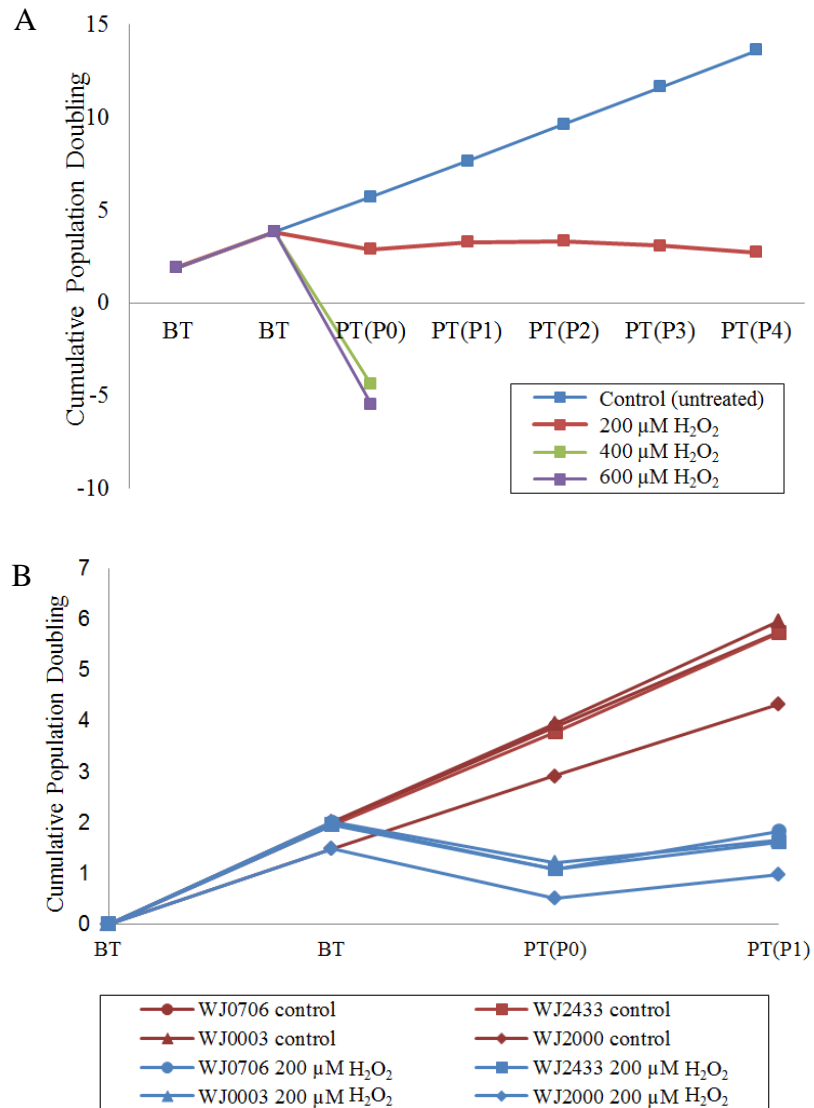


Figure 4.2 Cell growth profiles of H_2O_2 -treated WJ-MSCs relative to the respective untreated control cells determined by cumulative population doubling level. (A) WJ-MSC line WJ0706 was treated with different concentrations of H_2O_2 . (B) Different WJ-MSC lines, WJ0706, WJ0003, WJ2433 and WJ2000, served as biological replicates and were treated with 200 μM of H_2O_2 . Red lines represent the untreated control cells; blue lines represent 200 μM H_2O_2 -treated cells. BT: before treatment; PT: post treatment; P in bracket: passage

4.3 Validation of Senescence Characteristics in OSIPS WJ-MSCs

Validation of senescence state in three different H₂O₂-treated WJ-MSC lines WJ0619, WJ0706 and WJ2000 was carried out by examining morphological changes, senescence associated β -galactosidase (SA- β -gal) staining and mRNA expression levels of senescence biomarkers. On 200 μ M H₂O₂ treatments of WJ0619, WJ0706 and WJ2000, the cells all became irregularly enlarged, flattened in shape, multinucleated and were heavily granulated, as compared to the respective untreated control cells (Figure 4.3A). Additionally, all cells in three different H₂O₂-treated WJ-MSC lines were positively and strongly stained with blue colour of SA- β -gal staining, indicating the occurrence of senescence (Figure 4.3B).

To further validate senescence, qRT-PCR analysis of the mRNA expression levels of the senescence-related biomarkers, p16, p21, p53 and GLB1, was carried out in three different H₂O₂-treated WJ-MSC lines (Figure 4.4; Appendix A). Generally, all four markers were up-regulated in all the cell lines relative to the respective untreated control cells, except for p53 gene. The p53 gene was down-regulated in H₂O₂-treated WJ2000 and did not show large differences in WJ0619 and WJ0706 lines. The p16 and p21 genes were evidently up-regulated by two-fold or more in all three H₂O₂-treated WJ-MSC lines, despite the p16 level in WJ0619 was only increased by 1.29-fold. Similarly, the beta-galactosidase-1 (GLB1) that encodes the glycosyl hydrolase protein was also up-regulated in different WJ-MSC lines except for

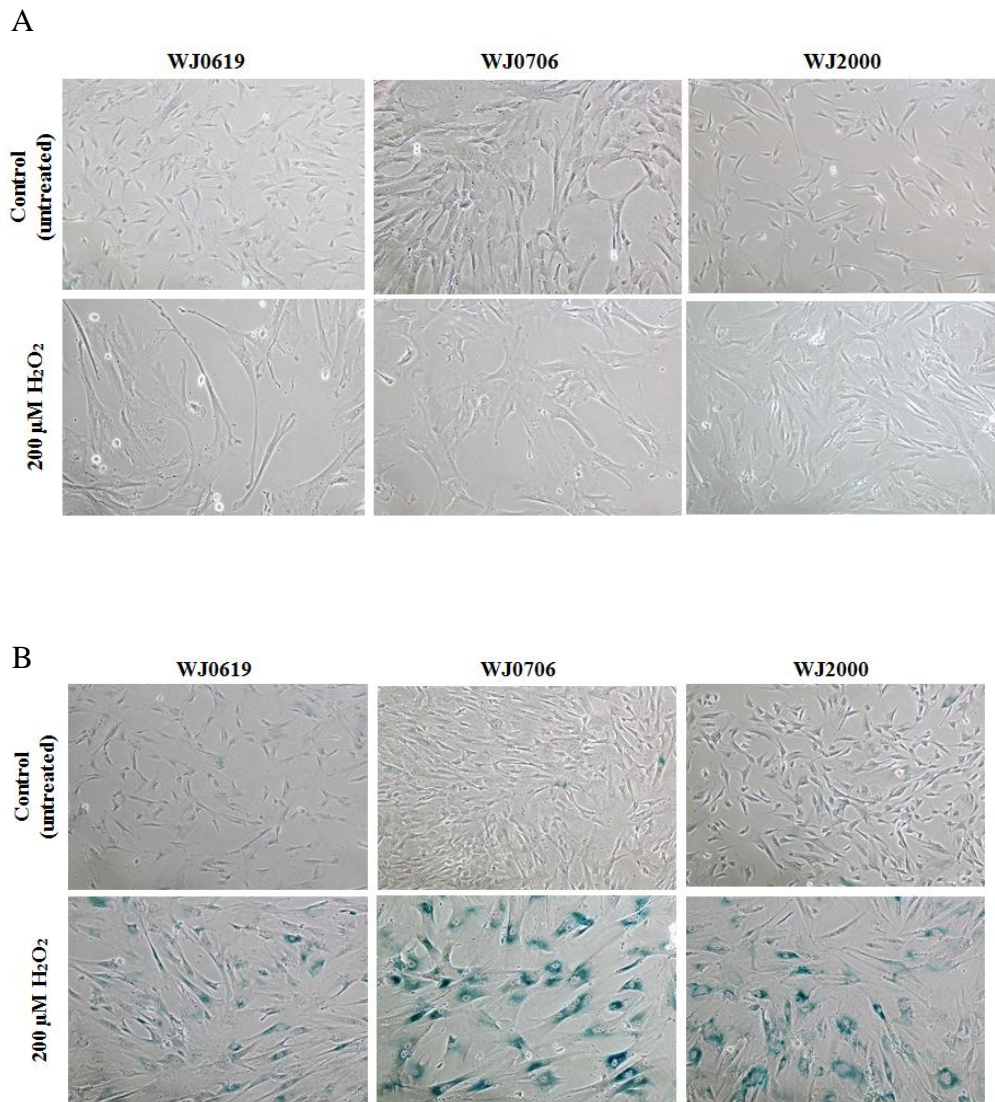


Figure 4.3 Senescence characteristics of 200 μM H_2O_2 -treated WJ-MSC lines. (A) Morphological changes and (B) SA- β -gal staining in WJ-MSC lines WJ0619, WJ0706 and WJ2000 before and after 200 μM H_2O_2 -treatment. All images were captured at 10x magnification.

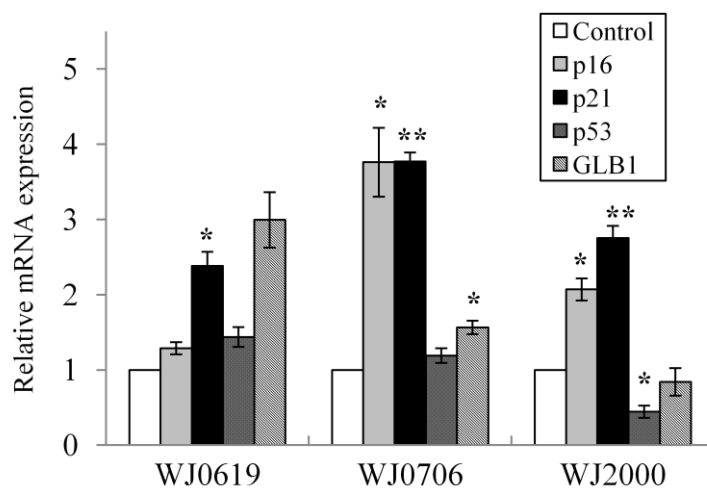


Figure 4.4 Expression of senescence biomarkers in H₂O₂-treated WJ- MSC lines WJ0619, WJ0706 and WJ2000 as determined by real-time PCR. Data presented were from three independent experiments done in triplicates. In all cases, * $p < 0.05$ and ** $p < 0.01$ were derived as compared to the untreated control samples, set as 1.0. The relative fold change values are shown in Appendix A.

WJ2000 that was not significantly affected, suggesting that different WJ-MSC lines might respond differently upon H₂O₂ treatment due to subtle biological differences.

Taken together, the results indicated that 200 μM H₂O₂ treatment successfully provoked oxidative stress-induced premature senescence (OSIPS) in three different WJ-MSC lines tested.

4.4 OSIPS WJ-MSCs Shared Similar Senescence Characteristics with Replicative Senescence (RS) WJ-MSCs

On prolong *in vitro* culture, WJ-MSCs enter replicative senescence (RS), a state of permanent growth arrest after a finite set of cell division. Hence, experiments were carried out to determine if oxidative stress-induced premature senescence (OSIPS) cells share common features with cells in replicative senescence using late-passage senescence WJ0706 cells, which have entered the RS state. Relative to the early passage (P) 7 cells, WJ0706 cells at the late passage (P) 23 became irregular, large and flattened in shape, and were stained positive for SA-β-gal, similar to H₂O₂-treated cells (Figure 4.5A). Out of the four senescence biomarkers tested by real-time RT-PCR as for OSIPS cells, only p21 and GLB1 expression was up-regulated in replicative senescence WJ0706 relative to P7 cells, unlike the OSIPS cells in which the four markers were generally up-regulated (Figure 4.5B; Appendix B). Taken together, OSIPS and replicative senescent WJ0706 shared similar senescence features.

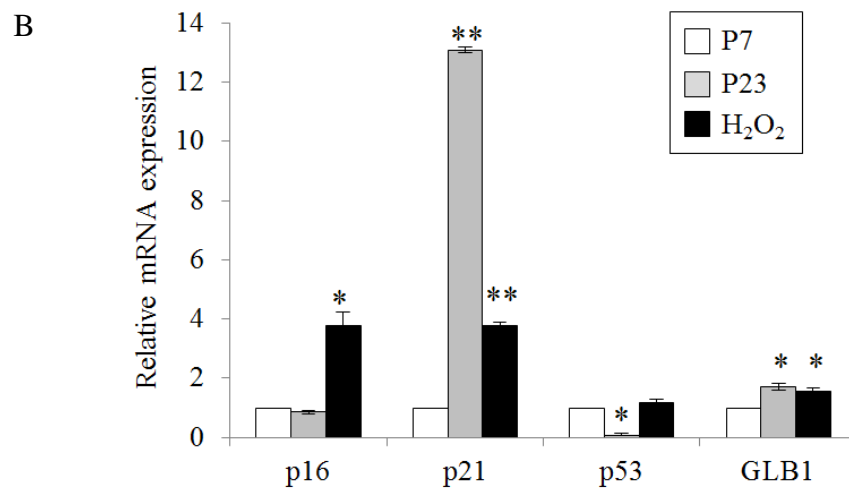
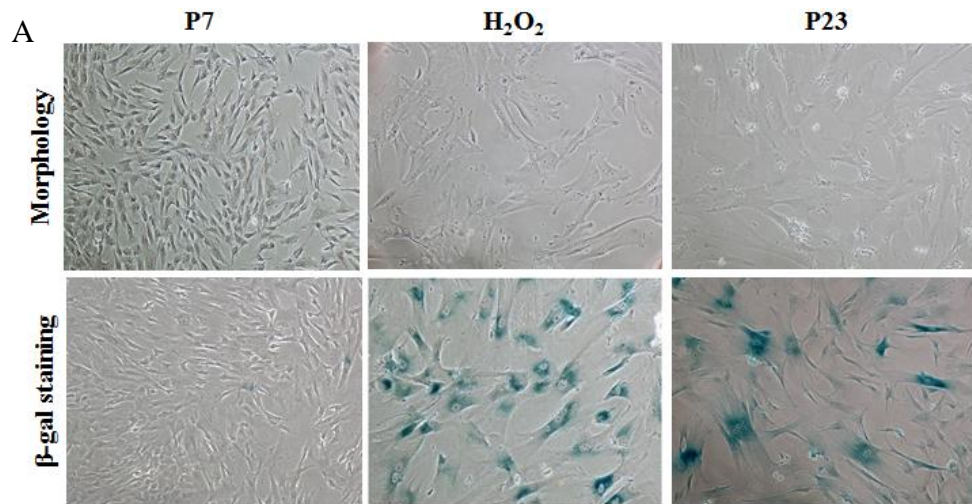


Figure 4.5 Senescence characteristics in early passage (P) 7 and late passage 23, and H₂O₂-treated OSIPS WJ0706 cells. (A) Cell morphology and SA-β-gal staining and (B) expression of senescence biomarkers in P7, P23 and OSIPS WJ0706. All cell images were captured at 10x magnification. Real-time RT-PCR data presented were from three independent experiments in triplicates. In all cases, * $p < 0.05$ and ** $p < 0.01$ were derived as compared to the untreated control samples, set as 1.0. The relative fold change values are shown in Appendix B.

4.5 Cell Cycle Arrest in OSIPS WJ-MSCs

WJ-MSCs possess the ability to self-renew, a process regulated by the G1/S-phase of the cell cycle (Neganova and Lako, 2008). In stem cells, the G1/S-phase is unblocked, accelerating the entry of cells into the S-phase of the cell cycle (Becker et al., 2006). On the contrary, cell cycle control is retarded in senescence cells, resulting in diminished proliferative capability and irreversible G1 cell cycle arrest (Shenghui et al., 2009; Alt et al., 2012). To elucidate the effects of H₂O₂ on the G1/S- and G2-phase of the cell cycle, the cell distribution of OSIPS MSCs and respective untreated control cells was examined by flow cytometry analysis (Table 4.1; Appendix C-E). In the all three OSIPS WJ-MSC lines tested as compared to the respective untreated controls, the percentage of G1-phase cells increased consistently, from 64.77 ± 2.68 to 75.60 ± 2.76 on the average, with concurrent decline, from 24.53 ± 3.60 to 15.83 ± 1.97 on the average, in the S-phase cell population. There were corresponding declines in the G2 cell population in two of the cell lines tested. The data indicated that the G1/S-phase of the cell cycle was blocked in OSIPS WJ-MSCs, suggesting that H₂O₂ treatment suppressed cell entry into the S-phase, consistent with reduced proliferation capacity (Chen et al., 2015).

Table 4.1 Cell cycle analysis in H₂O₂-treated and untreated WJ-MSC lines

Cell line	Treatment	Average cell population ¹		
		G1-phase	S-phase	G2-phase
WJ0619	Control	64.21 ± 14.68	27.09 ± 12.0	8.7 ± 4.36
	H ₂ O ₂ -treated	76.05 ± 17.47	15.21 ± 8.28	8.75 ± 9.23
WJ0706	Control	62.4 ± 5.25	26.1 ± 3.16	11.5 ± 2.17
	H ₂ O ₂ -treated	72.63 ± 7.57*	18.04 ± 12.71	9.32 ± 5.2
WJ2000	Control	67.68 ± 5.26	20.41 ± 7.23	11.91 ± 2.44
	H ₂ O ₂ -treated	78.11 ± 4.76	14.25 ± 3.6	7.64 ± 1.46**
Average	Control	64.77 ± 2.68	24.53 ± 3.60	10.70 ± 1.75
	H ₂ O ₂ -treated	75.60 ± 2.76**	15.83 ± 1.97*	8.57 ± 0.86

¹Average cell distribution obtained from three independent experiments, as represented by mean ± SD. **p*<0.05 and ***p*<0.01 were values obtained in comparison to the untreated control samples. The cell cycle histograms for each independent experiment for the three WJ-MSC lines are shown in Appendices C, D and E.

Part II

miRNA Profiling and Validation in Oxidative Stress-induced Premature Senescence in Wharton's Jelly-derived Mesenchymal Stem Cells (OSIPS WJ-MSCs)

4.6 RNA Concentration and Integrity Test

RNAs were isolated from the three OSIPS WJ-MSCs and respective untreated control lines. The concentration, purity and integrity of the isolated RNA samples were determined to ensure that the RNAs qualified for miRNA profiling analysis (Table 4.2 and Figure 4.6). The A_{260}/A_{280} ratios of the isolated RNA samples fell in the range of 1.8-2.0, and A_{260}/A_{230} ratio was > 1.5 , indicating high purity (Table 4.2). The RNA yields were sufficient for miRNA profiling analysis and further downstream analysis.

RNA analysis on non-denaturing agarose gel electrophoresis was carried out to check the integrity of RNA samples. Two intensive sharp bands that represented the 28S and 18S ribosomal RNAs were observed (Figure 4.6). The upper 28S bands were approximately double the intensity of the lower 18S bands at a ratio of 2:1, indicative of intact RNA samples.

Table 4.2: Purity and concentration of RNA samples isolated from untreated control and H₂O₂-treated WJ-MSCs for miRNA profiling analysis

Cell lines	Treatment	A ₂₆₀ /A ₂₈₀	A ₂₆₀ /A ₂₃₀	Concentration (ng/μL)
WJ0619	Control	1.967	1.504	358
	H ₂ O ₂ -treated	2.034	2.034	948
WJ0706	Control	2.068	2.230	1088
	H ₂ O ₂ -treated	2.057	1.763	2024
WJ2000	Control	2.020	2.174	1018
	H ₂ O ₂ -treated	1.905	1.519	240

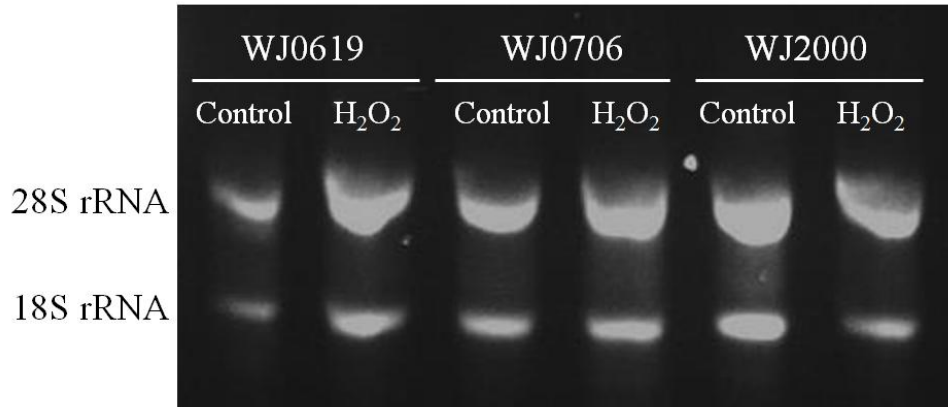


Figure 4.6 Integrity of RNA prepared from untreated control and OSIPS WJ-MSC lines WJ0619, WJ0706 and WJ2000. Total RNA (200 ng) isolated were subjected to 1% agarose gel electrophoresis at 70 V for 45 min. The gel was pre-stained with 3X GelRed nucleic acid stain and visualised by exposure to 302 nm UV light on a UVP BioSpectrum Imaging System.

4.7 Global miRNA Expression Profiling in OSIPS WJ-MSCs

To investigate the dysregulation of miRNAs in OSIPS WJ-MSCs, global miRNA expression profiling analysis was carried out using Gen. 7 version of miRCURY LNA™ microRNA Arrays. Out of the 1,896 human miRNAs included in the microarray, data analysis identified only minor differences in the miRNAs profile between the untreated and H₂O₂-treated group in the three WJ-MSC lines tested. After filtration, only 564 probes were deemed detectable above the background threshold for each sample. For the expression analysis, the *p*-values were calculated based on moderated *t*-statistics. The Benjamini and Hochberg multiple testing corrections that adjusted *p*-values derived from multiple statistical tests were done to filter out the false-positive results (Benjamini and Hochberg, 1995). All calculations were carried out in the software R/bioconductor using the LIMMA library (Smyth, 2005).

Amongst the 564 differentially expressed miRNAs identified, the top fifty differentially expressed miRNAs with the highest standard deviations were extracted for unsupervised hierarchical clustering analysis in a heatmap (Figure 4.7). The heatmap showed the result of a two-way hierarchical clustering of miRNAs and samples. Each row represented a miRNA and each column represented a MSC sample, which were further categorised into the control (untreated) and H₂O₂-treated groups as anticipated. miRNAs were organised according to the similarity and dissimilarity of the expression profiles and, hence, miRNAs with similar expression profiles were clustered in

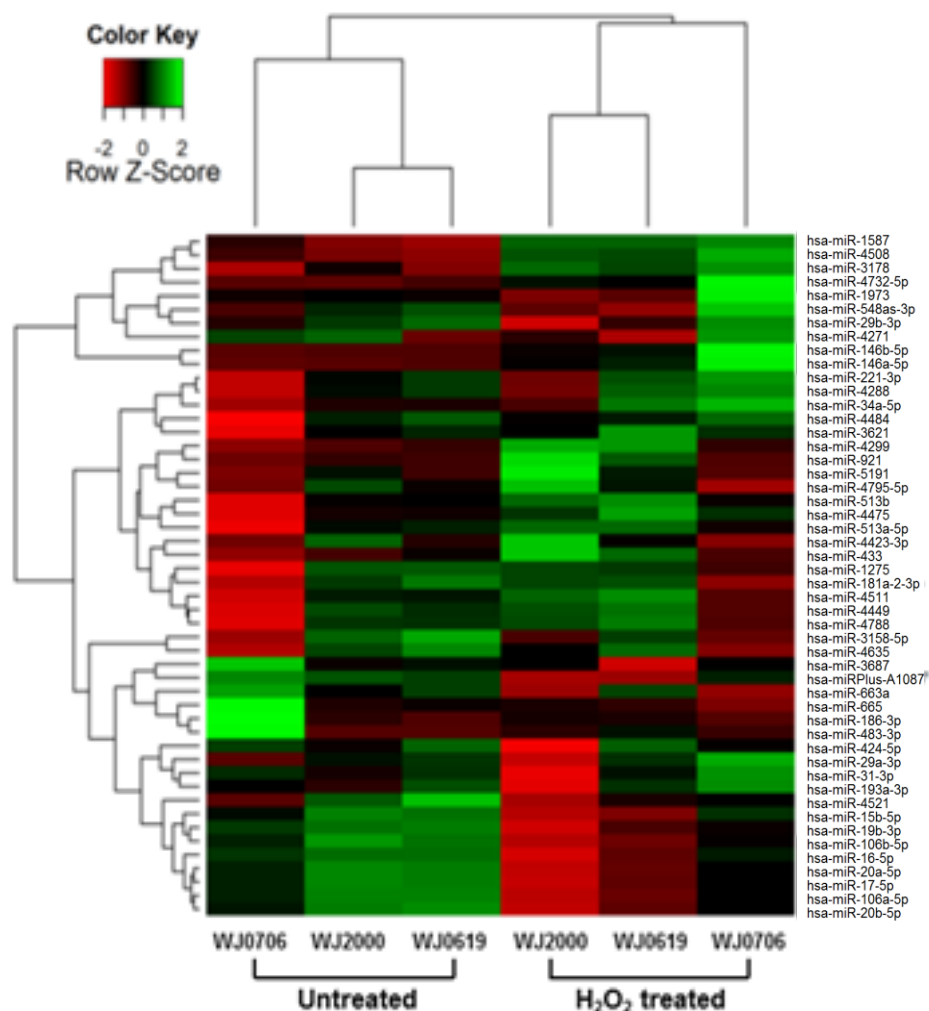


Figure 4.7 Differentially expressed miRNAs in H₂O₂-treated WJ-MSCs. Heatmap and unsupervised hierarchical clustering of the top fifty differentially expressed miRNAs in three H₂O₂-treated WJ-MSC lines WJ0706, WJ2000 and WJ0619 derived from microarray analysis. Clustering was performed using the complete-linkage method and the Euclidean distance measure. Colour code for relative miRNA expression levels: red and green represent expression levels below and above the reference channel, respectively. Normalised log₂(fold change) ratio values were used for the analysis.

the heatmap. The colour scale illustrated the relative expression level of miRNAs, whereby the red and green colours represented an expression level below or above the reference channel, respectively. A full list of top fifty differentially expressed miRNAs is shown in Table 4.3.

4.8 miRNA Expression Profiling Analysis Revealed Differentially Expressed miRNAs in OSIPS WJ-MSCs

Amongst the fifty differentially expressed miRNAs in OSIPS WJ-MSCs, only seven up-regulated and five down-regulated miRNAs fulfilled the criteria of $-1.0 > \log_2(\text{fold change}) > 1.0$ and $p < 0.05$. The \log_2 (fold change) values observed in OSIPS WJ-MSCs relative to untreated WJ-MSCs are shown in Table 4.4. The maximal up-regulation was 2.407 ± 1.51 in miR-146a-5p and maximal down-regulation was -1.281 ± 0.85 in miR-16-5p.

In the up-regulated group, both miR-146a-5p and miR-146b-5p belong to the miR-146 family and have been reported to be differentially expressed in late-passage fibroblasts cells (Bonifacio and Jarstfer, 2010). The remaining five miRNAs were recently reported miRNAs, as indicated by nomenclature numbering of four digits, including miR-1587, miR-3178, miR-4497, miR-4508 and miR-4732-5p. These miRNAs were first reported in deep sequencing of small RNA transcriptomes of several types of cancer, and await further annotation and study (Jima et al., 2010; Stark et al., 2010; Persson et al., 2011).

Table 4.3 Fifty top miRNAs up- or down-regulated in OSIPS WJ-MSCs

miRNA	Family ¹	Accession ¹	Chromosomal Location ¹	Sequence (5' → 3') ¹	Log ₂ (FC) ²
Up-regulated miRNA					
miR-146a-5p	miR-146	MI0000477	5q34	ugagaacugaaauccauggguu	2.407*
miR-146b-5p	miR-146	MI0003129	10q24.32	ugagaacugaaauccaauaggcu	2.029*
miR-4497		MI0016859	12q24.1	cuccgggacggcugggc	1.179**
miR-513a-5p	miR-506	MI0003191	Xq27.3	uucacaggaggugucau	1.142
miR-4732-5p		MI0017369	17q11.2	uguagagcaggagcaggaagcu	1.138*
miR-4508		MI0016872	15q11.2	gcggggcugggcgcgcg	1.055**
miR-3178		MI0014212	16p13.3	ggggcgcgccggaucg	1.043**
miR-1587		MI0016905	Xp11.4	uugggcugggcuggguuggg	1.019**
miR-4475		MI0016827	9	caagggaccaagcauucauuau	0.934*
miR-513b	miR-506	MI0006648	Xq27.3	uucacaaggaggugucauuuau	0.905
miR-4299		MI0015829	11	gcuggugacaugagaggc	0.817*
miR-921	miR-921	MI0005713	1q24.1	cuagugagggacagaaccaggauuc	0.792
miR-433	miR-433	MI0001723	14q32.2	uacggugagccugucauuauuc	0.790

Table 4.3 continue

miRNA	Family¹	Accession¹	Chromosomal Location¹	Sequence (5' → 3')¹	Log₂(FC)²
Up-regulated miRNA					
miR-3621		MI0016012	9	cgcggggucggggucugcagg	0.773
miR-5191		MI0018170	1	aggauaggaagaugaagugcu	0.745
miR-34a-5p	miR-34	MI0000268	1p36.22	uggcagugucuuagcugguugu	0.733
miR-4484	miR-4484	MI0016845	10	aaaaggcgggagaagcccca	0.623
miR-4511		MI0016877	15	gaagaacuguugcauuugcccu	0.607
miR-4788	miR-4788	MI0017435	3	uuacggaccagcuaagggaggc	0.441
miR-221-3p	miR-221	MI0000298	Xp11.3	agcuacauugucugcuggguuc	0.393
miR-4449	miR-4449	MI0016792	4	cgucccggggcugcgcgaggca	0.373
miR-4288		MI0015896	8	uugucugcugaguucc	0.366
miR-1275	miR-1275	MI0006415	6	gugggggagaggcuguc	0.294
miR-4795-5p		MI0017442	3	agaaguggcuaauauuuga	0.246
miR-4423-3p	miR-4423	MI0016760	1	auaggcaccaaaaagcaaca	0.187
miR-1973		MI0009983	4	accgugcaaagguagcaua	0.084

Table 4.3 continue

miRNA	Family¹	Accession¹	Chromosomal Location¹	Sequence (5' → 3')¹	Log₂(FC)²
Up-regulated miRNA					
miR-29a-3p	miR-29	MI000087	7q32.3	uagcaccaucugaaaucgguua	0.060
miR-181a-2-3p	miR-181	MI0000269	9q33.3	accacugaccguugacuguacc	0.018
Down-regulated miRNA					
miR-16-5p	miR-15	MI0000070	13q14.2	uagcagcacguaaauauuggcg	-1.281*
miR-17-5p	miR-17	MI0000071	13q31.3	caaagugcuuacagugcagguag	-1.268*
miR-20a-5p	miR-17	MI0000076	13q31.3	uaaagugcuuauagugcagguag	-1.265**
miR-20b-5p	miR-17	MI0001519	Xq26.2	caaagugcucauagugcagguag	-1.217**
miR-106a-5p	miR-17	MI0000113	Xq26.2	aaaagugcuuacagugcagguag	-1.158**
miR-106b-5p	miR-17	MI0000734	7q22.1	uaaagugcugacagugcagau	-0.943**
miR-19b-3p	miR-19	MI0000074	13q31.3	ugugcaaaucgaacaaaacuga	-0.927**
miR-15b-5p	miR-15	MI0000438	3q35.33	uagcagcacaucaugguuuaca	-0.883*
miR-663a	miR-663	MI0003672	20p11.1	aggcggggcgccgcccggaccgc	-0.827
miR-665	miR-665	MI0005563	14q32.2	accaggaggcugaggcccu	-0.766

Table 4.3 continue

miRNA	Family¹	Accession¹	Chromosomal Location¹	Sequence (5' → 3')¹	Log₂(FC)²
Down-regulated miRNA					
miR-4521		MI006887	17	gcuaaggaaguccugucucag	-0.697
miR-3687	miR-3687	MI0016088	21	cccggacaggcguucgugcgacgu	-0.685
miR-3158-5p	miR-3158	MI0014186	10	ccugcagagaggaagcccuuc	-0.582
miR-424-5p	miR-322	MI0001446	Xq26.3	cagcagcaauucauguuuugaa	-0.530
miR-29b-3p	miR-29	MI0000105	7q32.3	uagcaccuuugaaaucaguguu	-0.515
miR-186-3p	miR-186	MI0000483	1p31.1	gcccaaaggugaauuuuuuggg	-0.404
miR-4271		MI0015879	3	gggggaagaaaaggugggg	-0.384
miR-483-3p	miR-483	MI0002467	11p15.5	ucacuccucuccuccgucuu	-0.270
miR-31-3p	miR-31	MI0000089	9p21.3	ugcuaugccaacauauugccau	-0.214
miR-193a-3p	miR-193	MI0000487	17q11.2	aacuggccuacaaaguccagu	-0.155
miR-548a-3p	miR-548	MI0019132	13	uaaaaccacaauuauuguuugu	-0.146
miR-4635		MI0017262	5	ucuugaagucagaaccgcaa	-0.098

¹miRBase version 20 was used in data derivation. ²Microarray data of log₂(fold change), and **p*<0.05 or ***p*<0.01.

Table 4.4 Differentially expressed miRNAs in OSIPS WJ-MSCs

miRNA	Family ¹	Accession ¹	Chrom. Location ¹	Sequence (5' → 3') ¹	Log2(FC) ²
<u>Up-regulated miRNA</u>					
miR-146a-5p	miR-146	MI0000477	5q34	ugagaacugaa <u>uuccauggguu</u>	2.407±1.51*
miR-146b-5p	miR-146	MI0003129	10q24.32	ugagaacugaa <u>uuccauaggcu</u>	2.029±1.44*
miR-1587		MI0016905	Xp11.4	uugggcugggcuggguuggg	1.019±0.15**
miR-3178		MI0014212	16p13.3	ggggcgcggccggaucg	1.043±0.39**
miR-4497		MI0016859	12q24.1	cuccgggacggcugggc	1.179±0.36**
miR-4508		MI0016872	15q11.2	gcggggcugggcgcgcg	1.055±0.06**
miR-4732-5p		MI0017369	17q11.2	uguagagcagggagcaggaagcu	1.138±0.77*
<u>Down-regulated miRNA</u>					
miR-16-5p	miR-15	MI0000070	13q14.2	uagcagcacgaa <u>uauuggcg</u>	-1.281±0.85*
miR-17-5p	miR-17	MI0000071	13q31.3	caaagugcu uacagucagguag	-1.268±0.82*
miR-20a-5p	miR-17	MI0000076	13q31.3	uaaagugcu uauagucagguag	-1.265±0.81**
miR-20b-5p	miR-17	MI0001519	Xq26.2	caaagugcu cauagucagguag	-1.217±0.76**
miR-106a-5p	miR-17	MI0000113	Xq26.2	aaaagugcu uacagucagguag	-1.158±0.70**

¹miRBase version 20 was used in data derivation. ²Microarray data of log₂(fold change)(FC) >1.00 and <-1.00, and *p<0.05 or **p<0.01 were extracted.

The miRNAs shown were uniformly differentially expressed in all three cell line analysed. In the miR-17 family miRNA sequences, nucleotides in bold and italics indicate identical seed sequences of the miRNA family.

In the down-regulated group, miR-16-5p is a tumour suppressor miRNA that was involved in regulation of the cell cycle and apoptosis (Aqeilan et al., 2010; Kang et al., 2015; Mobarra et al., 2015). The other four down-regulated miRNAs, miR-17-5p, miR-20a-5p, miR-20b-5p and miR-106b-5p, are from the miR-17 family and share the same aaagugcu seed sequence. However, the paralogous genes encoding miR-17-5p and miR-20a-5p are located in the miR-17~92 cluster on chromosome 13, whereas miR-20b-5p and miR-106b-5p are located in the miR-106a~363 clusters on chromosomes X (Mogilyansky and Rigoutsos, 2013).

4.9 Experimental Validation of miRNA Expression in OSIPS and RS WJ-MSCs

To validate the microarray data, the two miR-146 and the four miR-17 family members were subjected to miRNA real-time RT-PCR analysis, as describe in Section 3.8.3. It was observed that miR-146a-5p was significantly up-regulated by up to 4.28- and 11.88-fold in WJ0706 and WJ2000, respectively; whilst miR-146b-5p was up-regulated by less than 2-fold changes (Figure 4.8, top row; Appendix F). Surprisingly in the OSIPS WJ0619 cells, both miR-146 miRNAs were down-regulated, suggesting intrinsic differences in the cell lines derived from different sources. On the other hand, all four miR-17 miRNAs were down-regulated in all the three OSIPS MSC lines, confirming the microarray data (Figure 4.8, bottom row; Appendix F).

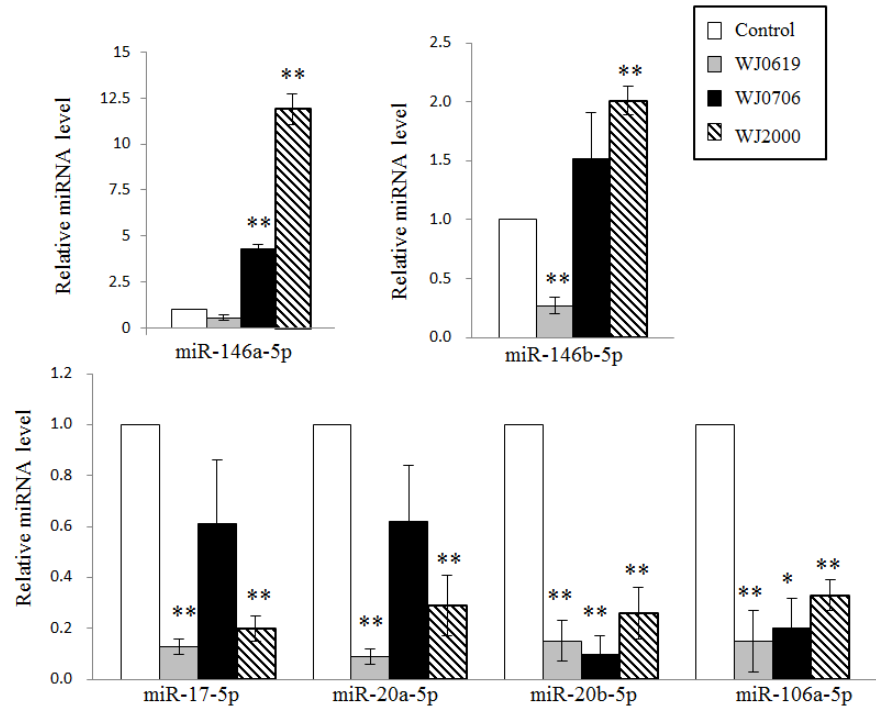


Figure 4.8 Validation of differentially expressed miRNAs in H₂O₂-treated WJ-MSCs by real-time RT-PCR. The top and bottom rows depict the up- and down-regulated groups of miRNAs, respectively. Data presented were from three independent experiments. In all cases, * $p < 0.05$ and ** $p < 0.01$ were considered significant compared to the untreated control samples, set as 1.0. The relative fold change values are shown in Appendix F.

In a comparative study, miRNA qRT-PCR was also carried out in the late-passage P23 replicative senescence (RS) WJ0706 relative to altered expression in the OSIPS cells established by the microarray analysis (Figure 4.9; Appendix G). In the up-regulated group, P23 RS WJ0706 showed 1.8-fold significant increase of miR-146a-5p, as observed in the OSIPS cells with 4.28-fold up-regulation; however, miR-146b-5p miRNA showed no significant changes in P23 RS cells (Figure 4.9, top row), which suggested that miR-146 family miRNAs may not be important in replicative senescence. On the other hand, all four miR-17 miRNAs were consistently suppressed in P23 RS cells as in the OSIPS cells (Figure 4.9, bottom row), further supporting possible role of miR-17 miRNAs in the senescence process.

4.10 Rapid and Irreversible Down-regulation of miR-20b-5p and miR-106a-5p in OSIPS WJ-MSCs

To examine the expression dynamics of miR-20b-5p and miR-106a-5p, WJ0706 cells were treated with H₂O₂ for 0.5 to 2 h. On H₂O₂ treatment for 0.5 h, the expression of miR-20b-5p and miR-106a-5p were rapidly down-regulated, and the suppressed miRNA levels were maintained for up to 2 h (Figure 4.10A; Appendix H). It was further shown that the suppressed miR-20b-5p and miR-106a-5p expression levels were maintained for up to 48 h in the cell recovery period post-H₂O₂ treatment (Figure 4.10B; Appendix I), suggesting irreversible down-regulation of these miRNAs in the OSIPS cells.

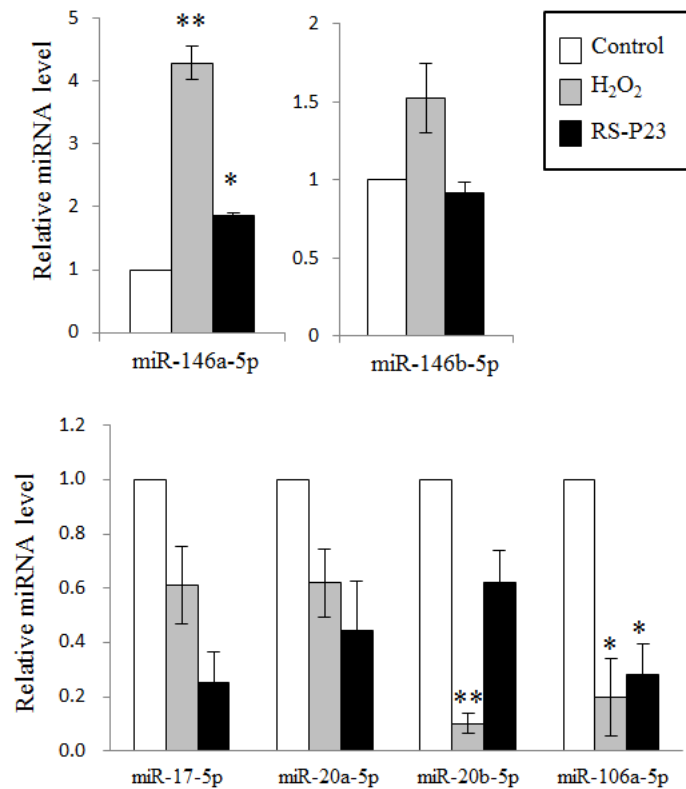


Figure 4.9 Validation of differentially expressed miRNAs in H₂O₂-treated or late-passage WJ0706 cells by real-time RT-PCR. The top and bottom rows depict the up- and down-regulated groups of miRNAs, respectively. Data presented were from three independent experiments. * $p < 0.05$ and ** $p < 0.01$ were considered significant compared to the untreated control samples, set as 1.0. The relative fold change values are shown in Appendix G.

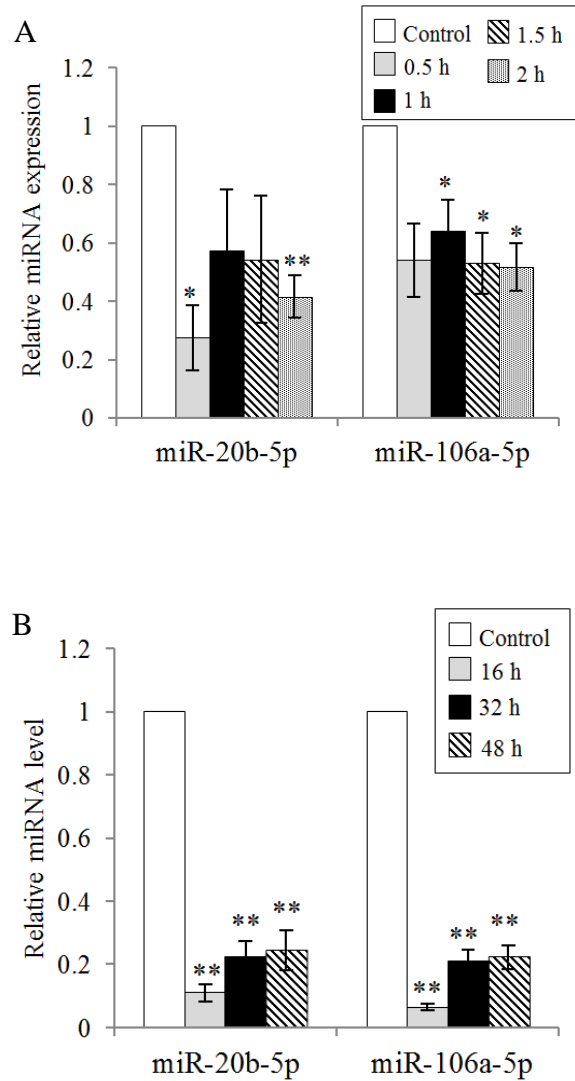


Figure 4.10 Down-regulated expression of miR-20b-5p and miR-106a-5p in H₂O₂-treated WJ-MSCs. (A - B) Expression of miR-20b-5p or miR-106a-5p in 200 μ M H₂O₂-treated WJ0706 cells for 0.5 to 2 h (A) and in similarly treated cells that were harvested at different time points post- H₂O₂ treatment (B), as compared to the early-passage untreated control cells, determined by real-time RT-PCR. Data presented were from three independent experiments. * p <0.05 and ** p <0.01 were considered significant compared to the control samples set as 1.0. The relative fold change values are shown in Appendix H and I.

Taken together, rapid and irreversible down-regulation suggests a possible role of miR-20b-5p and miR-106a-5p in senescence.

Part III

The Regulatory Role of miR-17 Family in the G1/S-phase of the Cell Cycle

4.11 miR-20b-5p and miR-106a-5p Promote Cell Proliferation in WJ- MSCs

Of the four down-regulated miR-17 miRNAs in OSIPS WJ-MSCs (Table 4.4), miR-17-5p and miR-20a-5p have previously been studied (Cloonan et al., 2008; Trompeter et al., 2011). The X-chromosomal miR-20b-5p and miR-106a-5p, which have not previously been examined, were the focus of this study in relation to oxidative stress-induced premature senescence in WJ-MSCs.

To elucidate the association between the miR-20b-5p and miR-106a-5p and cell proliferation, transient over-expression of the miRNA mimics in OSIPS and RS WJ0706 was performed, followed by cell growth analysis (Figure 4.11). Upon H₂O₂ treatment, the negative mimic-transfected control cells stopped in growth and entered growth arrest on day 2. On the other hand, the miR-20b-5p or miR-106a-5p mimic-transfected cells entered the log phase

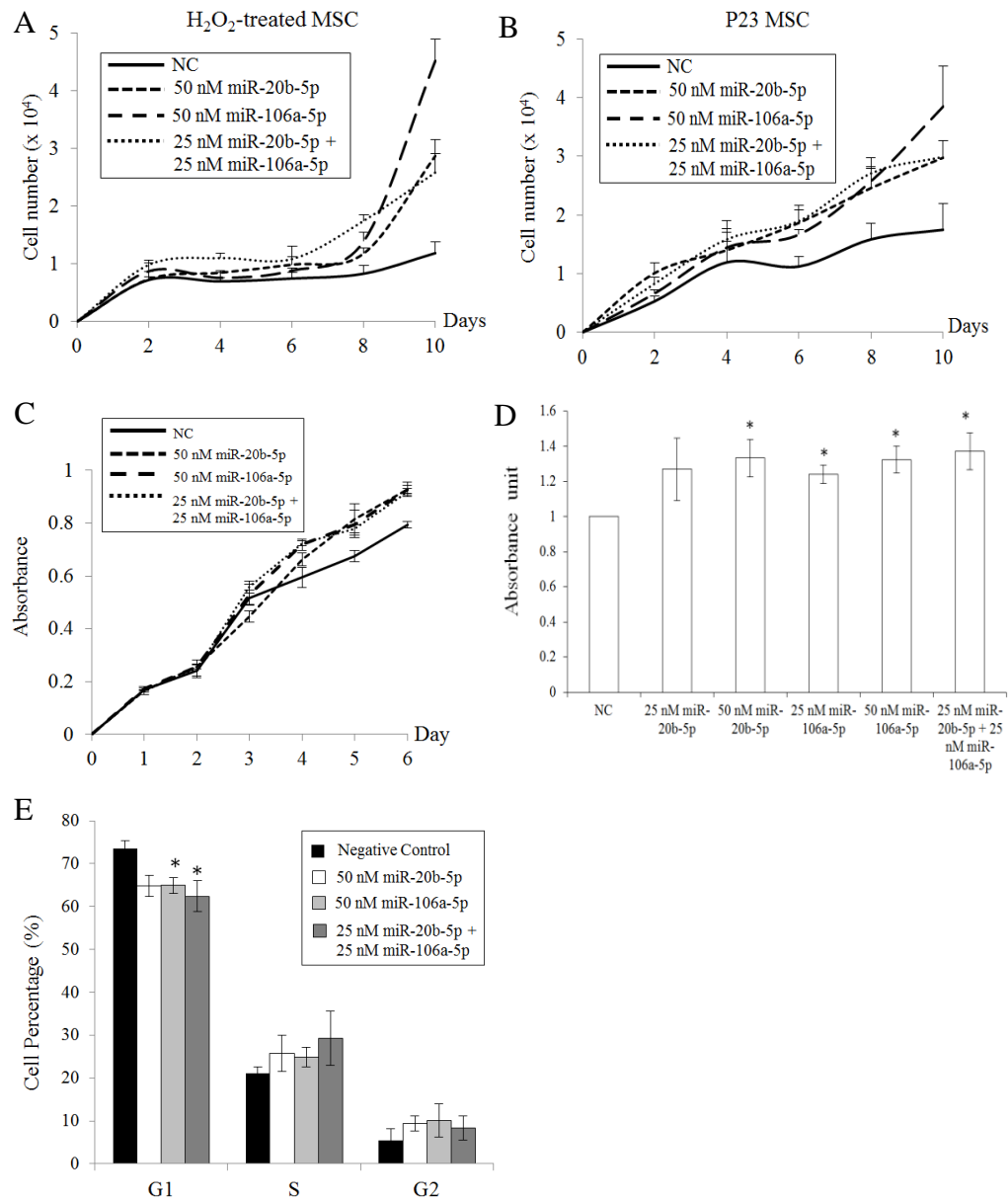


Figure 4.11 miR-20b-5p and miR-106a-5p promote cell proliferation in MSCs. (A - B) Growth curve of WJ0706 cells transfected with 25 or 50 nM miR-20b-5p and/or miR-106a-5p mimic, followed by 200 μ M H_2O_2 treatment (A), or in miRNA-transfected late-passage (P23) replicative senescent WJ0706 cells (B). The total cell numbers at specified days post-transfection and H_2O_2 treatment are determined. (C – E) Effects of over-expression of miR-20b-5p and/or miR-106a-5p mimics in WJ0706 cells on cell viability, determined by MTT analysis (B), DNA synthesis rate, determined by BrdU analysis (C), and distribution of G1-, S- or G2-phase cells in flow cytometry analysis (D). Data presented were from three independent experiments. * p <0.05 and ** p <0.01 were as compared to the nonspecific negative control (NC) mimic.

of growth on days 6 to 8 (Figure 4.11A). The miRNA mimic-transfected cells in the late passage RS entered exponential growth phase on day 4 onwards, while the negative mimic-transfected control cells were still growing at a slower rate (Figure 4.11B). Both growth analyses of OSIPS and RS cells indicated that miR-20b-5p or miR-106a-5p promoted the growth of senescence MSCs after a delayed period probably allowing for biochemical action of the transfected-miRNAs. The miR-20b-5p and miR-106a-5p mimics, when used individually at 50 nM, or in combination at a combined final concentration of 50 nM, displayed similar growth patterns. The results suggested these two miR-17 family miRNAs which shared the same seed sequence, behaved similarly and were probably interchangeable in promoting cell proliferation.

The role of miR-20b-5p and miR-106a-5p in enhancing cell proliferation was further shown in MTT analysis, BrdU assay and cell cycle analysis (Figures 4.11C - 4.11E). In MTT analysis, WJ0706 cells entered the exponential phase on day 3 post-transfection. On day 6, higher absorbance reading was obtained on over-expression of miR-20b-5p and/or miR-106a-5p mimics, indicating higher number of viable cells and thus greater cell proliferation rate (Figure 4.11C). The presumptive interchangeable behaviour between miR-20b-5p and miR-106a-5p mimics was similarly observed. BrdU assays also demonstrated that cells transfected with miR-20b-5p and/or miR-106a-5p mimics exhibited greater DNA synthesis rate than in the negative mimic-transfected control cells, as indicated by higher absorbance reading at 450 nm (Figure 4.11D). Besides, miRNA mimics at 50 nM concentration showed slightly greater DNA synthesis rate than at 25 nM concentration,

suggesting that the miRNA affected the DNA synthesis rate in a dosage-dependent manner. Cell cycle analysis showed that higher percentage of cells that transiently over-expressed miR-20b-5p and/or miR-106a-5p entered the S- and G2-phase of the cell cycle, further supporting that miR-20b-5p and miR-106a-5p act to promote cell proliferation (Figure 4.11E).

The results collectively lead to the proposal that miR-20b-5p and miR-106a-5p enhance cell proliferation in MSCs, echoing the microarray data whereby the two miRNAs were first shown to be down-regulated in senescence MSCs.

4.12 miR-20b-5p and miR-106a-5p Target G1/S-phase Cell Cycle Genes

Online databases, MicroT-CDS, miRTarBase, Miranda and TargetScan, were used to identify possible target transcripts of the down-regulated miR-17 family miRNAs in OSIPS MSCs and to further elucidate possible miR-17 involvement in senescence-related G1/S-phase regulatory pathways. The miR-17 miRNAs that are highly homologous and share identical seed sequences are predicted to target on cell cycle factors that streamline their regulatory effects on E2F1 transcription factor, thus directly governing G1/S-transition of the cell cycle (Figure 4.12). Interestingly, the predicted putative targets include both pro- and anti-proliferative genes. The X-chromosomal miR-20b-5p and miR-106a-5p, the focus of the present work, are predicted to regulate the pro-proliferative genes cyclin D1 and D2 (CCND1/2), CDK6 and E2F1 and the

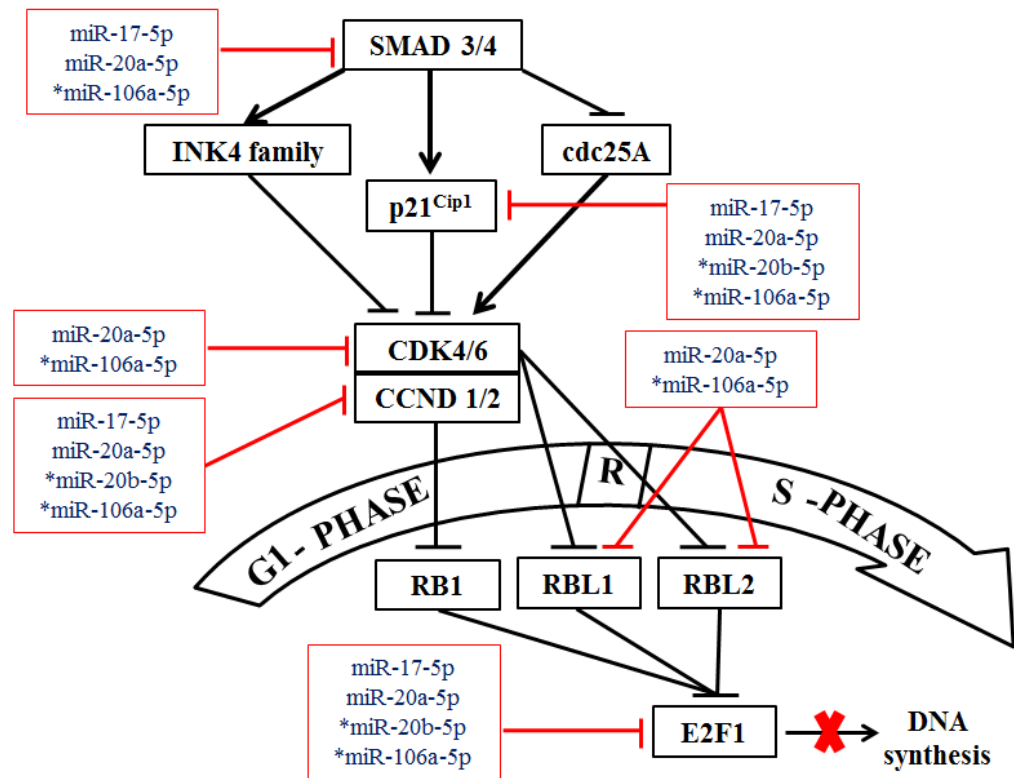


Figure 4.12 Predicted targets of the G1/S-phase cell cycle of the down-regulated miR-17 family miRNAs in OSIPS MSCs. Black arrows and black blunted lines show selected G1/S-phase factors (boxed in black) of the cell cycle. Blunted red lines indicate negative regulation by the miR-17 family miRNAs (boxed in red). R: the restricted entry point of the cell cycle

anti-proliferative gene p21 to govern the S-phase transition. The bioinformatics prediction is supported by previous reports on the involvement of miR-17 family miRNAs, viz. miR-17, miR-20a and miR-106b, in cell cycle regulation in human embryonic kidney (HEK) 293T cells, human cord blood derived unrestricted somatic stem cells and normal human fibroblast cells (Cloonan et al., 2008; Wang et al., 2008; Yu et al., 2008; Pickering et al., 2009; Trompeter et al., 2011).

Luciferase assays were performed to verify miR-20b-5p/miR-106a-5p direct targeting of transcripts of the cell cycle genes CCND1, CCND2, retinoblastoma transcriptional corepressor like 1 (RBL1/p107), retinoblastoma transcriptional corepressor like 2 (RBL2/p130), E2F1 and p21. Web-based bioinformatics analysis indicated that miR-20b-5p targeted multiple sites in the 3'-untranslated region (3'-UTR) of the CCND1/2, E2F1 and p21 transcripts, while miR-106a-5p was predicted to target all six cell cycle genes (Figure 4.13). Full-length or segments of 3'-UTR of each target transcript of interest were cloned into the dual luciferase (*Firefly/Renilla*) reporter vector pmirGLO (Trompeter et al., 2011). The verification of plasmids is shown in Appendix J.

Blank pmirGLO or pmirGLO/3'-UTR constructs were co-transfected into HCT-15 cells in the absence or presence of the miR-20b-5p or miR-106a-5p mimic, or a non-specific negative control, to test for effect of miRNAs on the luciferase activities (Figure 4.14). On co-transfection of the pmirGLO/3'UTR constructs and the miR-20b-5p mimic, only the anti-proliferative gene p21 showed significant reduction in luciferase activities,

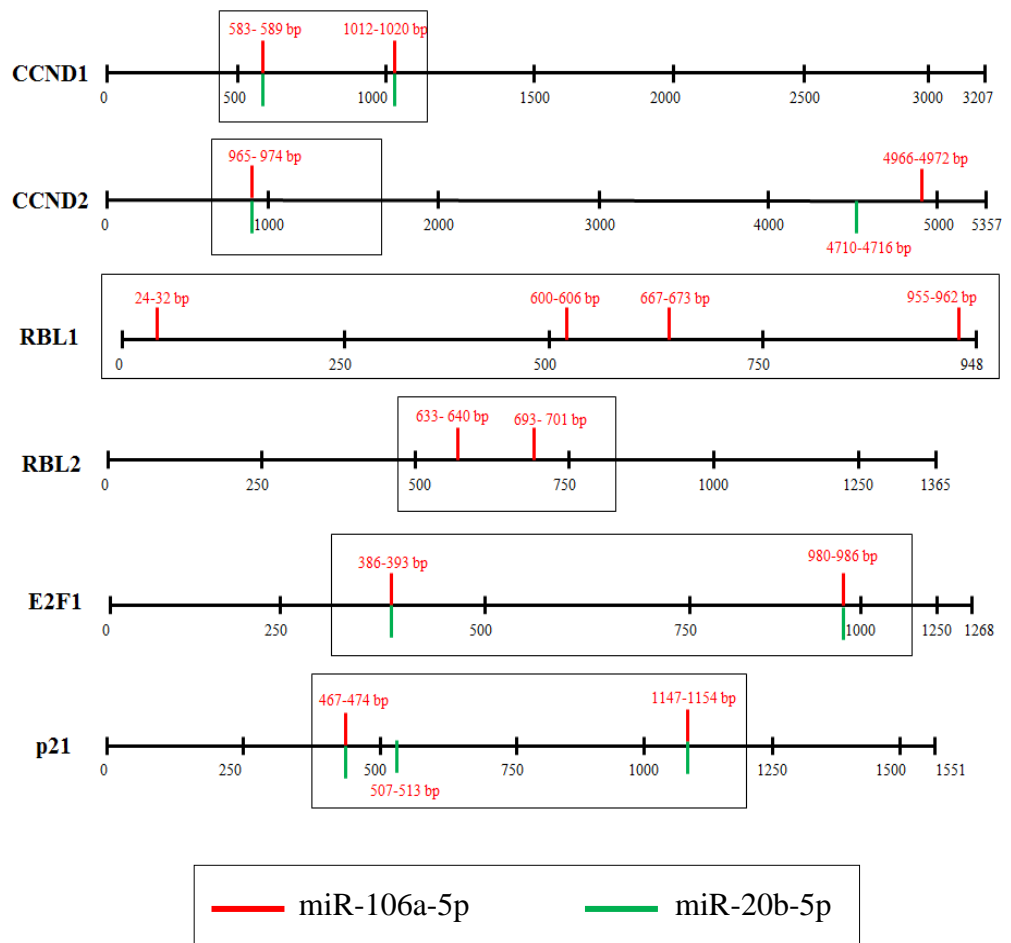


Figure 4.13 G1/S-phase cell cycle targets of the miR-20b-5p and miR-106a-5p. Schematic diagram displaying 3'-UTR of cell cycle transcripts, CCND1, CCND2, RBL1, RBL2, E2F1 and p21, with predicted miR-20b-5p (vertical green bar) and/or miR-106a-5p (vertical red bar) target sites (Trompeter et al., 2011). Black boxes indicate the 3'UTR segments cloned into the pmirGLO vector.

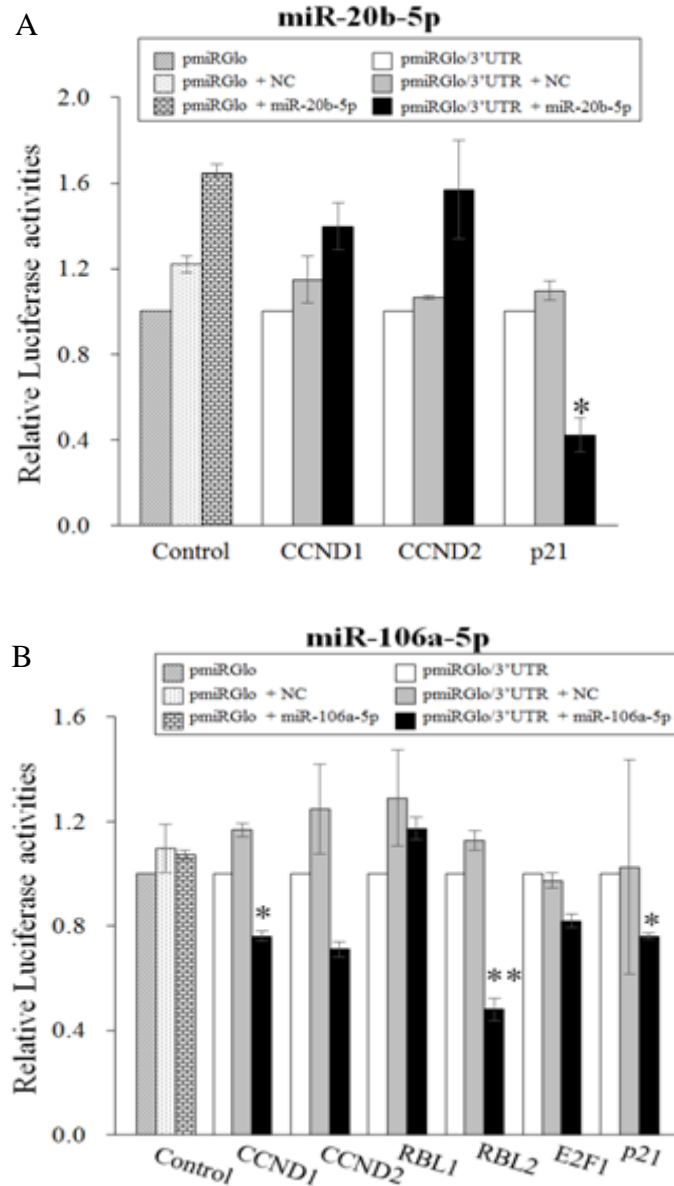


Figure 4.14 Validation of targeting of miR-20b-5p (A) and miR-106a-5p (B) at the cell cycle transcripts in luciferase assays. HCT-15 cells were co-transfected with pmirGLO/3'UTR, or the pmirGLO blank vector, and a miR-20b-5p or miR-106a-5p mimic, or a negative control mimic. Data presented were from two independent experiments, in triplicates. * $p < 0.05$ and ** $p < 0.01$ were considered significant compared to the pmirGLO or pmirGLO/3'-UTR vector, set as 1.0.

indicating specific targeting (Figure 4.14A). On the other hand, miR-106a-5p down-regulated the luciferase activities of all the G1/S-phase genes tested, with the exception of RBL1/p107, and weakly for E2F1 (Figure 4.14B). The luciferase assay data confirmed that miR-20b-5p and miR-106a-5p directly targeted on specific cell cycle-associated target genes.

The luciferase data were supported by an inverse association between miRNAs mimics and cell cycle transcripts levels as shown by qRT-PCR (Figure 4.15; Appendix K). On over-expression of miR-20b-5p/miR-106a-5p mimics in WJ0706, expression of anti-proliferative p21 and pro-proliferative CDK6, CCND1 and E2F1 was significantly suppressed. Taken together, the results demonstrated that miR-20b-5p and miR-106a-5p negatively regulate the expression of both pro- and anti-proliferative cell cycle genes.

4.13 miR-20b-5p and miR-106a-5p Regulate G1/S-phase Cell Cycle Genes

To confirm miR-20b-5p and miR-106a-5p regulation of G1/S-phase transcripts in OSIPS cells, changes in endogenous mRNA and protein expression levels of the cell cycle transcripts p21, CDK6, CCND1 and E2F1 in three OSIPS MSC lines were carried out. Real-time RT-PCR revealed that the mRNA levels of p21, CDK6 and CCND1 were significantly up-regulated in all three OSIPS MSC lines; however, E2F1 showed down-regulated expression (Figure 4.16; Appendix L). Western blot analysis confirmed similar increased

protein levels of p21, CDK6 and CCND1 in different OSIPS MSC lines except for CDK6 in WJ2000 cells (Figure 4.17). As miRNA negatively regulates target genes at the post-transcriptional level, up-regulated expression of CDK6, CCND1 and p21 is consistent with down-regulation of miR-20b-5p and miR-106a-5p in OSIPS MSC lines. Despite suppressed E2F1 mRNA level, the E2F1 protein level was down-regulated in WJ2000 cells but no significant changes were observed in other two OSIPS MSC lines. The data are consistent with the supposition that miR-20b-5p and miR-106a-5p contribute to premature senescence by targeting the p21/CDK/CCND/E2F1 pathway, resulting in blockage of the G1-to-S-phase transition.

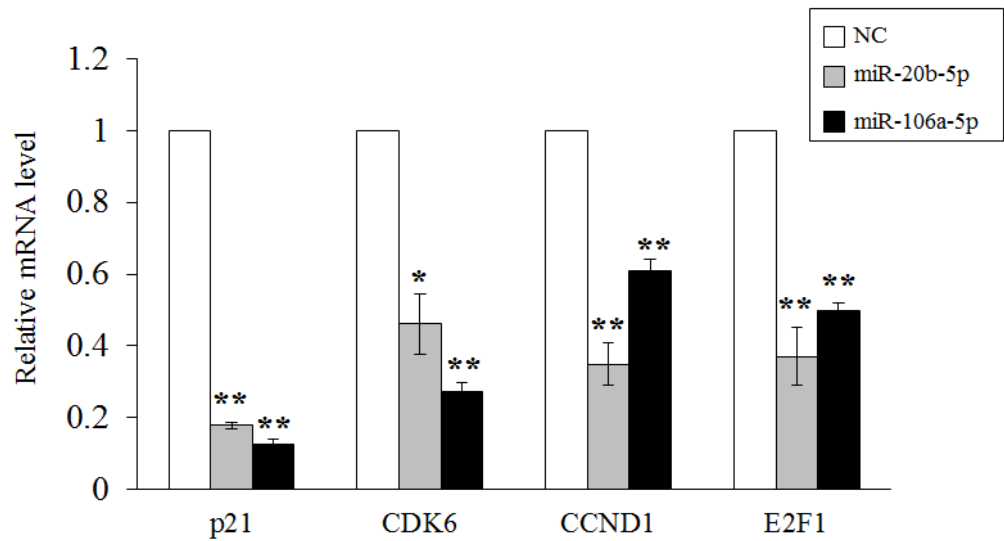


Figure 4.15 Inhibition of the cell cycle genes by miR-20b-5p/miR-106a-5p. WJ0706 cells were transfected with the miR-20b-5p or miR-106a-5p mimic, followed by qRT-PCR analysis. Data presented were from three independent experiments, in triplicates. * $p < 0.05$ and ** $p < 0.01$ were relative to the negative mimic-treated samples (NC), set as 1.0. The relative fold change values are shown in Appendix K.

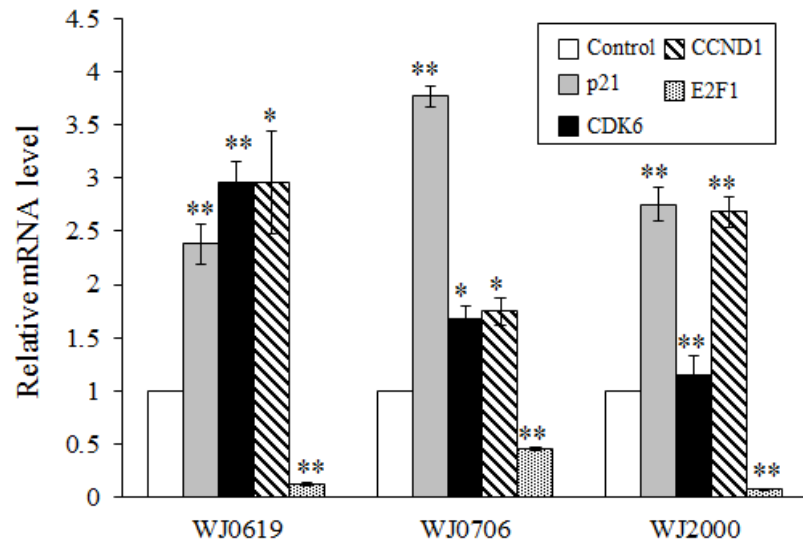


Figure 4.16 mRNA expression levels of the cell cycle target genes in H₂O₂-treated WJ-MSCs by real-time RT-PCR. Data presented were from three independent experiments, in triplicates. * $p < 0.05$ and ** $p < 0.01$ were derived compared to the untreated control samples, set as 1.0. The relative fold change values are shown in Appendix L.

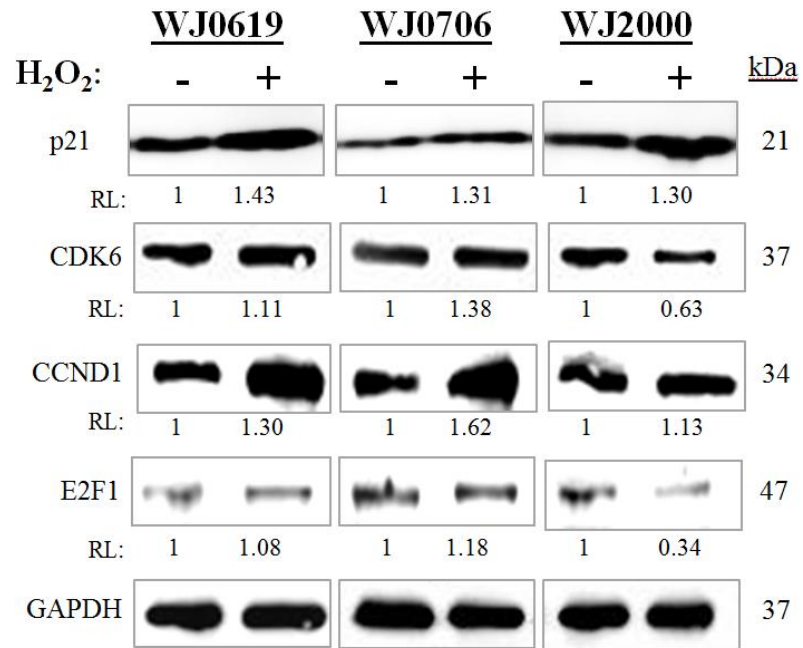


Figure 4.17 Protein expression levels of p21, CDK6, CCND1 and E2F1 in OSIPS WJ-MSCs by western blot analysis. GAPDH was included as a loading control. RL, relative levels compared to the untreated control samples, set as 1.0.

CHAPTER 5

DISCUSSION

5.1. Establishment of Premature Senescence in WJ-MSCs by Hydrogen Peroxide Treatment

Replicative senescence impairs the regenerative capacity of cells in general, thus hampering the applications of MSCs in tissue engineering and regenerative medicine (Gu et al., 2016). This study demonstrated that treatment of MSCs with hydrogen peroxide (H_2O_2) at 200 μ M for 2 h was sufficient to induce premature senescence in WJ-MSCs, a model which is useful for further studies on molecular mechanisms that regulate senescence. The premature senescence state in WJ-MSCs was validated by morphological changes, positive β -galactosidase staining, up-regulation of senescence biomarkers (Figure 4.3 – 4.4) and increased number of cell arrested at the G1-phase of the cell cycle (Table 4.1), consistent with the previous reports in stress-induced premature senescence MSCs isolated from bone marrow (BM-MSCs), human endometrium (hMESC) and umbilical cord blood (Brandl et al., 2011; Burova et al., 2013; Ko et al., 2012).

Burova et al. (2013) showed that MSCs derived from human endometrium (hMESC) was susceptible to H_2O_2 exposure up to 900 μ M. In contrast, H_2O_2 treatment at low dosage, i.e. 10 μ M, did not affect the

proliferation rate, morphology and β -galactosidase staining in bone marrow and adipose tissue-derived MSCs (hAMSCs) (Brandl et al., 2011; Chen et al., 2015). Another studies further showed that H_2O_2 at 50 μ M concentration required at least 24 h-prolonged treatment to trigger premature senescence in hMESC and hAMSCs (Burova et al., 2013; Chen et al., 2015). In this study, the MSCs derived from Wharton's Jelly were able to tolerate the oxidative stress up to 200 μ M concentration, whereby higher H_2O_2 concentrations led to cell death (Figure 4.2), suggesting that human MSCs from various sources may have different tolerance in response to oxidative stress (Ko et al., 2012).

Endogenous level of ROS is shown to be elevated in bone marrow-derived MSCs (BM-MSCs) under prolonged cultured, leading to onset of replicative senescence (RS) (Jeong and Cho, 2015). It has previously been shown that late-passage and H_2O_2 -treated hAMSCs shared similar senescence features, including cell proliferation rate, SA- β -Gal staining, cell cycle dynamics, multilineage differentiation capacity, and expression of pluripotency and cell cycle genes and differentiation markers (Chen et al., 2015). The observation was in line with the data presented in this study in which the OSIPS WJ-MSCs displayed similar cellular and molecular characteristic as cells in RS, as well as comparable miR-17 family miRNAs profile. The demonstrated similarities supported the use of OSIPS cells as study model to further dissect the molecular events in senescence.

5.2. Senescence-deregulated miRNAs are Frequently Associated with Cancer

miRNA microarray analysis was performed to compare the miRNA profiles of untreated control and OSIPS MSCs. In the up-regulated miRNAs in OSIPS MSCs (Table 4.4), the miR-146 family members, miR-146a and miR-146b, have previously been described as negative regulators of NF- κ B, and are involved in regulating immune response and tumour genesis and progression (Li et al., 2012; Yang and Wang, 2016). miR-146a was also shown to be differentially expressed in late-passage replicative senescence human fibroblasts and endothelial cells (Bonifacio and Jarstfer, 2010; Olivieri et al., 2013). Besides the miR-146 miRNAs, the other five four-digits miRNAs in the up-regulated group in OSISP MSCs were first reported in deep sequencing of small RNA transcriptome of normal and malignant B cells, melanoma and breast cancer (Jima et al., 2010; Stark et al., 2010; Persson et al., 2011). The miR-4372-5p gene is located closely to the ERBB2 receptor gene, which is frequently amplified and over-expressed in breast cancer cells (Persson et al., 2011). Over-expression of miR-3178 in hepatocellular carcinoma tumour endothelial cells was shown to inhibit cell proliferation and promote apoptosis and G1-phase arrest *in vitro* (Li et al., 2015), suggesting a possible role of miR-3178 in regulating senescence in OSIPS MSCs, a speculation which requires future experimental validation.

In the down-regulated miRNA group in the OSIPS cells (Table 4.4), miR-16 is a well-characterised tumour suppressor miRNA that regulates cell

proliferation and apoptosis, by targeting multiple oncogenes, including BCL2, MCL1, CCND1, WNT3A and SMAD3 (Aqeilan et al., 2010; Li et al., 2015). The four miR-17 family members, namely miR-17-5p, miR-20a-5p, miR-20b-5p and miR-106a-5p, are paralogous genes located in the miR-17/92 and miR-106a/363 clusters on chromosomes 13 and X, respectively (Figure 5.1) (Mogilyansky and Rigoutsos, 2013). Members of the chromosomal 13 miR-17/92 clusters have been extensively studied, mainly in their roles in tumorigenesis (Table 5.1). Over-expression of the oncogenic miR-17/92 cluster has been reported in the development of hepatocellular carcinoma, lung cancers, cardiovascular diseases and immune diseases (Mogilyansky and Rigoutsos, 2013; Yau et al., 2013; Zhu et al., 2015). Deregulation of the miR-17/92 targets, including E2F1, TP53INP1, TGF β and PTEN, has also been shown to contribute to abnormal cell proliferation, tumour growth, apoptosis and metastasis (Tan et al., 2014). The miR-106a/363 cluster was shown to behave as an oncogene under specific circumstances, but transcriptional regulation of the miRNA expression is still unclear (Concepcion et al., 2012). Taken together, the deregulated miR-17 miRNAs in OSIPS WJ-MSCs seem to share common regulatory mechanism(s) in senescence and in the tumorigenesis process.

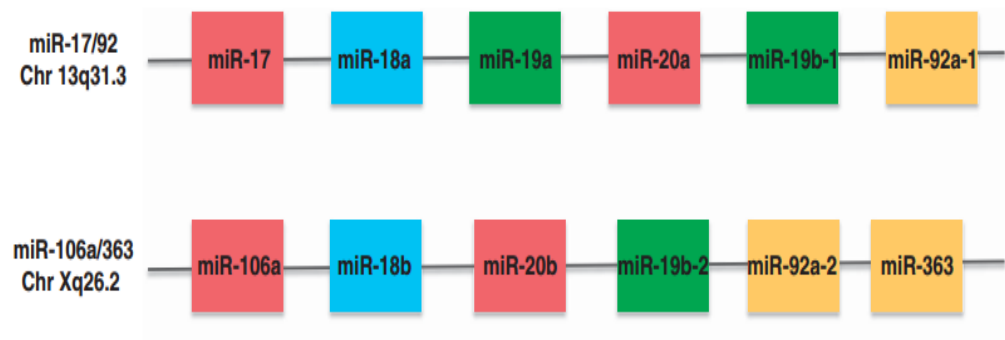


Figure 5.1 Schematic representation of the miR-17/92 and miR-106a/363 paralogs and their chromosomal location. Red indicates the miR-17 family members; blue indicates the miR-18 family members; green indicated the miR-19 family members; orange indicates the miR-92 family members. (Figure adapted from Mogilyansky and Rigoutsos, 2013)

Table 5.1 Relative expression of miRNAs from the miR-17/92 and miR-106a/363 clusters in normal development, cancer, other diseases and age-related conditions (Mogilyansky and Rigoutsos, 2013)

miRNAs	Normal development				Hematopoietic cancer								Cancer								Other diseases										
	Normal skeletal formation	Lung and heart development	B-cell development	T-cell development	B-cell lymphoma	Diffuse large B-cell lymphoma	B-cell CLL	MLL rearrangements	AML t (8;21)	AML t (15;17)	T-cell lymphoma	T-cell ALL	Multiple myeloma	Retinoblastoma	Colorectal cancer	Head and neck cancer	Pancreatic cancer	Breast cancer	Ovarian cancer	Lung cancer	Renal cancer	Hepatocellular carcinoma	Osteosarcoma	Gastric cancer	Nasopharyngeal cancer	Urothelial cancer	Autoimmunity	Cardiovascular diseases	Alzheimer's disease	Multiple sclerosis	Ageing
miR-17	*	*	*	*	+	+	+	+	-	+	+	+	+	+	+	+	+	+	+	+	+	+	+	+	+	+	+	+	-	-	-
miR-18a	*	*			+	+	+			+				+	+	+	+				+	+		+	+	+			+		
miR-19a	*	*			+	+	+			+				+	+	+	+				+	+	+			+	+				
miR-20a	*	*			+	+	+		-	-	+	+	+	+	+	+	+	+	+	+	+	+	+			+	+		-	-	-
miR-19b-1	*	*	*	*	+	+	+			+				+	+	+	+				+	+				+	+			-	-
miR-92a-1	*	*				+	+	+	-	+		+		+	+		+				+	+				+	+		-	-	-
miR-106a							+																						-	-	-
miR-18b																	+														

*: miRNA is important for normal development; '+': over-expressed miRNAs; '-': under-expressed

5.3. miR-17 miRNAs are Important Regulators of G1/S-phase Transition of the Cell Cycle in OSIPS WJ-MSCs

The down-regulated members of the miR-17 family miRNAs share the same seed sequences and target a large number of G1/S-phase cell cycle genes (Figure 4.12). It was validated in this work that the less studied miR-20b-5p and/or miR-106a-5p from the miR-106a/363 cluster targeted on both pro- and anti-proliferative genes, consistent with report by Cloonan et al. (2008) that demonstrated direct targeting of miR-17 and miR-20a, also of the miR-17 family, at genes in the cell cycle. Additionally, different members of miRNA clusters often act synergistically to target the same transcripts in a pathway (Concepcion et al., 2012), further supporting the interchangeability of the miR-20b-5p and miR-106a-5p in regulating G1/S-phase transcripts of the cell cycle (Figure 4.11; Figure 4.15). Other studies also showed that miR-17 family miRNAs affect the p21/CCND/CDK cascade in modulating E2F activity and the G1/S-phase of the cell cycle (Yu et al., 2008). In stress-induced premature senescence fibroblasts and human trabecular meshwork cells, miR-17 down-regulation induced p21 expression (Li et al., 2009), as observed in this work. CDK4/6 kinases are expressed throughout the cell cycle and are only activated upon binding to specific D-type cyclins. Activated CDK4/6-CCND complexes subsequently phosphorylate the retinoblastoma proteins (pRB), leading to the release of E2F for DNA synthesis and S-phase progression (Neganova and Lako, 2008). A negative correlation between miR-17 miRNAs and CCND1 was observed in OSIPS MSCs (Figure 4.15), echoing with the observations reported in the breast cancer cells (Yu et al., 2008).

In this study, miR-17 family miRNAs was shown not only to target at the upstream p21, but also various checkpoints along the CCND/CDK/RB cascade to modulate E2F transcription factor that govern the G1/S-transition of the cell cycle (Figure 4.14).

5.4. A Proposed Model on the Role of miR-17 miRNAs in Oxidative-stress Senescence

When the miR-17 family miRNAs members, miR-20b-5p and miR-106a-5p were down-regulated in OSIPS WJ-MSCs, targeted transcripts of the pro-proliferative genes, CDK4/6 and CCND1/2, and the anti-proliferative p21, were up-regulated (Figure 4.16). E2F1 is an important and immediate activator of the S-phase cell cycle progression, and is shown here in luciferase assay as a direct target of miR-106a-5p, over-expression of which resulted in E2F1 suppression (Figure 4.15). However, on miR-17 family miRNAs down-regulation, E2F1 mRNA levels in all three different OSIPS MSC lines were also down-regulated (Figure 4.16), while the protein expression levels of E2F1 were either unchanged, or was only mildly suppressed in one of the three cell lines (Figure 4.17). Instead of the anticipated negative regulation, a previous study also confirmed that miR-17 and miR-20a positively modulated E2F1 activity (Trompeter et al., 2011), as was observed in this study.

The pro- and anti-proliferative effects of miR-17 miRNAs on the cell cycle are likely modulated by multiple factors. Any miRNA-mRNA interaction

and regulation is dependent not only on the presence of transcriptional regulators, but also on the relative miRNA abundance and affinity to the target transcripts (Cloonan et al., 2008; Trompeter et al., 2011). In HEK293T cells, the inhibitory effects of miR-17 miRNAs on anti-proliferative proteins are more profound than the inhibitory effects on the pro-proliferative E2F1 (Trompeter et al., 2011). Another study also showed that although the inhibition of miR-17 and miR-20a up-regulated E2F1 expression, yet the percentage of BrdU-positive proliferative cells remained low (Pickering et al., 2009). The works of Trompeter et al. (2011) and Pickering et al. (2009) and our study collectively indicate the importance of the physiological state of the cells, and spatial- and temporal-dependent relative abundance of specific factors in E2F1 regulation and in senescence.

Based on the data presented in this work, a model on the participation of oxidative stress-induced down-regulated miR-17 family miRNAs, represented here by miR-20b-5p and miR-106a-5p, in a possible mechanism regulating premature senescence was proposed (Figure 5.2). It is proposed that H₂O₂-induced oxidative stress-induced senescence in WJ-MSCs is the consequence of cumulative effects of three separate events regulating E2F1 transcription factor. Firstly, oxidative stress down-regulates miR-17 family miRNAs and enhances the expression of p21 and the downstream cascade of CCND/CDK/RB. Secondly, miR-17 miRNAs individually target and regulate the factors of the p21 cascade, as shown in luciferase assays. Thirdly, and probably independent of miR-17 regulation, the oxidative stress-triggered DNA damages may have activated the single- and double-strand repair

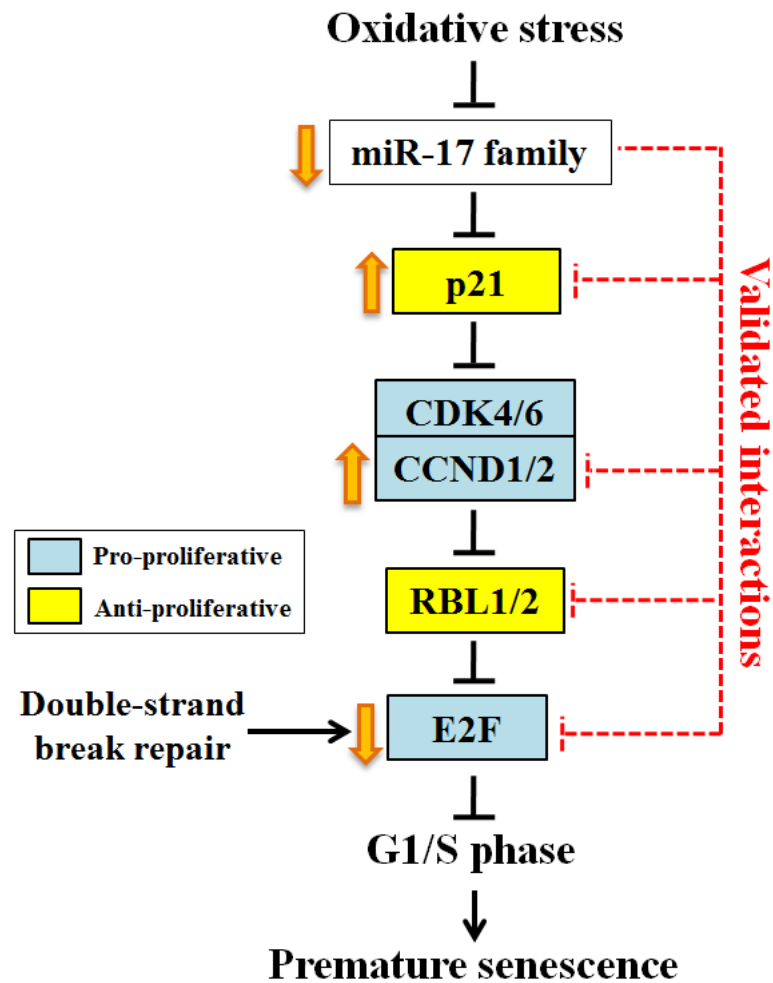


Figure 5.2 A proposed model illustrating the role of miR-17 family miRNAs in oxidative stress-induced premature senescence. The pro-proliferative genes are boxed in blue; the anti-proliferative genes are boxed in yellow. Thin arrows and solid blunt-ended lines indicate the proposed oxidative stress-initiated and miR-17-related cell cycle pathway leading to premature senescence. Red dashed lines show the G1/S-phase cell cycle targets of miR-17 miRNAs validated in luciferase assays in this study. Thick orange arrows represent changes in the mRNA or protein expression levels of the cell cycle genes validated in this study. See text for further description of the model.

mechanism to recruit E2F1 and CCND1 at the sites of the DNA breaks. E2F1 in turn promotes the localisation of repair factors at the damage sites (Castillo et al., 2015), and CCND1 further enhances the DNA damage repair mechanism (Casimiro et al., 2016). Subsequently, activated TopBP1 protein binds and positively modulates E2F1 to initiate temporary cell cycle arrest to endorse the DNA repair process under oxidative stress (Liu et al., 2004; Chen et al., 2011). The observed mild suppression or unaltered expression of E2F1 in the H₂O₂-treated cells may be the cumulative effects of the interactions and balances between the miR-17-dependent and miR-17-independent p21 regulatory pathway.

Taken together, the model illustrates that the observed down-regulated expression of miR-17 family miRNAs in H₂O₂-induced oxidative stress in MSCs lead to blockage of the G1/S-phase cell cycle transition by targeting at multiple G1/S-phase factors of the p21 pathway, and subsequently suppress cell proliferation and initiate premature senescence of MSCs.

CHAPTER 6

CONCLUSIONS

6.1 Conclusions

The use of mesenchymal stem cells (MSCs) in therapeutic applications is limited by the onset of senescence that diminishes the self-renewal and differentiation capacity of the cells. In this study, oxidative stress-induced premature senescence (OSIPS) in Wharton's Jelly-derived MSCs (WJ-MSCs) by H₂O₂ treatment was first established, which was then used as a model to study miRNA regulation in senescence. As the data showed high degree of resemblance between OSIPS WJ-MSCs and replicative senescence (RS) MSCs, the OSIPS WJ-MSC model may be a convenient source for cellular and molecular dissection in senescence studies.

In the microarray analysis, the identified dysregulated miRNAs in OSIPS WJ-MSCs were shown to be associated with cancer, suggesting a strong correlation between senescence-induced cell cycle arrest and cancer development. In the down-regulated miR-17 family in OSIPS cells, transient over-expression of the less studied miR-20b-5p and miR-106a-5p was shown to promote cell proliferation in WJ-MSCs. Bioinformatics and luciferase assay also validated that the miR-17 family members, miR-20b-5p and miR-106a-5p targeted and regulated both pro-and anti-proliferative cell cycle genes at the

G1/S-transition, further supporting significance roles of the miRNAs in cell cycle regulation. Based on the results obtained, a model on miR-20b-5p and miR-106a-5p regulation of MSCs senescence via regulation at G1/S-phase of the cell cycle was proposed.

Taken together, this study demonstrated that H₂O₂ induced oxidative stress in WJ-MSCs and down-regulated the expression of two miR-17 miRNAs, miR-20b-5p/miR-106a-5p, which regulate the G1/S-phase genes, leading to cell cycle arrest, inhibiting cell proliferation and subsequently triggering premature senescence.

6.2 Future Studies

Details of pathways and mechanisms involved in the onset of senescence, either prematurely or naturally, remain to be elucidated. H₂O₂-induced OSIPS MSCs are a promising model for further dissection on the molecular events in regulating premature, and possibly, replicative senescence. The OSIPS model may be useful for the screening of antioxidants and drugs that prevent, retard or revert cellular senescence. Furthermore, transcriptomic and proteomic studies may be carried out to investigate the effects of deregulated miRNAs on gene expression in OSIPS MSCs for better understanding on the basic elements of stress-induced senescence.

The results disclosed the important role of miR-17 miRNAs in senescence, suggested possible applications of miR-17 miRNAs to delay or revert senescence in that miRNA activities, gene regulatory network and signalling pathways may be restored by modulating miR-17 miRNA endogenous expression, thus inhibiting the onset of senescence. Delivery of miRNAs mimics into the cells for over-expression, or anti-miRNA for suppression, can be achieved by using chemically modified oligonucleotides and through adenoviral-, lentiviral- or nanoparticle-based technologies (Kota et al., 2009; Ma et al., 2010). However, it is also important to investigate possible side effects of miRNA-based therapy as each miRNA targets multiple transcripts; over-expression of miRNA mimics may interfere with the function of endogenous miRNAs and other target (Wang and Taniguchi, 2013). Thus, the safety and application of miRNAs as therapeutic agents need to be extensively studied. Detailed pharmacokinetics and pharmacodynamics studies should be carried out as well to determine the optimum dosage of oligonucleotides used in miRNAs-based treatment.

REFERENCES

- Acosta, J.C. et al., 2013. A complex secretory program orchestrated by the inflammasome controls paracrine senescence. *Nature cell biology*, 15(8), pp.978–990.
- Alt, E.U. et al., 2012. Aging alters tissue resident mesenchymal stem cell properties. *Stem Cell Research*, 8(2), pp.215–225.
- Andrades, J.A. et al., 2011. Skeletal Regeneration by Mesenchymal Stem Cells: What Else? In: Eberli, D., (ed.) *Regenerative Medicine and Tissue Engineering - Cells and Biomaterials*. InTech.
- Appelbaum, F.R., Forman, S.J., Negrin, R.S. and Blume, K.G., 2011. *Thomas' Hematopoietic Cell Transplantation*, Wiley.
- Aqeilan, R.I., Calin, G.A. and Croce, C.M., 2010. miR-15a and miR-16-1 in cancer: discovery, function and future perspectives. *Cell Death Differ*, 17(2), pp.215–220.
- Ayuzawa, R. et al., 2009. Naïve human umbilical cord matrix derived stem cells significantly attenuate growth of human breast cancer cells in vitro and in vivo. *Cancer letters*, 280(1), pp.31–37.
- Bartel, D.P., 2009. MicroRNAs: target recognition and regulatory functions. *Cell*, 136(2), pp.215–233.
- Batsali, A.K., Kastrinaki, M.C., Papadaki, H.A. and Pontikoglou, C., 2013. Mesenchymal stem cells derived from Wharton's Jelly of the umbilical cord: biological properties and emerging clinical applications. *Current stem cell research & therapy*, 8(2), pp.144–155.
- Becker, K.A. et al., 2006. Self-renewal of human embryonic stem cells is supported by a shortened G1 cell cycle phase. *Journal of cellular physiology*, 209(3), pp.883–893.
- Benjamini, Y. and Hochberg, Y., 1995. Controlling the false discovery rate: a practical and powerful approach to multiple testing. *Journal of the Royal Statistical Society. Series B (Methodological)*, pp.289–300.
- Bertoli, C., Skotheim, J.M. and de Bruin, R.A., 2013. Control of cell cycle transcription during G1 and S phases. *Nature reviews. Molecular cell biology*, 14(8), pp.518–28.
- Bilsland, A.E., Revie, J. and Keith, W., 2013. MicroRNA and senescence: the senectome, integration and distributed control. *Critical reviews in oncogenesis*, 18(4), pp.373–390.

- Boehm, M. and Slack, F., 2005. A developmental timing microRNA and its target regulate life span in *C. elegans*. *Science*, 310(5756), pp.1954–1957.
- Bonab, M.M. et al., 2006. Aging of mesenchymal stem cell in vitro. *BMC cell biology*, 7, p.14.
- Bonifacio, L.N. and Jarstfer, M.B., 2010. MiRNA profile associated with replicative senescence, extended cell culture, and ectopic telomerase expression in human foreskin fibroblasts. *PLoS ONE*, 5(9), pp.1–8.
- Brandl, A. et al., 2011. Oxidative stress induces senescence in human mesenchymal stem cells. *Experimental Cell Research*, 317(11), pp.1541–1547.
- Burova, E., Borodkina, A., Shatrova, A. and Nikolsky, N., 2013. Sublethal Oxidative Stress Induces the Premature Senescence of Human Mesenchymal Stem Cells Derived from Endometrium. *Oxid Med Cell Longev*, 2013.
- Campisi, J., 2013. Aging, cellular senescence, and cancer. *Annual review of physiology*, 75, pp.685–705.
- Can, A. and Karahuseyinoglu, S., 2007. Concise Review: Human Umbilical Cord Stroma with Regard to the Source of Fetus-Derived Stem Cells. *Stem Cells*, 25(11), pp.2886–2895.
- Caplan, A.I., 1991. Mesenchymal stem cells. *Journal of orthopaedic research : official publication of the Orthopaedic Research Society*, 9(5), pp.641–650.
- Caplan, A.I. and Dennis, J.E., 2006. Mesenchymal stem cells as trophic mediators. *Journal of cellular biochemistry*, 98(5), pp.1076–1084.
- Casimiro, M.C. et al., 2016. Cyclin D1 promotes androgen-dependent DNA damage repair in prostate cancer cells. *Cancer research*, 76(2), pp.329–338.
- Castillo, D.S. et al., 2015. E2F1 and E2F2 induction in response to DNA damage preserves genomic stability in neuronal cells. *Cell Cycle*, 14(8), pp.1300–1314.
- Castorina, A., Szychlinska, M., Marzagalli, R. and Musumeci, G., 2015. Mesenchymal stem cells-based therapy as a potential treatment in neurodegenerative disorders: is the escape from senescence an answer? *Neural Regeneration Research*, 10(6), p.850.
- Chaudhari, P., Ye, Z. and Jang, Y.Y., 2014. Roles of reactive oxygen species in the fate of stem cells. *Antioxidants & redox signaling*, 20(12), pp.1881–1890.
- Chen, G. et al., 2014. Monitoring the biology stability of human umbilical cord-derived mesenchymal stem cells during long-term culture in serum-free medium. *Cell and tissue banking*, 15(4), pp.513–521.

- Chen, J. et al., 2011. E2F1 promotes the recruitment of DNA repair factors to sites of DNA double-strand breaks. *Cell Cycle*, 10(8), pp.1287–1294.
- Chen, L.H. et al., 2010. MicroRNA and aging: A novel modulator in regulating the aging network. *Ageing Research Reviews*, 9(SUPPL.), pp.S59–S66.
- Chen, P.M. et al., 2015. c-Maf regulates pluripotency genes, proliferation/self-renewal, and lineage commitment in ROS-mediated senescence of human mesenchymal stem cells. *Oncotarget*, 6(34), pp.35404–35418.
- Cho, N.H. et al., 2004. Lifetime expression of stem cell markers in the uterine endometrium. *Fertility and sterility*, 81(2), pp.403–407.
- Christoffersen, N.R. et al., 2010. p53-independent upregulation of miR-34a during oncogene-induced senescence represses MYC. *Cell Death and Differentiation*, 17(2), pp.236–245.
- Cloonan, N. et al., 2008. The miR-17-5p microRNA is a key regulator of the G1/S phase cell cycle transition. *Genome biology*, 9(8), p.R127.
- Collins, S.D., Baffour, R. and Waksman, R., 2007. Cell therapy in myocardial infarction. *Cardiovascular revascularization medicine : including molecular interventions*, 8(1), pp.43–51.
- Concepcion, C.P., Bonetti, C. and Ventura, A., 2012. The microRNA-17-92 family of microRNA clusters in development and disease. *Cancer journal (Sudbury, Mass.)*, 18(3), pp.262–267.
- Conconi, M.T. et al., 2011. Phenotype and differentiation potential of stromal populations obtained from various zones of human umbilical cord: an overview. *The Open Tissue Engineering and Regenerative Medicine Journal*, 4, pp.6–20.
- Cong, Y.S., Wright, W.E. and Shay, J.W., 2002. Human telomerase and its regulation. *Microbiology and molecular biology reviews : MMBR*, 66(3), pp.407–425.
- Crisostomo, P.R. et al., 2008. Human mesenchymal stem cells stimulated by TNF-alpha, LPS, or hypoxia produce growth factors by an NF kappa B but not JNK-dependent mechanism. *American journal of physiology. Cell physiology*, 294(3), pp.C675–682.
- Dimri, G.P. et al., 1995. A biomarker that identifies senescent human cells in culture and in aging skin in vivo. *Proceedings of the National Academy of Sciences of the United States of America*, 92(20), pp.9363–9367.
- Ding, Y. et al., 2009. Mesenchymal stem cells prevent the rejection of fully allogenic islet grafts by the immunosuppressive activity of matrix metalloproteinase-2 and -9. *Diabetes*, 58(8), pp.1797–1806.

- Dominici, M. et al., 2006. Minimal criteria for defining multipotent mesenchymal stromal cells. The International Society for Cellular Therapy position statement. *Cytotherapy*, 8(4), pp.315–317.
- Dumble, M. et al., 2007. The impact of altered p53 dosage on hematopoietic stem cell dynamics during aging. *Blood*, 109(4), pp.1736–1742.
- Duscher, D. et al., 2014. Aging disrupts cell subpopulation dynamics and diminishes the function of mesenchymal stem cells. *Scientific reports*, 4, p.7144.
- Faraonio, R. et al., 2012. A set of miRNAs participates in the cellular senescence program in human diploid fibroblasts. *Cell Death and Differentiation*, 19(4), pp.713–721.
- Feliciano, A., Sánchez-Sendra, B., Kondoh, H. and Lleonart, M.E., 2011. MicroRNAs Regulate Key Effector Pathways of Senescence. *Journal of aging research*, 2011(August), p.205378.
- Friedenstein, A.J., Piatetzky-Shapiro, I.I. and Petrakova, K.V., 1966. Osteogenesis in transplants of bone marrow cells. *Journal of embryology and experimental morphology*, 16(3), pp.381–390.
- Fukada, S., Ma, Y. and Uezumi, A., 2014. Adult stem cell and mesenchymal progenitor theories of aging. *Frontiers in Cell and Developmental Biology*, 2(March), pp.1–9.
- Gauron, C. et al., 2013. Sustained production of ROS triggers compensatory proliferation and is required for regeneration to proceed. *Scientific reports*, 3, p.2084.
- Greco, S.J. and Rameshwar, P., 2012. Mesenchymal stem cells in drug/gene delivery: implications for cell therapy. *Therapeutic delivery*, 3(8), pp.997–1004.
- Gu, Y. et al., 2016. Changes in mesenchymal stem cells following long-term culture in vitro. *Molecular Medicine Reports*, 13(6), pp.5207–5215.
- Guo, W.T., Wang, X.W. and Wang, Y., 2014. Micro-management of pluripotent stem cells. *Protein & cell*, 5(1), pp.36–47.
- Haines, D.D., Juhasz, B. and Tosaki, A., 2013. Management of multicellular senescence and oxidative stress. *Journal of Cellular and Molecular Medicine*, 17(8), pp.936–957.
- Han, I. et al., 2014. Umbilical cord tissue-derived mesenchymal stem cells induce apoptosis in PC-3 prostate cancer cells through activation of JNK and downregulation of PI3K/AKT signaling. *Stem cell research & therapy*, 5(2), p.54.

- Harman, D., 2006. Free Radical Theory of Aging: An Update: Increasing the Functional Life Span. *Annals of the New York Academy of Sciences*, 1067(1), pp.10–21.
- Hayflick, L. and Moorhead, P.S., 1961. The serial cultivation of human diploid cell strains. *Experimental cell research*, 25, pp.585–621.
- Hekimi, S., Lapointe, J. and Wen, Y., 2011. Taking a "good" look at free radicals in the aging process. *Trends in cell biology*, 21(10), pp.569–576.
- Honzarenko, M. et al., 2006. Human bone marrow stromal cells express a distinct set of biologically functional chemokine receptors. *Stem cells (Dayton, Ohio)*, 24(4), pp.1030–1041.
- Hunt, J.S., Langat, D.K., McIntire, R.H. and Morales, P.J., 2006. The role of HLA-G in human pregnancy. *Reproductive biology and endocrinology : RB&E*, 4 Suppl 1(Suppl 1), p.S10.
- Insinga, A., Cicalese, A. and Pelicci, P.G., 2014. DNA damage response in adult stem cells. *Blood Cells, Molecules, and Diseases*, 52(4), pp.147–151.
- Ivey, K.N. et al., 2010. MicroRNAs as Regulators of differentiation and cell fate decisions. *Cell Stem Cell*, 7(1), pp.36–41.
- Jackson, K.A. et al., 2001. Regeneration of ischemic cardiac muscle and vascular endothelium by adult stem cells. *The Journal of clinical investigation*, 107(11), pp.1395–1402.
- Jeong, S.G. and Cho, G.W., 2015. Endogenous ROS levels are increased in replicative senescence in human bone marrow mesenchymal stromal cells. *Biochemical and Biophysical Research Communications*, 460(4), pp.971–976.
- Jeschke, M.G. et al., 2011. Umbilical cord lining membrane and Wharton's Jelly-derived mesenchymal stem cells: the similarities and differences. *The Open Tissue Engineering and Regenerative Medicine Journal*, 4, pp.21–27.
- Jima, D.D. et al., 2010. Deep sequencing of the small RNA transcriptome of normal and malignant human B cells identifies hundreds of novel microRNAs. *Blood*, 116(23), pp.118–128.
- Kanda, Y., Hinata, T., Kang, S.W. and Watanabe, Y., 2011. Reactive oxygen species mediate adipocyte differentiation in mesenchymal stem cells. *Life sciences*, 89(7-8), pp.250–258.
- Kang, W. et al., 2015. Targeting of YAP1 by microRNA-15a and microRNA-16-1 exerts tumor suppressor function in gastric adenocarcinoma. *Molecular cancer*, 14, p.52.

- Kassis, I. et al., 2006. Isolation of mesenchymal stem cells from G-CSF-mobilized human peripheral blood using fibrin microbeads. *Bone marrow transplantation*, 37(10), pp.967–976.
- Khan, W.S. et al., 2009. The epitope characterisation and the osteogenic differentiation potential of human fat pad-derived stem cells is maintained with ageing in later life. *Injury*, 40(2), pp.150–157.
- Kim, D.W. et al., 2013. Wharton’s Jelly-derived mesenchymal stem cells: phenotypic characterization and optimizing their therapeutic potential for clinical applications. *International Journal of Molecular Sciences*, 14(6), pp.11692–11712.
- Kim, N. and Cho, S.G., 2013. Clinical applications of mesenchymal stem cells. *The Korean Journal of Internal Medicine*, 28(4), pp.387–402.
- Kim, V.N., 2005. MicroRNA biogenesis: coordinated cropping and dicing. *Nature reviews. Molecular cell biology*, 6(5), pp.376–385.
- Kinzler, K.W. and Vogelstein, B., 1997. Cancer-susceptibility genes. Gatekeepers and caretakers. *Nature*, 386(6627), pp.761–763.
- Ko, E., Lee, K.Y. and Hwang, D.S., 2012. Human umbilical cord blood-derived mesenchymal stem cells undergo cellular senescence in response to oxidative stress. *Stem Cells and Development*, 21(11), pp.1877–1886.
- Kota, J. et al., 2009. Therapeutic microRNA delivery suppresses tumorigenesis in a murine liver cancer model. *Cell*, 137(6), pp.1005–1017.
- Krishnamurthy, J. et al., 2006. p16INK4a induces an age-dependent decline in islet regenerative potential. *Nature*, 443(7110), pp.453–457.
- Kuilman, T., Michaloglou, C., Mooi, W.J. and Peeper, D.S., 2010. The essence of senescence. *Genes and Development*, 24(22), pp.2463–2479.
- Lander, A.D., 2009. The “stem cell” concept: is it holding us back? *Journal of biology*, 8(8), p.70.
- Lee, J.Y. et al., 2010. mTOR activation induces tumor suppressors that inhibit leukemogenesis and deplete hematopoietic stem cells after Pten deletion. *Cell stem cell*, 7(5), pp.593–605.
- Leow, S.N. et al., 2015. Safety and efficacy of human Wharton’s Jelly-derived mesenchymal stem cells therapy for retinal degeneration. *PLoS ONE*, 10(6), pp.1–20.
- Lenkala, D. et al., 2014. The impact of microRNA expression on cellular proliferation. *Human genetics*, 133(7), pp.931–938.

- Lewis, C.M. and Suzuki, M., 2014. Therapeutic applications of mesenchymal stem cells for amyotrophic lateral sclerosis. *Stem cell research & therapy*, 5(2), p.32.
- Li, G. et al., 2009. Alterations in microRNA expression in stress-induced cellular senescence. *Mechanisms of Ageing and Development*, 130(11-12), pp.731–741.
- Li, L. et al., 2015. MicroRNA-16-5p Controls Development of Osteoarthritis by Targeting SMAD3 in Chondrocytes. *Current pharmaceutical design*, 21(35), pp.5160–5167.
- Li, W. et al., 2015. Regulation of tumorigenesis and metastasis of hepatocellular carcinoma tumor endothelial cells by microRNA-3178 and underlying mechanism. *Biochemical and biophysical research communications*, 464(3), pp.881–887.
- Li, X. et al., 2012. 53BP1 functions as a tumor suppressor in breast cancer via the inhibition of NF- κ B through miR-146a. *Carcinogenesis*, 33(12), pp.2593–2600.
- Liu, K., Luo, Y., Lin, F.T. and Lin, W.C., 2004. TopBP1 recruits Brg1/Brm to repress E2F1-induced apoptosis, a novel pRb-independent and E2F1-specific control for cell survival. *Genes & development*, 18(6), pp.673–686.
- Lombard, D.B. et al., 2005. DNA repair, genome stability, and aging. *Cell*, 120(4), pp.497–512.
- López-otín, C. et al., 2013. Europe PMC funders group the hallmarks of aging. *Cell*, 153(6), pp.1194–1217.
- Lynam-Lennon, N., Maher, S.G. and Reynolds, J.V., 2009. The roles of microRNA in cancer and apoptosis. *Biological reviews of the Cambridge Philosophical Society*, 84(1), pp.55–71.
- Ma, L. et al., 2010. Therapeutic silencing of miR-10b inhibits metastasis in a mouse mammary tumor model. *Nature biotechnology*, 28(4), pp.341–347.
- Melton, C. and Blelloch, R., 2010. MicroRNA regulation of embryonic stem cell self-renewal and differentiation. *Advances in experimental medicine and biology*, 695, pp.105–117.
- De Miguel, M.P. et al., 2012. Immunosuppressive properties of mesenchymal stem cells: advances and applications. *Current molecular medicine*, 12(5), pp.574–591.
- Minieri, V. et al., 2015. Persistent DNA damage-induced premature senescence alters the functional features of human bone marrow mesenchymal stem cells. *Journal of Cellular and Molecular Medicine*, 19(4), pp.734–743.

- Mobarra, N. et al., 2015. Overexpression of microRNA-16 declines cellular growth, proliferation and induces apoptosis in human breast cancer cells. *In Vitro Cellular & Developmental Biology-Animal*, 51(6), pp.604–611.
- Mogilyansky, E. and Rigoutsos, I., 2013. The miR-17/92 cluster: a comprehensive update on its genomics, genetics, functions and increasingly important and numerous roles in health and disease. *Cell death and differentiation*, 20(12), pp.1603–1614.
- Molofsky, A.V. et al., 2006. Increasing p16INK4a expression decreases forebrain progenitors and neurogenesis during ageing. *Nature*, 443(7110), pp.448–452.
- Morrison, S.J. and Spradling, A.C., 2008. Stem cells and niches: mechanisms that promote stem cell maintenance throughout life. *Cell*, 132(4), pp.598–611.
- Mundra, V., Gerling, I.C. and Mahato, R.I., 2013. Mesenchymal stem cell-based therapy. *Molecular pharmaceuticals*, 10(1), pp.77–89.
- Neganova, I. and Lako, M., 2008. G1 to S phase cell cycle transition in somatic and embryonic stem cells. *Journal of Anatomy*, 213(1), pp.30–44.
- Nelson, G. et al., 2012. A senescent cell bystander effect: senescence-induced senescence. *Aging cell*, 11(2), pp.345–349.
- Nombela-Arrieta, C., Ritz, J. and Silberstein, L.E., 2011. The elusive nature and function of mesenchymal stem cells. *Nature reviews. Molecular cell biology*, 12(2), pp.126–131.
- O'Donnell, K. a et al., 2005. c-Myc-regulated microRNAs modulate E2F1 expression. *Nature*, 435(7043), pp.839–843.
- Ohtani, N., Mann, D.J. and Hara, E., 2009. Cellular senescence: Its role in tumor suppression and aging. *Cancer Science*, 100(5), pp.792–797.
- Olivieri, F. et al., 2013. MiR-146a as marker of senescence-associated pro-inflammatory status in cells involved in vascular remodelling. *Age*, 35(4), pp.1157–1172.
- Olivieri, F. et al., 2015. DNA damage response (DDR) and senescence: shuttled inflamma-miRNAs on the stage of inflamm-aging. *Oncotarget*, 6(34), pp.35509–35521.
- Pan, J.S., Hong, M.Z. and Ren, J.L., 2009. Reactive oxygen species: a double-edged sword in oncogenesis. *World journal of gastroenterology*, 15(14), pp.1702–1707.
- Park, K. and Kim, K.B., 2013. miRTar Hunter: a prediction system for identifying human microRNA target sites. *Molecules and cells*, 35(3), pp.195–201.

- Persson, H. et al., 2011. Identification of new microRNAs in paired normal and tumor breast tissue suggests a dual role for the ERBB2/Her2 gene. *Cancer Res.*, 71(1), pp.78–86.
- Pervaiz, S., Taneja, R. and Ghaffari, S., 2009. Oxidative stress regulation of stem and progenitor cells. *Antioxidants & redox signaling*, 11(11), pp.2777–2789.
- Pickering, M.T., Stadler, B.M. and Kowalik, T.F., 2009. miR-17 and miR-20a temper an E2F1-induced G1 checkpoint to regulate cell cycle progression. *Oncogene*, 28(1), pp.140–145.
- Pittenger, M.F. et al., 1999. Multilineage potential of adult human mesenchymal stem cells. *Science (New York, N.Y.)*, 284(5411), pp.143–147.
- Power, C. and Rasko, J.E., 2011. Promises and challenges of stem cell research for regenerative medicine. *Annals of internal medicine*, 155(10), pp.706–713, W217.
- Racz, G.Z. et al., 2014. Immunomodulatory and potential therapeutic role of mesenchymal stem cells in periodontitis. *Journal of physiology and pharmacology: an official journal of the Polish Physiological Society*, 65(3), pp.327–339.
- Raghuram, G.V. and Mishra, P.K., 2014. Stress induced premature senescence: a new culprit in ovarian tumorigenesis? *The Indian journal of medical research*, 140 Suppl(Suppl 1), pp.S120–129.
- Røslund, G.V. et al., 2009. Long-term cultures of bone marrow-derived human mesenchymal stem cells frequently undergo spontaneous malignant transformation. *Cancer research*, 69(13), pp.5331–5339.
- Rüster, B. et al., 2006. Mesenchymal stem cells display coordinated rolling and adhesion behavior on endothelial cells. *Blood*, 108(12), pp.3938–3944.
- Ritchie, M.E. et al., 2007. A comparison of background correction methods for two-colour microarrays. *Bioinformatics (Oxford, England)*, 23(20), pp.2700–2707.
- Schellenberg, A. et al., 2011. Replicative senescence of mesenchymal stem cells causes DNA-methylation changes which correlate with repressive histone marks. *Aging*, 3(9), pp.873–888.
- Shenghui, H.E. et al., 2009. Mechanisms of stem cell self-renewal. *Annual Review of Cell and Developmental*, 25, pp.377–406.
- Signer, R.A. and Morrison, S.J., 2013. Mechanisms that Regulate Stem Cell Aging and Life Span. *Cell Stem Cell*, 12(2), pp.152–165.

- Sikora, E., Arendt, T., Bennett, M. and Narita, M., 2011. Impact of cellular senescence signature on ageing research. *Ageing Research Reviews*, 10(1), pp.146–152.
- Smyth, G.K., 2005. Limma: linear models for microarray data. In: *Bioinformatics and computational biology solutions using R and Bioconductor*. Springer, pp. 397–420.
- Son, B.R. et al., 2006. Migration of bone marrow and cord blood mesenchymal stem cells in vitro is regulated by stromal-derived factor-1-CXCR4 and hepatocyte growth factor-c-met axes and involves matrix metalloproteinases. *Stem cells (Dayton, Ohio)*, 24(5), pp.1254–1264.
- Stark, M.S. et al., 2010. Characterization of the melanoma miRNAome by deep sequencing. *PLoS ONE*, 5(3), p.e9685.
- Stolzing, A., Jones, E., McGonagle, D. and Scutt, A., 2008. Age-related changes in human bone marrow-derived mesenchymal stem cells: consequences for cell therapies. *Mechanisms of ageing and development*, 129(3), pp.163–173.
- Suzuki, M. and Boothman, D. a, 2008. Stress-induced Premature Senescence (SIPS). *Journal of Radiation Research*, 49(2), pp.105–112.
- Sylvestre, Y. et al., 2007. An E2F/miR-20a autoregulatory feedback loop. *Journal of Biological Chemistry*, 282(4), pp.2135–2143.
- Tamura, M. et al., 2011. Wharton's Jelly stem cells as agents for cancer therapy. *The Open Tissue Engineering and Regenerative Medicine Journal*, 4, pp.39–47.
- Tan, W., Li, Y., Lim, S.G. and Tan, T.M., 2014. miR-106b-25/miR-17-92 clusters: Polycistrons with oncogenic roles in hepatocellular carcinoma. *World Journal of Gastroenterology*, 20(20), pp.5962–5972.
- Tazawa, H., Tsuchiya, N., Izumiya, M. and Nakagama, H., 2007. Tumor-suppressive miR-34a induces senescence-like growth arrest through modulation of the E2F pathway in human colon cancer cells. *Proceedings of the National Academy of Sciences*, 104(39), pp.15472–15477.
- Toussaint, O. et al., 2000. Stress-induced premature senescence. Essence of life, evolution, stress, and aging. *Annals of the New York Academy of Sciences*, 908, pp.85–98.
- Trompeter, H.I. et al., 2011. MicroRNAs miR-17, miR-20a, and miR-106b act in concert to modulate E2F activity on cell cycle arrest during neuronal lineage differentiation of USSC. *PLoS ONE*, 6(1).
- Uccelli, A., Moretta, L. and Pistoia, V., 2008. Mesenchymal stem cells in health and disease. *Nature reviews. Immunology*, 8(9), pp.726–736.

- Ullah, I., Subbarao, R.B. and Rho, G.J., 2015. Human mesenchymal stem cells - current trends and future prospective. *Bioscience reports*, 35(2).
- Vasudevan, S., Tong, Y. and Steitz, J.A., 2007. Switching from repression to activation: microRNAs can up-regulate translation. *Science (New York, N.Y.)*, 318(5858), pp.1931–1934.
- Wagner, W. et al., 2008. Replicative senescence of mesenchymal stem cells: A continuous and organized process. *PLoS ONE*, 3(5).
- Wagner, W., Ho, A.D. and Zenke, M., 2010. Different facets of aging in human mesenchymal stem cells. *Tissue Engineering Part B: Reviews*, 16(4), pp.445–453.
- Wang, Q. et al., 2008. miR-17-92 cluster accelerates adipocyte differentiation by negatively regulating tumor-suppressor Rb2/p130. *Proceedings of the National Academy of Sciences of the United States of America*, 105(8), pp.2889–2894.
- Wang, Q. et al., 2016. Comparative analysis of human mesenchymal stem cells from fetal-bone marrow, adipose tissue, and Warton’s jelly as sources of cell immunomodulatory therapy. *Human vaccines & immunotherapeutics*, 12(1), pp.85–96.
- Wang, Y. and Taniguchi, T., 2013. MicroRNAs and DNA damage response: implications for cancer therapy. *Cell cycle (Georgetown, Tex.)*, 12(1), pp.32–42.
- Watson, N. et al., 2015. Discarded Wharton jelly of the human umbilical cord: a viable source for mesenchymal stromal cells. *Cytotherapy*, 17(1), pp.18–24.
- Wei, X. et al., 2013. Mesenchymal stem cells: a new trend for cell therapy. *Acta Pharmacologica Sinica*, 34(6), pp.747–754.
- Williams, A.R. and Hare, J.M., 2011. Mesenchymal stem cells: Biology, patho-physiology, translational findings, and therapeutic implications for cardiac disease. *Circulation research*, 109(8), pp.923–940.
- Yamakuchi, M. and Lowenstein, C.J., 2009. MiR-34, SIRT1, and p53: The feedback loop. *Cell Cycle*, 8(5), pp.712–715.
- Yang, Y. and Wang, J.K., 2016. The functional analysis of MicroRNAs involved in NF- κ B signaling. *European review for medical and pharmacological sciences*, 20(9), pp.1764–1774.
- Yau, W.L. et al., 2013. Over-expression of miR-106b promotes cell migration and metastasis in hepatocellular carcinoma by activating epithelial-mesenchymal transition process. *PloS one*, 8(3), p.e57882.

- Ye, J. et al., 2012. Primer-BLAST: A tool to design target-specific primers for polymerase chain reaction. *BMC Bioinformatics*, 13(1), p.134
- Yu, Z. et al., 2008. A cyclin D1/microRNA 17/20 regulatory feedback loop in control of breast cancer cell proliferation. *Journal of Cell Biology*, 182(3), pp.509–517.
- Yun, M.H., 2015. Changes in regenerative capacity through lifespan. *International journal of molecular sciences*, 16(10), pp.25392–25432.
- Zhang, J. and Li, L., 2008. Stem cell niche: microenvironment and beyond. *J Biol Chem*, 283(15), pp.9499–9503.
- Zhang, Q. et al., 2011. Direct differentiation of atrial and ventricular myocytes from human embryonic stem cells by alternating retinoid signals. *Cell research*, 21(4), pp.579–587
- Zhu, H., Han, C. and Wu, T., 2015. MiR-17-92 cluster promotes hepatocarcinogenesis. *Carcinogenesis*, 36(10), pp.1213–1222.
- Zou, L., 2007. Single- and double-stranded DNA: building a trigger of ATR-mediated DNA damage response. *Genes & development*, 21(8), pp.879–885.
- Zuk, P.A. et al., 2001. Multilineage cells from human adipose tissue: implications for cell-based therapies. *Tissue engineering*, 7(2), pp.211–228.

APPENDICES

APPENDIX A

Fold change of senescence biomarkers in H₂O₂-treated WJ-MSC lines relative to the untreated control calculated by comparative $\Delta\Delta C_t$ method

Senescence biomarkers	Log(fold change) (Mean \pm SD)		
	WJ0619	WJ0706	WJ2000
p16	1.29 \pm 0.08	3.76 \pm 0.46*	2.07 \pm 0.15*
p21	2.38 \pm 0.19*	3.77 \pm 0.12**	2.75 \pm 0.16**
p53	1.44 \pm 0.13	1.19 \pm 0.10	0.44 \pm 0.08*
GLB1	2.99 \pm 0.37	1.56 \pm 0.09*	0.84 \pm 0.18

Three independent experiments were carried out. * $p < 0.05$ and ** $p < 0.01$ were derived as compared to the respective untreated control samples, set as 1.0. (Equivalent to Figure 4.4)

APPENDIX B

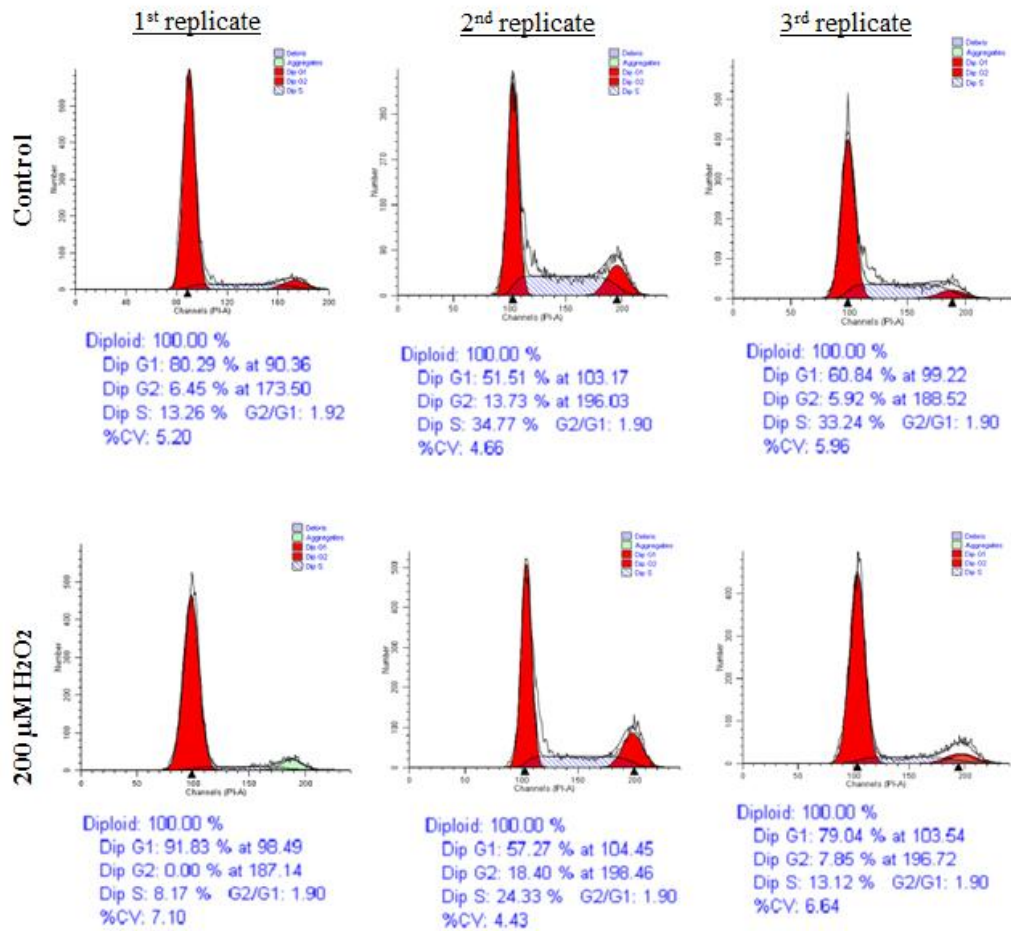
Fold change of senescence biomarkers in H₂O₂-treated and replicative senescence P23 WJ0706 relative to the untreated control calculated by comparative $\Delta\Delta C_t$ method

Senescence biomarkers	Log(fold change) (Mean \pm SD)		
	Control P7 WJ0706	H ₂ O ₂ -treated WJ0706	P23 WJ0706
p16	1	3.76 \pm 0.46*	0.86 \pm 0.07
p21	1	3.77 \pm 0.12**	13.09 \pm 0.09**
p53	1	1.19 \pm 0.10**	0.07 \pm 0.06*
GLB1	1	1.56 \pm 0.09	1.71 \pm 0.13*

Three independent experiments were carried out. * $p < 0.05$ and ** $p < 0.01$ were derived as compared to the untreated P7 control sample, set as 1.0. (Equivalent to Figure 4.5B)

APPENDIX C

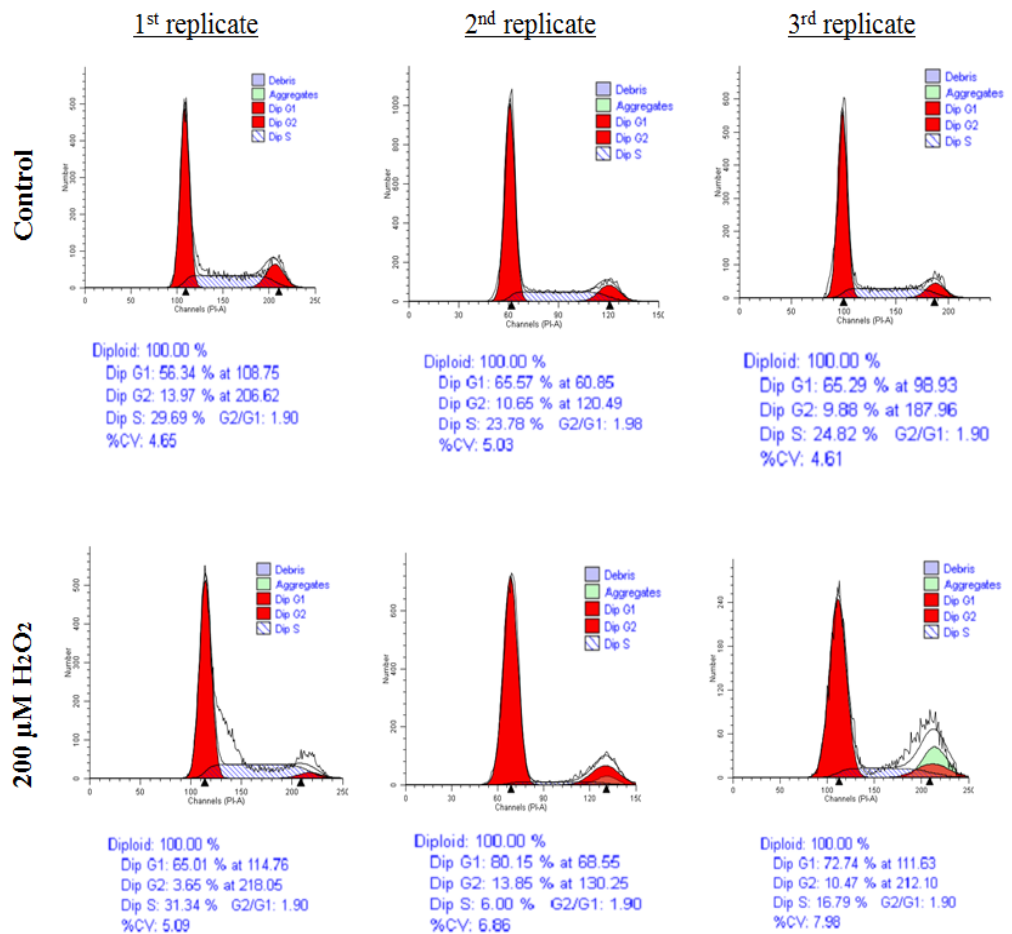
Cell cycle histograms of untreated control and H₂O₂-treated WJ0619 line by ModFit LT™ software (BD Biosciences)



Three independent experiments were carried out. (Equivalent to Table 4.1)

APPENDIX D

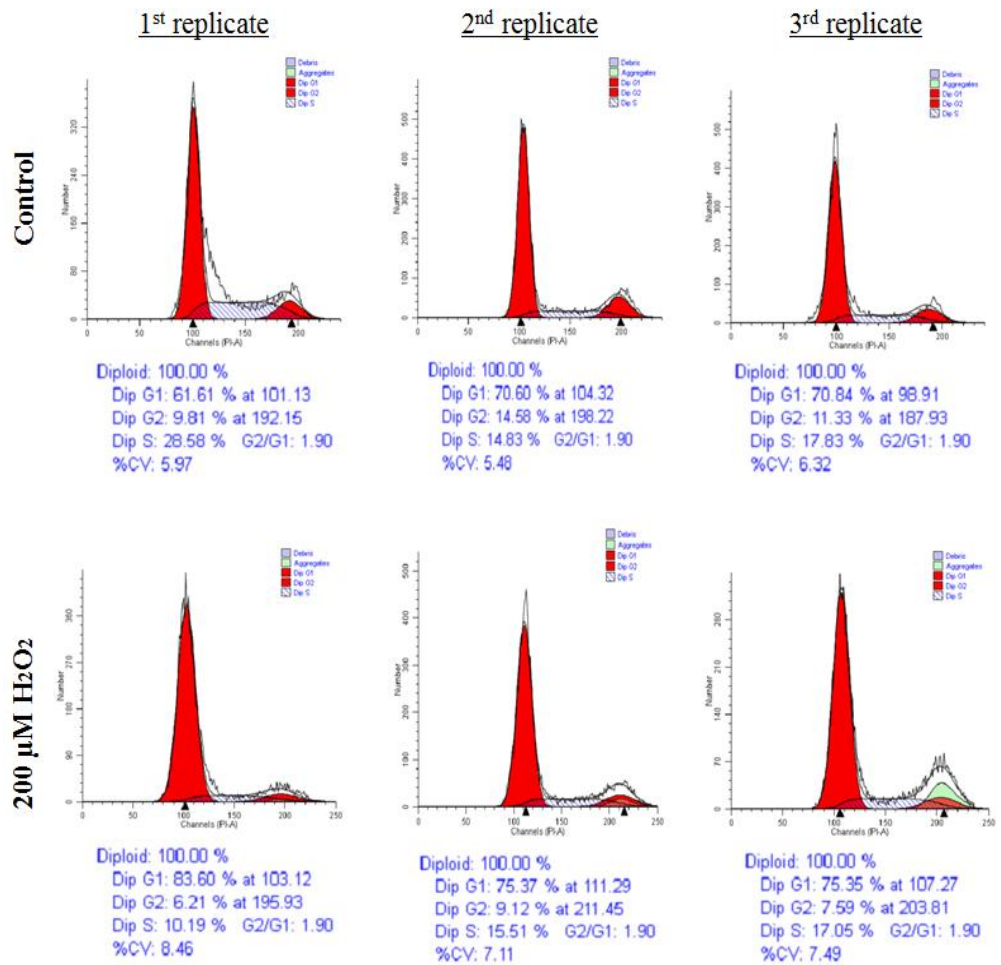
Cell cycle histograms of untreated control and H₂O₂-treated WJ0706 line by ModFit LT™ software (BD Biosciences)



Three independent experiments were carried out. (Equivalent to Table 4.1)

APPENDIX E

Cell cycle histograms of untreated control and H₂O₂-treated WJ2000 line by ModFit LT™ software (BD Biosciences)



Three independent experiments were carried out. (Equivalent to Table 4.1)

APPENDIX F

Fold change of miRNAs in three OSIPS WJ-MSC lines relative to the respective untreated control calculated by comparative $\Delta\Delta C_t$ method

miRNAs	Log(fold change) (Mean \pm SD)		
	WJ0619	WJ0706	WJ2000
	<u>Up-regulated group</u>		
miR-146a-5p	0.57 \pm 0.15	4.29 \pm 2.59**	11.88 \pm 0.82**
miR-146b-5p	0.27 \pm 0.04**	1.52 \pm 0.22	2.01 \pm 0.07**
	<u>Down-regulated group</u>		
miR-17-5p	0.13 \pm 0.02**	0.61 \pm 0.14	0.20 \pm 0.03**
miR-20a-5p	0.09 \pm 0.02**	0.62 \pm 0.12	0.29 \pm 0.07**
miR-20b-5p	0.15 \pm 0.05**	0.10 \pm 0.04**	0.25 \pm 0.06**
miR-106a-5p	0.15 \pm 0.07**	0.20 \pm 0.14*	0.33 \pm 0.03**

Three independent experiments were carried out. * $p < 0.05$ and ** $p < 0.01$ were derived as compared to the respective untreated control samples, set as 1.0. (Equivalent to Figure 4.8)

APPENDIX G

Fold change of miRNAs in H₂O₂-treated and replicative senescence P23 WJ0706 relative to the untreated control calculated by comparative $\Delta\Delta C_t$ method

miRNAs	Log(fold change) (Mean \pm SD)		
	Control WJ0706	H ₂ O ₂ -treated WJ0706	P23 WJ0706
<u>Up-regulated group</u>			
miR-146a-5p	1	4.29 \pm 2.59**	1.85 \pm 0.04*
miR-146b-5p	1	1.52 \pm 0.22	0.92 \pm 0.06
<u>Down-regulated group</u>			
miR-17-5p	1	0.61 \pm 0.14	0.25 \pm 0.11
miR-20a-5p	1	0.62 \pm 0.12	0.44 \pm 0.18
miR-20b-5p	1	0.10 \pm 0.04**	0.62 \pm 0.12
miR-106a-5p	1	0.20 \pm 0.14*	0.28 \pm 0.11*

Three independent experiments were carried out. * $p < 0.05$ and ** $p < 0.01$ were derived as compared to the untreated control WJ0706, set as 1.0. (Equivalent to Figure 4.9)

APPENDIX H

Fold change of miR-20b-5p and miR-106a-5p in H₂O₂-treated WJ0706 for 0.5 to 2 h, relative to the untreated control calculated by comparative $\Delta\Delta C_t$ method

Duration of 200 μ M H ₂ O ₂ treatment	Log(fold change) (Mean \pm SD)	
	miR-20b-5p	miR-106a-5p
Untreated control	1	1
0.5 h	0.27 \pm 0.19*	0.54 \pm 0.22
1 h	0.57 \pm 0.37	0.64 \pm 0.22*
1.5 h	0.54 \pm 0.38	0.53 \pm 0.18*
2 h	0.42 \pm 0.13**	0.52 \pm 0.14*

Three independent experiments were carried out. * $p < 0.05$ and ** $p < 0.01$ were derived as compared to the untreated control WJ0706, set as 1.0. (Equivalent to Figure 4.10A)

APPENDIX I

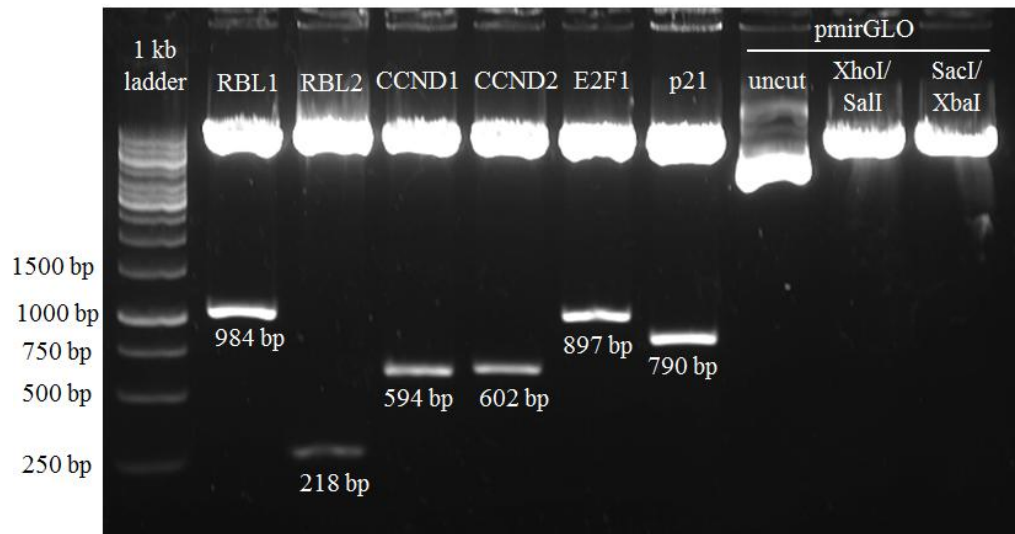
Fold change of miR-20b-5p and miR-106a-5p in H₂O₂-treated WJ0706 cultured in complete medium for different time points relative to the untreated control calculated by comparative $\Delta\Delta C_t$ method

Time points	Log(fold change) (Mean \pm SD)	
	miR-20b-5p	miR-106a-5p
Untreated control	1	1
16 h	0.11 \pm 0.05**	0.06 \pm 0.02**
32 h	0.22 \pm 0.09**	0.21 \pm 0.06**
48 h	0.24 \pm 0.11**	0.22 \pm 0.06**

Three independent experiments were carried out. * $p < 0.05$ and ** $p < 0.01$ were derived as compared to the untreated control WJ0706, set as 1.0. (Equivalent to Figure 4.10B)

APPENDIX J

Restriction enzyme digestion of plasmid DNA followed by gel electrophoresis



Plasmid pmirGLO carrying 3'-UTR of RBL1 gene was cut with XhoI/SalI restriction enzymes; pmirGLO carrying 3'-UTR of RBL2, CCND1/2, E2F1 and p21 were cut with SacI/XbaI restriction enzymes; pmirGLO without any insertion was cut with either XhoI/SalI or SacI/XbaI restriction enzymes or left uncut, as the control. 1kb ladder was use as the lane marker.

APPENDIX K

Fold change of cell cycle genes in WJ0706 cells over-expressed with miR-20b-5p or miR-106a-5p relative to the negative mimic control calculated by comparative $\Delta\Delta C_t$ method

Cell cycle genes	Log(fold change) (Mean \pm SD)		
	Negative mimic Control	miR-20b-5p	miR-106a-5p
p21	1	0.18 \pm 0.02**	0.12 \pm 0.03**
CDK6	1	0.46 \pm 0.14*	0.27 \pm 0.04**
CCND1	1	0.35 \pm 0.10**	0.61 \pm 0.06**
E2F1	1	0.37 \pm 0.14**	0.50 \pm 0.04**

Three independent experiments were carried out. * $p < 0.05$ and ** $p < 0.01$ were relative as compared to the negative mimic control sample, set as 1.0. (Equivalent to Figure 4.15)

APPENDIX L

**Fold change of cell cycle genes in three OSIPS WJ-MSC lines
relative to the respective untreated control cells
calculated by comparative $\Delta\Delta C_t$ method**

Cell cycle genes	Log(fold change) (Mean \pm SD)		
	WJ0619	WJ0706	WJ2000
p21	2.38 \pm 0.32**	3.77 \pm 0.17**	2.75 \pm 0.28**
CDK6	2.96 \pm 0.35**	1.68 \pm 0.21*	1.15 \pm 0.31**
CCND1	2.96 \pm 0.83*	1.75 \pm 0.23*	2.68 \pm 0.25
E2F1	0.12 \pm 0.02**	0.46 \pm 0.02**	0.08 \pm 0.01**

Three independent experiments were carried out. * $p < 0.05$ and ** $p < 0.01$ were derived as compared to the respective untreated control samples, set as 1.0. (Equivalent to Figure 4.16)